UNIVERSITY OF CALIFORNIA
RIVERSIDE

Developing Agent-Based Distributed Cooperative Vehicle-Infrastructure Systems in the Connected and Automated Vehicle Environment

A Dissertation submitted in partial satisfaction
of the requirements for the degree of

Doctor of Philosophy

in

Mechanical Engineering

by

Ziran Wang

June 2019

Dissertation Committee:
Dr. Matthew J. Barth, Chairperson
Dr. Marko Princevac
Dr. Guoyuan Wu

The Dissertation of Ziran Wang is approved:

_____

_____

_____

Committee Chairperson

University of California, Riverside

ACKNOWLEDGMENT

First and foremost, I want to sincerely thank my Ph.D. advisor, Dr. Matthew J. Barth. During the past three years I spent in the Transportation System Research (TSR) lab at UCR, he has been providing me a perfect environment to conduct research regarding my favorite topic: Connected and automated vehicles. He never hesitated to give me valuable advices regarding my research, my projects, and even my life-long career plan. Besides his expertise in our research field, I also learnt a lot from the way he communicates with people from different backgrounds, which I think will benefits me for my whole life.

I would also like to thank Dr. Marko Princevac and Dr. Guoyuan Wu for their services in my dissertation committee. Specifically, I deeply appreciate Dr. Princevac for his help before I got admitted and during my first year at UCR, when he was the graduate advisor of our department. Special thanks for Dr. Wu's patient and detailed guidance towards my dissertation, since many of my research topics originated from the brainstorms between us, and those topics cannot be transferred into so many solid publications without the help from him. He has also been willing to recommend me to the people he knows and help me expand my social network in our research field. My thanks also go to another two research faculties in our lab, Dr. Peng Hao and Dr. Kanok Boriboonsomsin, for their managements and collaborations on the projects I involved in.

In addition to the aforementioned research advisors, my Ph.D. career cannot be successful without the help from so many people at UCR. I want to thank all my colleagues in our lovely TSR lab, including Mike Todd, Dr. George Scora, Alexander Vu, Dr. Ji Luo, Dr. Xuewei Qi, Dr. Danyang Tian, Fei Ye, Nigel Williams, Chao Wang, Roland David

Oswald, Zhouqiao Zhao, Zhensong Wei, Xishun Liao, Yuan-Pu Hsu, Yu Wang, Yu Jiang, Pingbo Ruan, Shangrui Liu, Xuanpeng Zhao, Hangquan Zhao and many more. I truly appreciate my classmates and dear friends Yin-Chen Liu and Kris Suvitcharnpun for spending time with me working on different courses and projects, and also my graduate student mentor Benjamin Sommerkorn for welcoming me to UCR. I want to sincerely thank Dr. Wei Ren with his former students Dr. Shaocheng Wang and Dr. Peng Wang, for their kindly guidance regarding my Ph.D. career during my first year at UCR. My appreciation should also be sent to Jun Wang, who has been continuously supporting me during my four years at UCR.

Finally, I would like to acknowledge the Department of Mechanical Engineering at UCR, College of Engineering-Center for Environmental Research and Technology (CE-CERT) at UCR, United States Department of Energy, United States Department of Transportation, National Center for Sustainable Transportation (NCST), Toyota Motor North America, and Volvo Group North America, for fully or partially supporting my study and research in this dissertation.

The major contents in this dissertation have been published in the Institute of Electrical and Electronics Engineers (IEEE) Transactions on Intelligent Transportation Systems, IEEE Transactions on Intelligent Vehicles, Society of Automotive Engineers (SAE) International Journals of Connected and Automated Vehicles, Hindawi Journal of Advanced Transportation, IEEE Intelligent Transportation Systems Conference, IEEE Intelligent Vehicles Symposium, SAE World Congress, American Control Conference, and Transportation Research Board Annual Meeting, respectively.

DEDICATION

This dissertation is dedicated to the people who encouraged me to study abroad and chase my dreams. I want to sincerely thank my wife Ziwei Zhang (张紫薇) for her endless love during the past ten years in our relationship, and her continuous companion and support during my four years of Ph.D. career in the United States. Without her, I have no idea where I would have been, and what I could have achieved by now.

Of course, I would not be who I am today without my parents Youping Pan (潘有萍) and Xiaoyong Wang (王晓勇). They provided me the opportunities to firstly attend college in Beijing, and then pursue my Ph.D. degree in the United States. They have been always showing their countless supports to me, both emotionally and financially. Additionally, without the suggestion and guidance from my uncle Andrew Pan (潘明), I could not even think about one day I would become a doctor in the field of engineering.

Last but not least, I want to thank Chongqing Nankai Secondary School (重庆南开中学), where I met my wife and spent the best years of my youth. My outlook on life, values, and the world were formed and shaped by so many excellent educators there during those unforgettable six years. I would like to end this dedication with my motto, which was originated from the Chinese philosopher Hu Shih and was quoted by the chancellor of Nankai at our high school commencement:

成功不必在我，而功力必不唐捐

ABSTRACT OF THE DISSERTATION

Developing Agent-Based Distributed Cooperative Vehicle-Infrastructure Systems in the Connected and Automated Vehicle Environment

by

Ziran Wang

Doctor of Philosophy, Graduate Program in Mechanical Engineering
University of California, Riverside, June 2019
Dr. Matthew J. Barth, Chairperson

The rapid development of our transportation systems has brought much convenience to our daily lives, while also introducing various issues related to safety, mobility, and environmental sustainability. To address these transportation system issues, connected and automated vehicle (CAV) technology has had significant development during the last decade. With CAV technology, the capabilities of vehicles is greatly improved, allowing for equipped vehicles to not only drive partially or fully automatically using information from on-board sensors, but also behaving cooperatively through vehicle-to-everything (V2X) communications.

In this dissertation research, agent-based distributed cooperative vehicle-infrastructure systems have been developed to evaluate CAV applications from the perspective of safety, mobility and environmental sustainability, both qualitatively and quantitatively. Specifically, the proposed CAV systems described in this dissertation are divided into two major categories: The first category is based only on vehicle-to-vehicle

(V2V) communication among CAVs, while the second category is based on both V2V and infrastructure-to-vehicle (I2V) communication.

In this dissertation, three different cooperative automation applications are addressed, including cooperative adaptive cruise control (CACC), cooperative eco-driving at signalized intersections, and cooperative merging at highway on-ramps. Different agent-based motion control algorithms of CAVs are proposed and evaluated, including a distributed consensus control algorithm, an online feedforward/feedback control algorithm, and an optimal control algorithm. All proposed applications are qualitatively and quantitatively evaluated using numerical simulations and/or microscopic traffic simulations, showing their benefits of avoiding collisions, increasing traffic flow, decreasing travel time, and/or decreasing energy consumption and pollutant emissions. Field implementations with real vehicles traveling in the real-world traffic environment have also been conducted to evaluate the effectiveness of the proposed algorithms.

Additionally, studies of the aforementioned cooperative automation applications were also carried out using a game engine, which provided a simulation environment with more realistic vehicle models and road networks. Human-in-the-loop simulations were conducted on the driving simulator platform, and a learning-based approach was developed to model the human factors.

TABLE OF CONTENTS

LIST OF TABLES

LIST OF FIGURES

1 INTRODUCTION

1.1 Motivation

The rapid development of our transportation system has brought a large amount of convenience into our daily lives, allowing both passengers and goods to be transported domestically and internationally in a quicker fashion. It is estimated that more than one billion motor vehicles are owned by people over the globe, and this number will likely double within one or two decades [1]. However, a number of negative consequences related to our transportation system growth are also generated by such a huge number of motor vehicles. In terms of safety, more than 30,000 people perish from roadway accidents on U.S. highways every year [2]. In terms of mobility, Los Angeles, for instance, topped the global ranking in traffic congestion during 2016, with 104 excess hours being spent per commuter [3]. And in terms of environmental sustainability, 11.7 billion gallons of fuel were wasted worldwide due to traffic congestion in 2015 [4].

To address the aforementioned issues, *cooperative vehicle-infrastructure systems* has had some major developments during the last decade. By taking advantage of various communication approaches, intelligent vehicles can communicate with each other, and also with the infrastructure to conduct cooperative decisions and maneuvers such as crash avoidance, trip planning, toll collection, etc. An illustration of such cooperative vehicle-infrastructure systems can be seen in Figure 1-1.

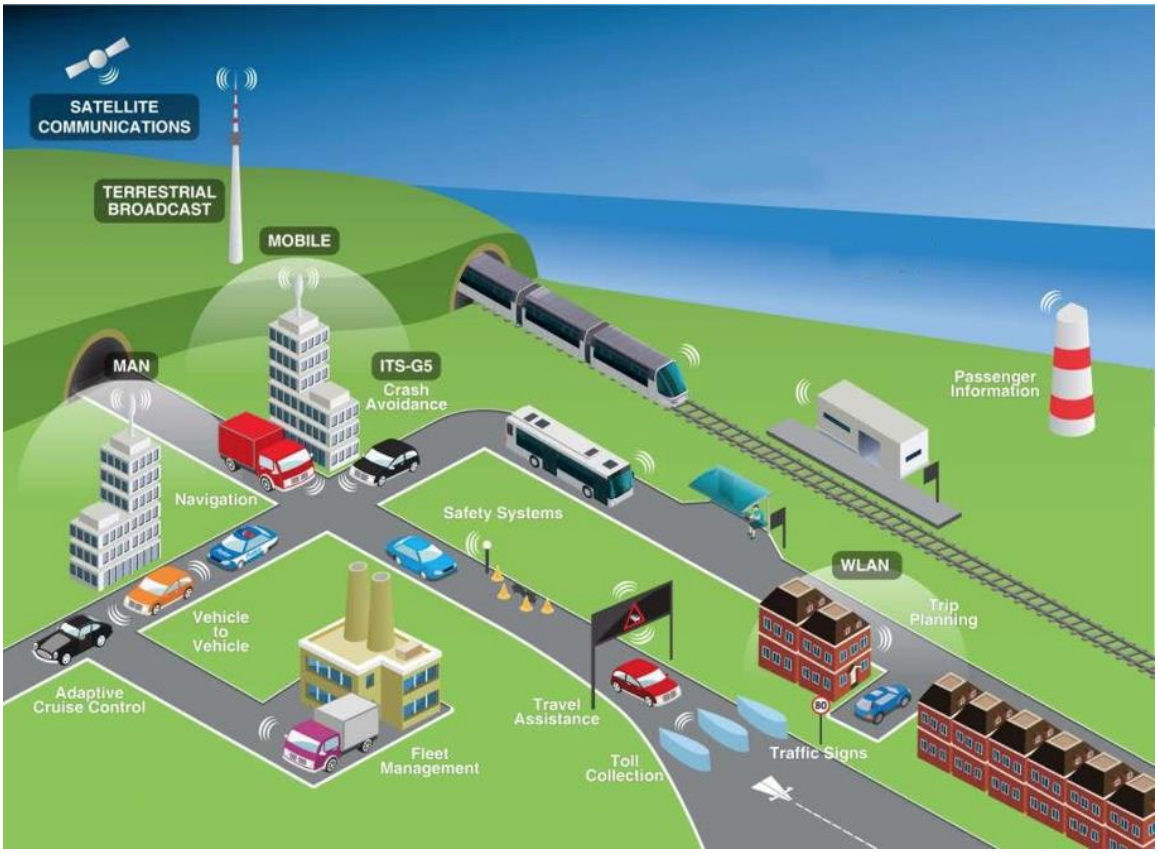

Figure 1-1. Illustration of Cooperative Vehicle-Infrastructure Systems [5]

A specific type of intelligent vehicle in such systems is a Connected and Automated vehicle (CAV), which is now attracting significant research interest around the globe. With CAV technology, the level of connectivity and automation of vehicles can be greatly improved, allowing for equipped vehicles to not only drive partially or fully automatically using information from on-board sensors, but also behave cooperatively through vehicle-to-everything (V2X) communications. Cooperative automation of CAVs has been widely studied by researchers around the world recently, whereby CAVs cooperative with each other to form or maintain certain formations by use of motion control systems that rely on their on-board sensors and vehicle-to-vehicle (V2V) and/or infrastructure-to-vehicle (I2V)

communication. The V2V communication mainly provides real-time state information about the forward vehicle or vehicles (i.e., state information such as acceleration, speed, position), while the I2V communication mainly provides information about downstream traffic conditions or local speed suggestions as part of an active traffic management approach.

By cooperatively controlling the motion of different CAVs, some or all of the following benefits are brought to the transportation system: 1) Roadway capacity can be increased due to the reduction of gaps between vehicles; 2) Energy consumption and pollutant emissions are reduced due to the reduction of unnecessary velocity changes and aerodynamic drag on following vehicles; 3) Driving safety is improved since the detection and actuation time is shortened compared to manually driven cases, and downstream traffic information can be propagated upstream sooner; and 4) Customer satisfaction is improved since the system behavior can be more responsive to traffic changes, and the shorter following gaps can deter cut-ins of other vehicles [6].

1.2 Problem Statement and Contribution of the Dissertation Research

It is well recognized that CAVs have great potential to bring system-wide benefits to our current transportation systems, with respect to safety, mobility, and environmental sustainability. However, much of the existing research on CAV systems come from a traffic system perspective, without considering the detailed specific vehicle-level planning and control logic. These high-level CAV system designs are often not that realistic and accurate, since many detailed parameters such as vehicle dynamics and V2V/I2V communication capabilities are neglected.

In this dissertation research, an *agent-based distributed approach* is adopted to develop a more effective cooperative vehicle-infrastructure system. The approach of agent-based modeling and simulation allows us to build CAV systems in a distributed manner, focusing on their heterogeneities and internal relations. In this research, we not only adopt V2V communication to develop distributed cooperative vehicle-infrastructure systems, but also I2V communication, where the infrastructure is considered as an agent of the cooperative automation system. The proposed agent-based approach allow agents in the transportation systems to reach global goals (in terms of safety, mobility, and sustainability) through distributed collaboration.

The specific contributions of this dissertation can be summarized as:

- A high-level architecture for agent-based distributed cooperative vehicle-infrastructure systems is developed.
- Multiple cooperative automation applications in the CAV environment under V2V and/or I2V communication are proposed, with each of them bringing one or more benefits to the transportation system
- Multiple motion control algorithms are developed to realize the desired movements of CAVs in the proposed CAV applications, where algorithms were analyzed qualitatively and quantitatively by various simulation approaches.

1.3 Organization of the Dissertation Research

The dissertation is organized as follows: Chapter 2 describes the research background of this dissertation and conducts a literature review on several related topics, including the general architecture of CAV systems, different cooperative vehicle-

infrastructure systems in the transportation systems, and the agent-based modeling and simulation. Chapter 3 introduces the distributed cooperative systems proposed during this dissertation using only V2V communication, such as distributed consensus-based cooperative adaptive cruise control (CACC) systems and distributed optimal control-based CACC systems. Chapter 4 introduces the distributed cooperative systems proposed during this dissertation using both V2V communication and I2V communication, such as cooperative eco-driving at signalized intersections and cooperative merging at highway on-ramps. Chapter 5 concludes this dissertation with presenting the publications resulted from this dissertation, as well as pointing out some future directions in the future research.

The general framework of this dissertation could be illustrated as Figure 1-2.

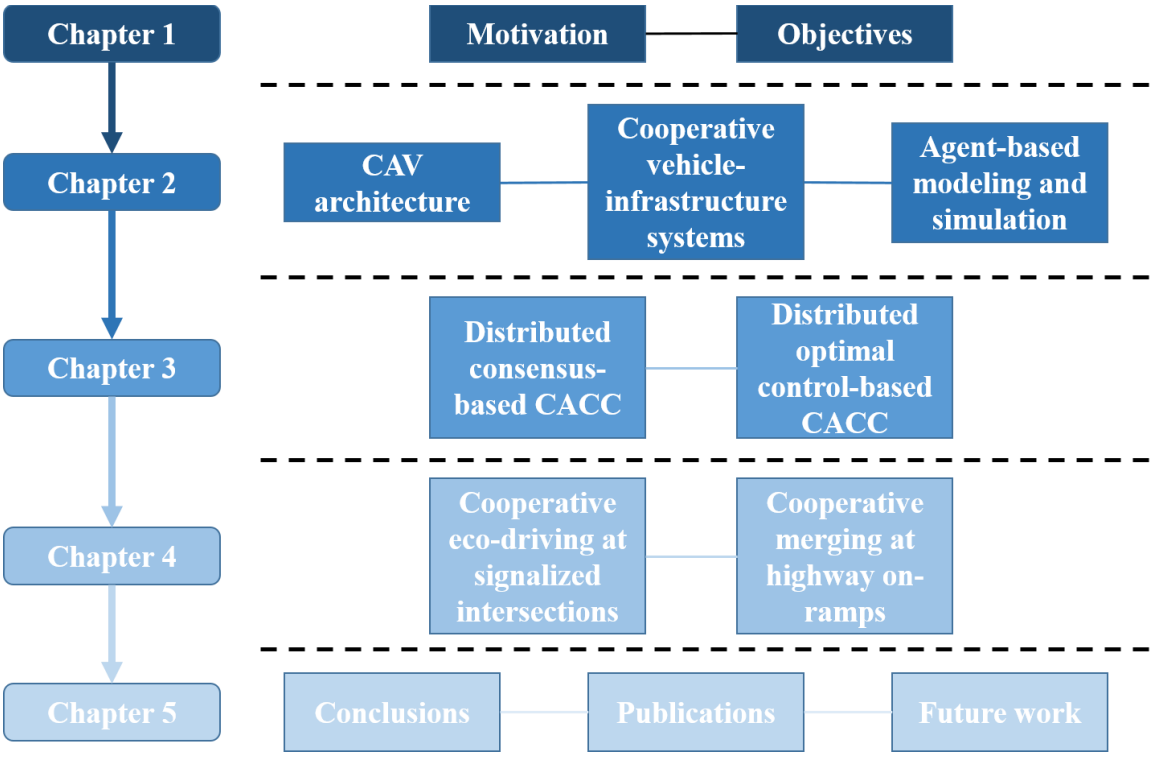

Figure 1-2. General framework of the dissertation

2 RESEARCH BACKGROUND AND LITERATURE REVIEW

2.1 General Architecture of Connected and Automated Vehicle Systems

In this section, different modules of CAV systems are introduced, providing background information for this dissertation. Many related publications are reviewed to explain the functions of separate components of a CAV system, including the communication component, the perception component, the localization component, the planning component, and the control component. In general, the architecture of such CAV systems can be illustrated as shown in Figure 2-1.

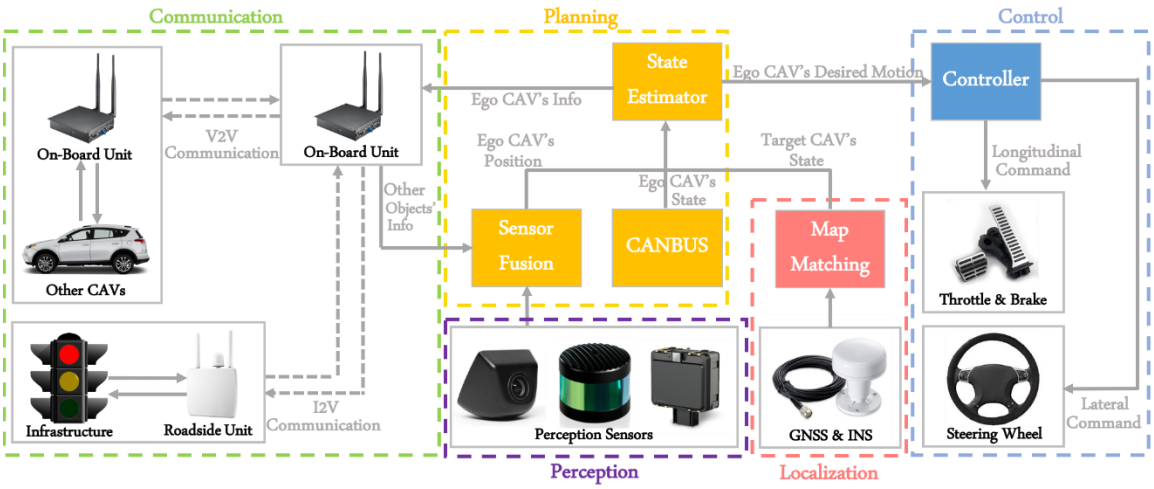

Figure 2-1. General architecture of a CAV system

2.1.1 Communication Module

The communication module of CAV system facilitates real-time, and reliable wireless V2V and I2V communication. The bandwidths of both communication approaches are possibly insufficient as the number of CAVs increases inside the coverage

area [1]. Therefore, short-range wireless technologies become advantageous in such scenarios, and specifically, Dedicated Short Range Communications (DSRC) has been selected as the standard communication protocol for V2V communication. The term "Dedicated" in DSRC points to the fact that the U.S. Federal Communication Commission allocated 75 MHz of licensed spectrum in the 5.9 GHz band for DSRC [8]. V2V safety messages are expected to be exchanged on Channel 172, which is a safety-specific channel that the aforementioned licensed spectrum has [9]. The term "Short Range" in DSRC refers that this communication protocol operates over a distance of several hundred meters, which is shorter than cellular and WiMax services [10].

However, one of the key drawbacks of DSRC is its low scalability, which often fails to provide the required time-probabilistic characteristics when traveling in a dense traffic [11]. The asynchronous disadvantage of DSRC may also lead to performance degradation by the collisions with hidden node problem in carrier sense multiple access with collision avoidance (CSMA/CA) [12]. With versatile communication types from one-to-one to one-to-many transmissions, 4G-LTE systems has been enhanced to enable V2V and I2V communication [13]. Not only software-based simulations, but also field experiments of 4G-LTE for V2V and I2V communication were conducted by researchers worldwide during the past decade [14], [15]. Furthermore, given the characteristics of very high data rates, massive number of devices, very low latency and very high reliability, the next generation of cellular networks, 5G, is also considered one feasible approach for V2V and I2V communication [16], [17].

As can be seen from the communication module in Figure 2-1, hardware communication devices installed on the ego CAV receive information from other CAVs, meanwhile also sending its own information to others through V2V communication. Additionally, it can also exchange information with the roadside infrastructure through I2V communication. The information sent through V2V communication includes vehicle dynamics (e.g., position, velocity, acceleration, yaw angle, and yaw rate) and CAV formation-related messages (e.g., formation status and formation leader ID). The communication topology (i.e., information flow topology) defines the origins and destinations of information transmission among vehicles and the infrastructure, thus playing a very important role in information exchange and sharing [18]. Some of the representative information flow topologies of CAVs are illustrated in Figure 2-2. The first four are V2V-only communication topologies, while the last two are V2V/I2V-hybrid communication topologies. More detailed information is listed as: (a) predecessor-following (PF), (b) predecessor+leader-following (PLF), (c) multiple-predecessor-following (MPF), (d) bidirectional (BD), (e) predecessor-following (PF) with the infrastructure sending information to the leader, and (f) predecessor-following (PF) with the infrastructure broadcasting information.

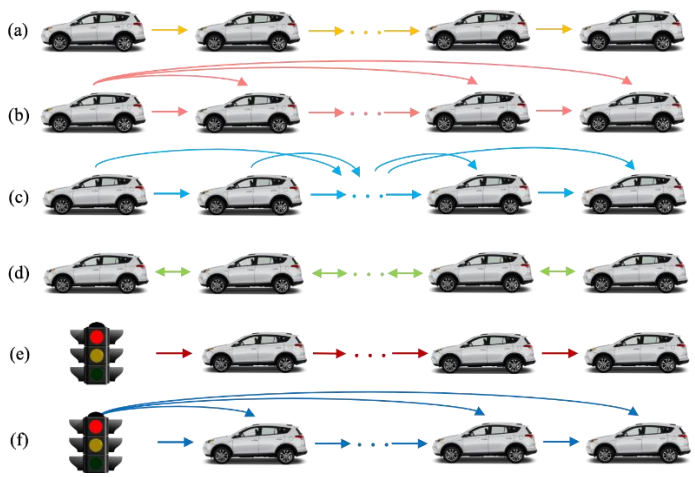

Figure 2-2. Typical information flow topologies

2.1.2 Perception Module

Perception sensors equipped on a CAV system are the primary source of the information with respect to surrounding vehicles and the road environment provided to the sensor fusion component of the planning module. The communication module of a CAV system can provide additional information that cannot be detected by perception sensors, and can generally provide it more quickly. This includes:

- Information from other vehicles that are beyond sensor range or that are occluded from view by intermediate vehicles or horizontal or vertical road curvature;
- Information about the status of other vehicles that cannot be sensed by remote sensors (wheel speeds, fault status, performance capabilities, etc.)
- Immediate notification of speed change or steering commands as soon as they have been issued to another vehicle's actuators, even before the vehicle's motion has begun to change.

- Negotiations between cooperative vehicles regarding desired maneuvers (merging, lane changing), so that these can be done more safely and efficiently.

The perception sensors also play a crucial fallback role in terms of acquiring information about the driving environment, when information about other CAVs or the infrastructure from V2V/I2V wireless communication is impeded by wireless dropouts or channel congestion. Note that the scope of this dissertation is limited to longitudinal motion control of CAV, where most existing related implementations are Level 1 automation as defined by SAE [24]. Lateral control maneuvers like lane keeping and lane changing are conducted by the human driver of the CAV. Therefore, the perception sensors of such CAV systems need to focus primarily on providing the preceding vehicles' information, like detecting the speeds of the preceding vehicles and the clearance with respect to the immediately preceding vehicle.

2.1.3 Localization Module

The localization module of a CAV system consists of two different hardware components: GNSS & INS (i.e., global navigation satellite system and inertial navigation system) and map matching.

The GNSS & INS component serves as a combined satellite & inertial-based navigation system, which can be optionally augmented by terrestrial reference stations [19]. This component can provide precise position, movement, and posture measurements for the self-localization and attitude determination of CAVs by differential correction. It should be noted that the relative positioning accuracy between the ego CAV and other equipped objects (i.e., other CAVs and/or infrastructure features) is not solely determined

by the GNSS update frequency. It is also based on the accuracy of the GNSS position measurements, and communication delay. Considering the aforementioned factors, a GNSS update rate of 10 Hz is sufficient for general cooperative automation applications, and a faster sampling rate based on GNSS & INS integrated measurements will reduce positioning errors at higher vehicle speeds [23].

Map matching is important to a CAV system, especially for some of the applications where the ego CAV needs to adjust its longitudinal speed to merge with other CAVs coming from another lane at an intersection or a highway ramp. The correct assignment of CAVs to lanes is important, as well as their relative longitudinal gaps. Therefore, a map of the implementation environment can be built a priori, and match with the vehicle coordinates (i.e., longitude, latitude, heading) received from the GNSS & INS component. To compute distances between the ego vehicle with other vehicles, traffic lights, merging point or other objects, they need to be adjusted to their closest lane by retrieving the nearest neighbor GPS track vertex [19]. Each object's coordinate can be then matched onto the associated lane to obtain its project point, and then the relative longitudinal distance between two objects can be derived by summing the segment lengths falling in between those projection points on the same GPS track (if they are on the same lane), or by calculating the difference of distances to the merging point of two GPS tracks.

2.1.4 Planning Module

The planning module processes data received from the communication module, the localization, as well as the perception module, and sends the motion commands of the ego vehicle to the control module. The planning module of a CAV system usually includes the

following components: sensor fusion, vehicle controller area network (CANBUS), and state estimator.

The sensor fusion component processes all sensing data received from the perception sensors and the communication module of the CAV system, and sends it to the state estimator component. Unlike more highly automated vehicle systems that require the entire surrounding environment to be precisely measured by multiple perception sensors, the cooperative longitudinal motion control discussed in this dissertation requires less information regarding the surrounding environment, and therefore less data are fused in the sensor fusion component. However, this component is crucial in harnessing the complementary nature of vehicle's sensors and communication systems, based on the following issues that Kianfar et al. encountered during the development of their CAV system [12]: 1) When the ego CAV is under tunnels or bridges, information from GNSS will be unreliable. Therefore, in addition to the INS, the position of the CAV can also be improved by using the sensing data measured by the perception sensors if it can be associated with a reference map; 2) When the V2V communications are impaired, the data measured by perception sensors will still be available to estimate the relative position, speed, and acceleration of the immediately preceding vehicle.

Although the GNSS & INS component is able to provide the speed of the ego CAV, its measurement is highly affected by the GNSS connection and precision. For example, if the ego CAV is traveling through a tunnel, the measured speed would be much likely less accurate than in an open space. More accurate and timely speed measurements should be obtained from the wheel-speed sensors that are an integral element of production anti-lock

braking and traction control systems. Therefore, wheel speed measured from the ABS system on the CANBUS could be much more accurate. CANBUS also allows the planning module of the CAV system to get access to many other vehicle states data.

The state estimator component receives data from the sensor fusion, CANBUS, as well as map matching, and then computes a desired motion of the ego CAV for the control module to realize. Motion planning has been developed in various ways for high-level automated vehicles, including graph search-based planners, sampling-based planners, interpolating curve planners and numerical optimization approaches [25]. However, since we only focus on the longitudinal motion of CAVs in this dissertation, the planning process in the state estimator component becomes much easier: Simply choose when and by how much to accelerate or decelerate, or else keep the current longitudinal speed. As mentioned in the CAV system developed by Martensson et al. [20], the accuracy of the state estimate highly depends on the quality of the available data (e.g., the accuracy, latency or the outage duration of the GNSS measurements or V2V communication, the performance of the perception sensors under the existing environmental conditions), and also the quality of the process estimation models.

2.1.5 Control Module

The control module of CAV systems consists of a software part and a hardware part: A controller component that integrates the motion control algorithms of the CAV, and the physical actuators of the CAV that actuate the longitudinal and/or lateral commands generated by the controller component. Although lateral control is not within the scope of

this dissertation, we still put it into Figure 2-1 to make the CAV system architecture complete.

The controller component in this control module receives the ego CAV's desired motion from the planning module, which includes information such as the reference trajectory or desired path of the CAV [26], the decision whether to join or leave a vehicle platoon [20], the desired position of the ego CAV in the vehicle platoon [22], or the desired arriving time at a specific location (e.g., traffic signal or ramp merging point) [27]. The cooperative longitudinal motion control, which is the major topic of this dissertation, will be developed and implemented in this controller component to determine the reference acceleration or speed at each time step. This reference value will then be converted into longitudinal commands for the engine and brakes of this CAV, thereby allowing it to achieve the desired motion determined by the planning module [21].

2.2 Cooperative Vehicle-Infrastructure Systems in the CAV Environment

The cooperative automation of CAVs can introduce benefits to current transportation systems with respect to safety, mobility, and environmental sustainability. As one of its major tasks, cooperative longitudinal motion control of multiple vehicles has been widely studied. Many researchers have been focusing on the mathematical modeling and software simulation of cooperative longitudinal motion control under different cases in transportation systems, while some others have been contributing much efforts to the testing of such systems on full-scale vehicles to verify their effectiveness in realistic traffic conditions. In this section, relevant studies are categorized into five different operational

concepts (vehicle cooperative ACC and platooning on highways, cooperative merging at highway on-ramps, variable speed limits near highway bottlenecks, coordination at isolated intersections, and eco-driving at signalized corridors), where each type reviews both simulation-based theoretical work and experimental work.

As shown in the performance matrix Table I, we evaluate these five operational concepts based on five different criteria: 1) The extent of theoretical research reported to date; 2) The extent of experimental research reported to date; 3) The potential transportation safety benefits; 4) The potential mobility benefits; 5) The potential environmental benefits. The first two criteria are independent from the latter three criteria, so we differentiate them by different markings in the performance matrix. Number of stars denotes the extent of work conducted, and the extent of the benefits to current transportation systems.

Table I Performance Matrix of Different Cooperative Vehicle-Infrastructure Systems.

	Extent of Work using CAVs		Potential Benefit to Transportation Systems		
	Theoretical Work	Experimental Work	Safety Benefit	Mobility Benefit	Environment Benefit
A. Cooperative adaptive cruise control and platooning	✦✦✦	✦✦	★	★★★	★★
B. Cooperative merging at highway on-ramps	✦✦	✦	★★	★★★	★
C. Speed harmonization on highways	✦✦	✦	★★	★½	★
D. Cooperative eco-driving at signalized intersections	✦	½	★	★★	★★½
E. Automated coordination at non-signalized intersections	✦½			★★	★

2.2.1 Cooperative Adaptive Cruise Control (CACC) and Platooning

Cooperative adaptive cruise control (CACC) and platooning are terms that have been adopted and utilized relatively loosely during recent years, such that different researchers visualize different functions and capabilities when discussing CACC or platoon

systems. At the heart of the concept is the merging of adaptive cruise control (ACC), a subset of the broader class of automated longitudinal speed control systems, with a cooperative module enabled with V2V communication and/or I2V communication [28]. In this subsection, only V2V communication based CACC and platoon studies are discussed, while some I2V communication based CACC studies are covered in some of the latter subsections.

Extensive research has been conducted in the field of CACC, where the literature reviews conducted by Dey *et al.* covered several different aspects of this operational concept of CAVs [29]. Specifically, the cooperative longitudinal motion control is considered as the core of a CACC system, since it keeps the string stability of a CACC string and avoids rear-end collisions of multiple CAVs.

Linear feedback control has been widely adopted as the key cooperative methodology for much previous CACC work. Milanes et al. developed a classic PD controller for the gap regulation, and a simple linear function for the gap-closing of each vehicle in a CACC string [21]. Van Arem *et al.* developed a feedback control algorithm to compute the reference acceleration, so it could be further converted to a position of gas/brake pedal by the vehicle model and control the motion of the CAV [29]. This proposed methodology was simulated in the microscopic traffic simulation model MIXIC to examine the impact of CACC on the traffic flow. Double-integrator consensus algorithms have been adopted widely for the cooperative longitudinal motion control of CACC vehicle strings. Similar to van Arem *et al.*, many other double-integrator consensus

algorithms also compute a reference acceleration based on the speed and position of the ego CAV and its predecessor [31], [32].

Optimal control has been considered as another approach for the longitudinal cooperation in a CACC string by many research projects. In general, the design of an optimal controller can be equivalently formulated as a structured convex optimization problem with multiple objectives (e.g., minimizing energy consumption) and system constraints. Unlike most linear feedback control approaches that only consider vehicle speed and position as inputs, optimal control approaches often take nonlinearity and constraints into account, such as vehicle powertrain and vehicle aerodynamics. Van de Hoef et al. formulated a convex optimization problem with linear constraints for a group consisting of a coordination leader and its coordination followers, aiming to maximize the fuel savings [33]. Turri et al. studied the cooperative look-ahead control of a heavy-duty CACC system, where the fuel calculation of vehicles is formulated as an optimal control problem to find the optimal engine speed to minimize fuel consumption [34].

Although many cooperative longitudinal motion control methodologies have been proposed for CAVs to form CACC string from a theoretical perspective, fewer field experiments of this use case have been conducted over the past decades. One of the early-stage well-known demonstration was given by University of California at Berkeley's PATH Program at San Diego, California, in 1997 [35]. Another pioneering work was accomplished by TNO in the Netherlands, where Toyota Prius were installed with CACC functions to conduct highway vehicle platooning [36]. Advanced vehicle platooning projects were completed in the Grand Cooperative Driving Challenge (GCDC) held in the

Netherlands in 2011[37]. This challenge aims to support and accelerate the introduction of CAVs in everyday traffic, and competitions like this greatly benefits the practical case of vehicle platooning based on theoretical studies.

It should be noted that, a very large portion of cooperative control methodologies of CACC are developed for heavy-duty trucks, where researchers around the world used to refer them as "truck platooning" [38]. In the United States, the PATH Program has developed three generations of proof-of-concept prototype truck platooning systems, including the first two based on Freightliner Century model tractors, and the third one based on a Volvo tractor. Specifically, in their truck platooning project with Volvo, different cooperative operational concepts were proposed, including string formation, steady-state cruising, string split maneuvers, and faults or abnormal operating conditions [39]. In Japan, the Energy ITS project led to the development of an automated truck platoon system, which can introduce 14 % energy saving when the trucks are empty-loaded and the gap is 10 m, and 15 % energy saving when the trucks are ordinarily loaded and the gap is 4 m [40]. In Europe, similar work was conducted by RWTH Aachen University's "KONVOI" project, where the field test was conducted on German highways with one leading human-driven truck and three following automated trucks [41]. So far, it is clear to researchers that, truck platooning mainly aims at reducing air drag and thereby energy consumption, which is slightly different from passenger vehicle platooning which aims at improving travel efficiency.

2.2.2 Cooperative Merging at Highway On-Ramps

Cooperative merging at highway onramps is a major conflict zone that generates safety and mobility concern. The difficulty for the driver along the on-ramp where he/she has to discern whether to accelerate or decelerate to enter the main line safely. Meanwhile, the drivers on main lane may have to modify their speeds to permit the entrance of merging vehicle, thus affecting the traffic flow [42]. To address these issues, cooperative automation of CAVs has been widely studied and applied to highway on-ramp merging case, where different control algorithms have been proposed and implemented to allow CAVs to merge with each other in a cooperative manner. Existing related work were reviewed by Rios-Torres et al. and Scarinci et al. [43], [44].

The concept of virtual vehicle or "ghost" vehicle of a CACC system in the highway on-ramps cooperative merging case was originated from Uno et al. [45]. The proposed approach maps a virtual vehicle onto the highway main road before the actual merging happens, allowing vehicles to perform safer and smoother merging maneuver. Lu et al. applied a similar idea in their proposed systems, where they first formulated the merging problems differently with respect to two different geometric layouts of the road (i.e., either with or without a parallel lane), and then proposed a speed based closed-loop adaptive control method to control the longitudinal speed of merging CAVs [46].

Other than virtual vehicle concept, many other approaches were also proposed to realize the cooperative merging case. Specifically, Dao et al. proposed a distributed control protocol to assign vehicles into vehicle strings in the merging scenario [61]. Rios-Torres et al. presented an optimization framework and an analytical closed-form solution that

allowed online coordination of CAVs at on-ramp merging zones [47]. Besides, Liu et al. investigated the impact of CACC vehicle string operation on the on-ramp merging areas [48]. Their study revealed that the highway capacity increases greatly as the CACC market penetration rate increases, with a maximum value of 3080 veh/hr/lane at 100% market penetration.

While aforementioned simulations are encouraging, their transition to experimental implementations are far from straightforward, given the difficulty to model the nonlinear gasoline-propelled vehicle dynamics at very low speeds. Therefore, much less experimental implementations of cooperative merging have been conducted by researchers worldwide. Researchers from PATH program conducted experimental tests on their cooperative automated merging systems both on their RFS test track and on the Crows Landing test track [50]. The proposed general real-time algorithm was successfully implemented on their CAVs which had magnet-based speed and steering control. Milanes et al. proposed a fuzzy logic-based controller to act on the CAV's longitudinal motion control actuators (i.e., throttle and brake pedals), following the references set by a decision algorithm [42]. A local control station (LCS) was developed to serve as an infrastructure, which receives information from the CAVs in its domain, analyzes this information to determine when a potentially risky situation might arise, and notifies the CAVs of suggested maneuvers through I2V communication. Their experimental implementation emulates a congested traffic situation by allowing two Citroens to perform ACC between them at low speed. Another Citroen came from the ramp and merged between these two vehicles, which was decided by LCS. This work was part of their AUTOPIA program,

which aimed to develop autonomous vehicles using produced vehicles, and tested them in real-world traffic [51].

2.2.3 Speed Harmonization on Highways

Speed harmonization is a highway traffic strategy framework with an objective to reduce temporal and spatial variations of traffic speed, so as to increase safety and mobility of the transportation systems, while at the same time reducing negative impacts on the environment [52]. Traffic approaches of speed harmonization include variable speed limit, ramp metering, and some other hybrid approaches that changes. Within the scope of this survey, we review the cooperative longitudinal motion control methods of existing CAV-based speed harmonization case on highways.

Many research efforts focus on only sharing speed harmonization information with connected vehicles and allow their drivers to behave according to that information. However, within the scope of this survey, we only review the speed harmonization cases where the longitudinal motion of vehicles is also controlled by developed cooperative longitudinal motion control methods. Li et al. proposed and analyzed a describing-function based approach for speed harmonization. A V2V communication based cooperative longitudinal motion control algorithm was proposed, taking leading CAV's status as the input of the algorithm. The simulation results showed the proposed method effectively suppressed development of oscillation, and therefore mitigated energy consumption and emission.

However, more researchers applied variable speed limit (VSL) to the speed harmonization case on highways. Wang et al. developed a VSL based longitudinal motion

control algorithm for CAVs using I2V communication, showing this speed harmonization approach reduces total travel time and average energy consumption [53]. Kondaker et al. firstly established an I2V-based VSL system, where CAVs with CACC functions can receive downstream information much in advance [54]. The sensitivity analysis showed that the developed approach outperformed the uncontrolled scenario by 20% travel time reductions, 6-11% safety improvements, and 5-16% energy consumption reductions, respectively.

Although there were quite a few practices and field tests of speed harmonization cases worldwide during the past decade, such as the ones conducted in the U.S., Germany [57], France [58], Sweden [59], and Greece [52], none of these used CAV technology. More recently, there were only a very few experimental implementations of CAV-based speed harmonization cases. Federal Highway Administration (FHWA) conducted a speed harmonization implementation on interstate I-66, Washington, DC with three CAVs that are equipped with I2V communication, and three more probe vehicles [52]. A simplified speed harmonization algorithm was proposed to control the longitudinal motion of CAVs, where those three CAVs were positioned in a row to regulate the upstream traffic speed along highway. The impacts of this speed harmonization implementation were measured by those three probe vehicles, showing the traffic stream trajectories after this speed harmonization approach reduced oscillatory behavior as characterized using the power spectral densities of the measurements.

2.2.4 Cooperative Eco-Driving at Signalized Intersections

Eco-driving at signalized intersections using I2V communication has been a research interest for multiple research organizations globally, including “Eco-Approach and Departure” application proposed by University of California at Riverside in the U.S. [74], and “GLOSA” application proposed by University of Surrey in the U.K. [61]. In their applications, the signal phase and timing (SPaT) information is sent to the approaching CAV, so it can plan its longitudinal speed trajectory to avoid unnecessary speed change or full stop.

Based on the existing I2V communication-based eco-driving case, some researchers proposed to integrate it with V2V communication-based case such as CACC, aiming to increase the system-wide benefits. As illustrated in Fig. 6, the leader of a CACC vehicle string can receive SPaT information from the roadside equipment unit, and share it with its following CAVs while traveling at signalized corridors [62]. A typical scenario of this case would be that, when the leading CAV decides to decelerate and slowly approach the intersection to avoid a full stop at the intersection during the red phase, upstream CAVs can also follow its maneuver through V2V communication based cooperative longitudinal motion controllers to save energy.

Yang et al. developed a cooperative longitudinal motion control algorithm for CAVs traveling through isolated signalized intersections, where the optimal longitudinal speed trajectory was computed to minimize the energy consumption, ensuring that each CAV arrives at the intersection as soon as the last CAV in the queue is discharged [63]. Microscopic traffic simulation showed that the proposed system produces vehicle energy

savings up to 40% when the CAV market penetration rate is 100%. Zhao et al. developed a cooperative eco-driving longitudinal motion control scheme for a group of vehicles with mixed CAVs and conventional vehicles [64]. A complicated interaction scheme was developed by them to allow CAVs and conventional vehicles cooperate with each other, and the numerical simulations with different penetration rates showed the overall energy consumption continues to drop while the penetration rate of CAVs increases.

Another scenario at signalized intersections that the cooperative longitudinal motion control can make a significant difference is likely to be the coordinated start of CAVs. Shladover et al. specified in their work that, even if the I2V communication is not adopted in this scenario, the first CAV stopped at a signal in a queue can broadcast its state information so that any following CAVs can accelerate in a synchronized fashion [28]. It was expected that, the cooperative longitudinal motion control of multiple CAVs in the string enable a much quicker clearance of the queue at the signal, increasing the intersection throughput or facilitating the selection of shorter signal cycles without sacrificing throughput.

The basic concept of eco-driving is an important element in the AERIS Project's Eco-Signal Operations scenario, however, that scenario focused more on providing advice to the driver about the recommended speed, which assumes the vehicle is controlled by the human driver [65]. The Multi-Modal Intelligent Traffic Signal System (MMITSS) project is developing a family of intersection signal control applications for CAVs, and aims to reach the goal of eco-driving and improving efficiency and throughput of the transportation systems [66]. When CAVs reach a high market penetration and the cooperative

longitudinal motion control can be applied, the general intelligent traffic signal control (ISIG) can ensure that CACC strings are not broken by signal phase changes, allowing all CAVs in the string to travel through the intersection within the same green phase.

Given the limited amount of theoretical research in the use case of cooperative eco-driving at signalized intersections, there is no published experimental implementation of this use case. However, including the AERIS and MMITSS projects, there are several ongoing projects in the U.S. that are looking into testing this use case with realistic CAVs. It could be expected that more experimental implementations on eco-driving at signalized intersections will be conducted by federal agencies and research organizations worldwide in the coming years.

2.2.5 Automated Coordination at Non-Signalized Intersections

The cooperative automation of CAVs at non-signalized intersections has been another popular topic in the research field of intelligent transportation systems for a long time. Since intersection is considered as one of the most common traffic cases that cause traffic conflicts, much work has been conducted to increase traffic safety by applying V2V communication and/or I2V communication. Specifically, approaching CAVs are assigned with specific sequences by the proposed planning/scheduling algorithms, and their motions can be controlled by the proposed cooperative longitudinal motion controllers once the planning/scheduling is finished.

In 2004, Neuendorf et al. firstly proposed a decentralized cooperative longitudinal motion controller for CAVs at autonomous intersections by adopting the idea of the virtual platoon concept, where the general idea can be illustrated by Fig. 7 [67]. Medina et al.

further developed an autonomous intersection system for CAVs using similar approach, which consists of a bi-level architecture: A supervisory level with subsystems Target Vehicle Assignment and Control Reconfiguration; An execution level with cooperative vehicle motion control design [68], [69]. Xu et al. also adopted the virtual platoon methodology to project vehicles approaching from different directions of an intersection into a virtual lane [70].

Upon addressing the safety issue at conflict-free intersections, some proposed cooperative longitudinal motion control methods also considered the mobility and efficiency issues of CAVs. Bashiri et al. adopted the capability of V2V communication to improve the efficiency of the intersection in terms of average delay time per vehicle [71]. In the simulation study, the proposed cooperative autonomous control scheme was able to reduce average delay by up to 40% while reducing variance by 50% compared to the traditional stop sign policy. Jin et al. proposed a multi-agent motion management protocol for CAVs to form platoons based on V2V communication before approaching to the non-signalized intersection [72]. Compared to the conventional traffic signal control system, the proposed system shortens the average travel time by 30% and reduces the energy consumption by 23%. Diab et al. developed a scaled testing platform with four 1:14 scaled CAVs to test the proposed safe intersection management system [73]. A PI controller was developed to control the longitudinal motion of CAVs, and different crossing modes for CAVs in the CACC platoon were designed, including pass, stop, split, and join.

For the use case of conflict-free coordination at non-signalized intersections, there were a few experimental implementations conducted by European research organizations,

such as Cybercars project and Cybercars-2 project in France [74], [75]. However, including the aforementioned two projects, most testing projects put their research focus on the motion planning of CAVs, i.e., how to plan the trajectories of CAVs so they will not collide with each other while travelling through the intersection. Very limited literature could be found that discussed about the motion control of CAVs in their implementations of conflict-free coordination at non-signalized intersections. This could be a potential research field that organizations worldwide could contribute to in their future developments.

2.3 Agent-Based Modeling and Simulation

Agent-based modeling and simulation (ABMS) focuses on microscale models that simulate the simultaneous operations and interactions of multiple agents [76]. There is no universal definition of the term "agent", however, certain characteristics are often shared by agents from a modeling standpoint [77]. Those characteristics include:

- An agent is identifiable, a discrete individual with a set of characteristics and rules governing its behaviors and decision-making capability. Agents are self-contained. The discreteness requirement implies that an agent has a boundary and one can easily determine whether something is part of an agent, is not part of an agent, or is a shared characteristic.
- An agent is situated, living in an environment with which it interacts with other agents. Agents have protocols for interaction with other agents, such as communication protocols, and the capability to respond to the environment. Agents have the ability to recognize and distinguish the traits of other agents.

- An agent is goal-directed, having goals to achieve (not necessarily objectives to maximize) with respect to its behaviors.
- An agent is autonomous and self-directed. An agent can function independently in its environment and in its dealings with other agents, at least over a limited range of situations.
- An agent is flexible, and has the ability to learn and adapt its behaviors over time based on experience. This requires some form of memory. An agent may have rules that modify its rules of behavior.

Given the fact that CAVs can fulfill the above characteristics to large extent, ABMS is considered an attractive approach for modeling transportation systems comprised of CAVs.

There are many existing tools to model and simulate cooperative vehicle-infrastructure systems, from the traditional four-step travel demand models, to the state-of-the-art agent-based models, they all have their unique advantages and thus are suited for different purposes [78]. In this subsection, we give some brief introduction on the tools that are used in this dissertation study, including MATLAB/Simulink, PTV VISSIM, Unity, and MOtor Vehicle Emission Simulator (MOVES).

MATLAB is a widely-used multi-paradigm numerical computing environment and proprietary programming language developed by MathWorks [79]. Simulink is a graphical programming environment for modeling, simulating and analyzing multi-domain dynamical systems, and it offers tight integration with the MATLAB environment [80]. Since its capabilities to numerically model dynamic systems, MATLAB/Simulink is used

in this dissertation as a fundamental tool to model CAV dynamic systems, developing and analyzing the motion planner and controller of CAVs.

PTV VISSIM is a microscopic multi-modal traffic flow simulation software package developed by Planung Transport Verkehr AG in Germany [81]. Specifically, VISSIM Application Programmer's Interface (API) package enables users to integrate external applications to take influence on the traffic simulation. In this dissertation, we implement the proposed vehicle control methodologies in the DriverModel.DLL by C++, which can be assigned to specific vehicle types in VISSIM and overwrite the standard driving behavior. Additionally, the EmissionsModel.DLL is provided by VISSIM to add user-defined emission models, where we implement the MOVES model to perform analysis on the environmental impacts of the system.

The emergence of the CAV technology triggers a challenging system modeling problem: Traditional modeling tools that consider only one target vehicle can no longer be adopted since we need to also consider a CAV's surrounding environment, such as other vehicles, road infrastructure, and pedestrians. Microscopic traffic simulators, such as SUMO, Aimsun, and aforementioned PTV VISSIM, provide the options for researchers to model a relatively large amount of vehicles in a traffic environment [82], [83]. However, users of such simulators cannot model full dynamics of vehicles, and neither can they get involved in the control of vehicles. Conversely, game engines are able to model complex virtual reality environments, and also allow users (i.e., game players) to get fully immersed in the simulation game.

The Unity game engine used in this dissertation integrates a custom rendering engine with the Nvidia PhysX physics engine and Mono, the open source implementation of Microsoft's .NET libraries [84]. Unity has been widely used to build simulation platforms. Graighead et al. implemented the Search and Rescue Game Environment (SARGE) with Unity, where robotic vehicles in this environment are equipped with various sensors, such as 3D camera, GPS, odometer, inertial measurement unit (IMU), and planar laser ranging [85]. KTH Royal Institute of Technology in Sweden conducted several studies on the visualization of truck platooning using Unity [86], [87]. Toyota InfoTechnology Center in USA also contributed a series of work to the vehicle prototyping research by Unity. Yamaura et al. built a virtual prototype of advanced driver-assistance systems (ADAS) with a closed-loop simulation framework that consists of four tools: Unity, Simulink, OpenMETA, and Dymola [88]. Kim et al. proposed several research directions and potential approaches for testing autonomous vehicle software in a virtual prototyping environment using Unity, from the perspective of test criteria and test case generation [89]. As an extended work of that work, Dai et al. presented a co-simulation tool-chain for the automated optimization of various parameters in the virtual prototyping environment [90]. In general, Unity has the following advantages over other simulation tools:

- Graphics and visualization: Since Unity is designed for developers to develop 3D video games, it has an impressive capability of graphics rendering and visualization. It streamlines the demonstration of the proposed CAV technology to the audience,

especially to the general public (without knowing technical details). This is the primary reason why we selected Unity for performing ABMS of CAVs.

- Integration with driving simulator: Unity provides easy access to change the input equipment, which makes it possible to integrate it with driving simulator hardware. Since we want to compare the proposed CAV technology with the baseline, using driving simulator hardware with human-in-the-loop simulation is more realistic than simply applying some human driver models in the simulation.
- Asset store: Unity has an official asset store where Unity developers and users can upload and download different Unity assets, which allows Unity users to develop their own game environment based on others' previous work, instead of building things from scratch.
- Documentation and community: Unity provides thorough, well-organized, and easy-to-read documentation covering how to use each component in Unity, and an online commUnity website for all Unity users to ask and answer questions.

MOVES is developed by U.S. Environmental Protection Agency (EPA), which creates emission factors or emission inventories for both on-road motor vehicles and non-road equipment [99]. Its purpose is to provide an accurate estimate of emissions from cars, trucks and non-highway mobile sources under a wide range of user-defined conditions. In this dissertation, we extract the main functions of MOVES based on the database provided on U.S. EPA's official website, and develop customized versions in MATLAB and PTV VISSIM. In such a manner, the energy consumption and pollutant emission results can be

directly computed during our simulations, instead of outputting vehicle speed profiles in each simulation scenario and inputting them in the official MOVES' application.

3 DISTRIBUTED COOPERATIVE SYSTEMS WITH V2V COMMUNICATION

3.1 Introduction and Background

Recently, the rapid development of our transportation systems has led to a world-wide economic prosperity, where transportation for both passengers and goods is much more convenient both domestically and internationally. The number of motor vehicles worldwide is estimated to be more than 1 billion now, and will double again within one or two decades [1]. Such a huge quantity of motor vehicles and intensive transportation activities have brought about various social-economic issues. For example, more than 30,000 people still perish from roadway crashes on U.S. highways every year [2]. For the past few years, cities that have experienced more economic improvements are at a higher risk to face worsening traffic conditions, resulting in increased pollutant emissions and decreased travel efficiency. In terms of average time wasted on the road, Los Angeles for example tops the global ranking with 104 hours spent in congestion per commuter during the year of 2016 [3]. It was also estimated by [4] that there were 3.1 billion gallons of energy wasted worldwide due to traffic congestion in 2014, which equated to approximately 19 gallons per commuter.

Significant efforts have been made around the world to address these transportation issues. Many propose to simply expand our existing transportation infrastructure to help solve these traffic-related problems. However, this is not only costly, but also has many negative social and environmental effects. As an alternative solution, the development of connected and automated vehicle (CAV) can help better manage traffic, thus improving

traffic safety, mobility, and reliability without the cost of infrastructure buildout. One of the more promising CAV applications is Cooperative Adaptive Cruise Control (CACC), which extends Adaptive Cruise Control (ACC) with CAV technology (e.g., mainly via V2V communication) [6]. By sharing information among vehicles, a CACC system allows vehicles to form platoons and be driven at harmonized speeds with constant time headways between vehicles. The main advantages of a CACC system are: a) connected and automated driving is safer than human driving by minimizing driver distractions; b) roadway capacity is increased due to the reduction of inter-vehicle time gaps without compromising safety; c) fuel consumption and pollutant emissions are reduced due to the reductions of both unnecessary acceleration maneuvers and aerodynamic drag on the vehicles in the platoon [91].

3.2 Distributed Consensus-Based CACC System

3.2.1 Problem Statement

Given the second-order dynamics of a vehicle i

$$\dot{r}_i(t) = v_i(t) \tag{3-1}$$

$$\dot{v}_i(t) = a_i(t) \tag{3-2}$$

$$a_i(t) = \frac{1}{m}\left[F_{net_i}(t) - R_i T_{br_i}(t) - c_{vi} v_i(t)^2 - c_{pi} v_i(t) - d_{mi}(t)\right] \tag{3-3}$$

where $r_i(t)$, $v_i(t)$ and $a_i(t)$ denote the longitudinal position, longitudinal speed and longitudinal acceleration of vehicle i at time t, respectively, m_i denotes the mass of vehicle i, $F_{net_i}(t)$ denotes the net engine force of vehicle i at time t, which mainly depends on the vehicle speed and the throttle angle, R_i denotes the effective gear ratio from

the engine to the wheel of vehicle i, $T_{br_i}(t)$ denotes the brake torque of vehicle i at time t, c_{vi} denotes the coefficient of aerodynamic drag of vehicle i, c_{fi} denotes the coefficient of friction force of vehicle i, $d_{mi}(t)$ denotes the mechanical drag of vehicle i at time t.

The following equations can then be derived from the principle of vehicle dynamics when the braking maneuver is deactivated, i.e., vehicle i is accelerating by the net engine force:

$$F_{net_i}(t) = \ddot{x}_i(t)m_i + c_{vi}\dot{x}_i(t)^2 + c_{pi}\dot{x}_i(t) + d_{mi}(t) \tag{3-4}$$

and when the braking maneuver is activated, i.e., vehicle i decelerates by the brake torque:

$$T_{br_i}(t) = \frac{\ddot{x}_i(t)m_i + c_{vi}\dot{x}_i(t)^2 + c_{pi}\dot{x}_i(t) + d_{mi}(t)}{R_i} \tag{3-5}$$

It should be noted that the net engine force is a function of the vehicle speed and the throttle angle, which is generally based on the steady-state characteristics of engine and transmission systems, and the mathematical derivation can be referred to [94], [95].

Generally, the longitudinal control command of a vehicle is based on a hierarchical strategy, where the high-level controller (eq. (3-1) and (3-2)) generates a target acceleration, while the low-level controller commands the vehicle actuators to track the target acceleration (eq. (3-3)). In this dissertation, we focus on the high-level vehicle controller, where we propose the online feedforward/feedback longitudinal controller based on the predecessor following information flow topology of a string of vehicles, where the following vehicle only gets information from its immediate leading vehicle through V2V communications.

In this section, we propose the different algorithms based on the predecessor following information flow topology of a string of vehicles, where the following vehicle only gets information from its immediate leading vehicle through V2V communications. Given that, the problem can be generalized as a car-following problem shown as the following figure.

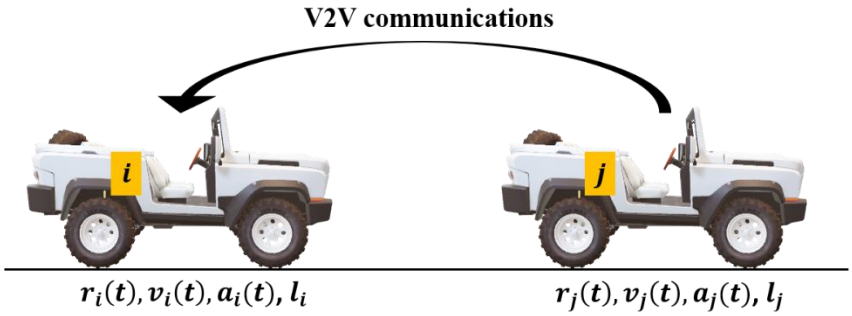

Figure 3-1. Typical information flow topologies

In this figure, the term l_j denotes the length of vehicle j. As can be seen, the following vehicle i receives information from the leading vehicle j through V2V communications. Therefore, the problem of forming a predecessor following string of vehicles can be formulated as that, given determined l_i and l_j, and $r_i(0)$, $v_i(0)$, $a_i(0)$, $r_j(0)$, $v_j(0)$, $a_j(0)$, how to apply a longitudinal control algorithm such that

$$r_i(t) \to r_j(t) - r_{headway} \tag{3-6}$$

$$v_i(t) \to v_j(t) \tag{3-7}$$

$$a_i(t) \to a_j(t) \tag{3-8}$$

where "→" means the value on the left-hand side converges to the value on the right-hand side, $r_{headway}$ is the desired distance headway between two vehicles.

3.2.2 Distributed Consensus Algorithm

We represent the information flow topology of a distributed network of vehicles by using a directed graph $\mathcal{G} = (\mathcal{V}, \mathcal{E})$, where $\mathcal{V} = \{1, 2, \dots, n\}$ is a finite nonempty node set and $\mathcal{E} \subseteq \mathcal{V} \times \mathcal{V}$ is an edge set of ordered pairs of nodes, called edges. The edge $(i, j) \in \mathcal{E}$ denotes that vehicle j can obtain information from vehicle i. However, it is not necessarily true in reverse. The neighbors of vehicle i are denoted by $\mathcal{N}_i = \{j \in \mathcal{V}: (i, j) \in \mathcal{E}\}$. The topology of the graph is associated with an adjacency matrix $\mathcal{A} = [a_{ij}] \in \mathbb{R}$, which is defined such that $a_{ij} = 1$ if edge $(j, i) \in \mathcal{E}$, $a_{ij} = 0$ if edge $(j, i) \notin \mathcal{E}$, and $a_{ii} = 0$. $\mathcal{L} = [\ell_{ij}] \in \mathbb{R}$ (i.e., $\ell_{ij} = -a_{ij}$, $i \neq j$, $\ell_{ii} = \sum_{j=1, j\neq i}^{n} a_{ij}$) is the nonsymmetrical Laplacian matrix associated with $\mathcal{G}$. A directed spanning tree is a directed tree formed by graph edges that connects all the nodes of the graph.

Before proceeding to designing our distributed consensus algorithm for the CACC system, we recall here some basic consensus algorithms which can be used to apply similar dynamics on the information states of vehicles. If the communication between vehicles in the distributed networks is continuous, then a differential equation can be used to model the information state update of each vehicle.

The single-integrator consensus algorithm [92] is given by

$$\dot{r}_i(t) = -\sum_{j=1}^{n} g_{ij} k_{ij} \left(r_i(t) - r_j(t) \right), i \in V \tag{3-9}$$

where $x_i \in \mathbb{R}$, $k_{ij} > 0$, $g_{ij} = 1$ if information flows from vehicle j to i and 0 otherwise, $\forall i \neq j$. The adjacency matrix A of the information flow topology is defined accordingly as

$a_{ii} = 0$ and $a_{ij} = g_{ij}k_{ij}, \forall i \neq j$. This consensus algorithm guarantees convergence of multiple agents to a collective decision via local interactions.

The former equation can be extended to second-order dynamics to better model the movement of a physical entity, such as a CAV. For a second-order model, the double-integrator consensus algorithm [93] is given by

$$\begin{cases} \dot{r}_i(t) = v_i(t) \\ \dot{v}_i(t) = -\sum_{j=1}^{n} g_{ij}k_{ij}\left(r_i(t) - r_j(t)\right) \\ \qquad\qquad +\gamma g_{ij}k_{ij}\left(v_i(t) - v_j(t)\right), i \in V \end{cases} \tag{3-10}$$

where $x_i \in \mathbb{R}$, $v_i \in \mathbb{R}$, $k_{ij} > 0$, $\gamma > 0$, and $g_{ij} = 1$ if information flows from vehicle j to i and 0 otherwise, $\forall i \neq j$.

3.2.3 Feedforward/Feedback Consensus Algorithm

3.2.3.1 Introduction

Most existing relevant works adopt the same set of control parameters (i.e., damping gains) independently of certain driving scenario characteristics [30], [31], [96], [97]. Such uniform assignment of control gains may not guarantee the constraints of the proposed longitudinal control algorithms under some driving scenarios. For example, the algorithm might work well when the initial speed difference of two vehicles are relatively small, and the initial headway is relatively large. However, when the initial conditions of these parameters change dramatically but the control gains remain the same, some overshoot of the headway might appear during the convergence process. Although the dynamics of two vehicles will still converge to consensus eventually, safety constraints cannot be satisfied since rear-end collision between vehicles will happen. The convergence

to stability might also take a very long time, making the algorithm inefficient. Additionally, the speed or acceleration can change dramatically during a short period without considering the riding comfort of human passengers. These are the issues we want to address in this dissertation by developing an online feedforward/feedback longitudinal controller, where the block diagram is shown as Figure 3-2.

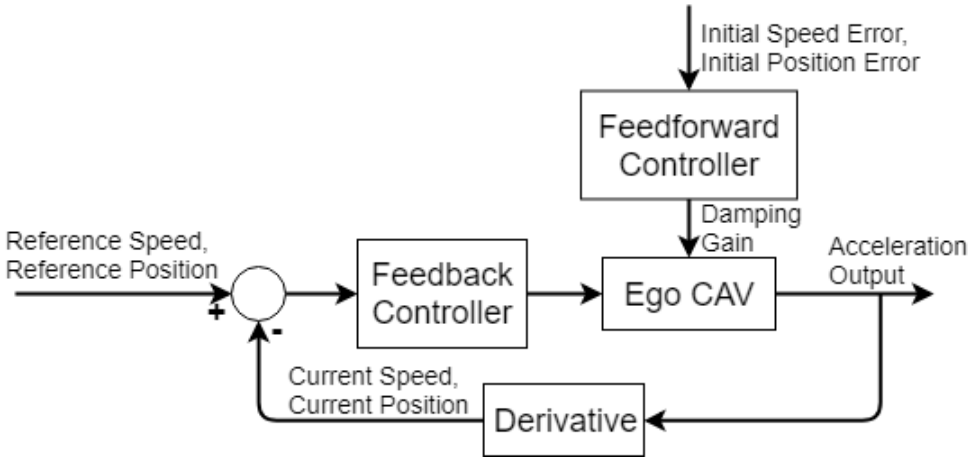

Figure 3-2. Typical information flow topologies

3.2.3.2 Feedback Control: Distributed Consensus Algorithm

Based on aforementioned consensus algorithm eq. (3-10), a double-integrator distributed consensus longitudinal control algorithm for CAVs is proposed as

$$\dot{r}_i(t) = v_i(t) \tag{3-11}$$

$$\dot{v}_i(t) = -\alpha_{ij} k_{ij} \cdot \left[\left(r_i(t) - r_j\left(t - \tau_{ij}(t)\right) + l_j + v_i(t) \cdot \left(t_{ij}^g(t) + \tau_{ij}(t)\right)\right) + \gamma_i \cdot \left(v_i(t) - v_j\left(t - \tau_{ij}(t)\right)\right)\right],\ i, j \in \mathcal{H} \tag{3-12}$$

where $\tau_{ij}(t)$ denotes the time-variant communication delay between two vehicles, $t_{ij}^g(t)$ is the time-variant desired time gap between two vehicles, which can be adjusted by many factors like road grade, vehicle mass, braking ability, etc. The term $\left[l_j + v_i(t) \cdot\right.$

$\left(t_{ij}^{g}(t)+\tau_{ij}(t)\right)\Big]$ is another form of the term $r_{headway}$. The longitudinal position and speed converges to position consensus and speed consensus, respectively as

$$r_i(t) \to [r_j\left(t-\tau_{ij}(t)\right)-l_j-v_i(t)\cdot\left(t_{ij}^{g}(t)+\tau_{ij}(t)\right)] \tag{3-13}$$

$$v_i(t) \to v_j\left(t-\tau_{ij}(t)\right) \tag{3-14}$$

If we define $\tilde{r_i}$ and $\tilde{v_i}$ as the position error and speed error of vehicle i with respect to the leading vehicle of a vehicle string (i.e., the desired values of all following vehicles in the string), then this problem can be rewritten as

$$\dot{r}_i(t) = v_i(t) \tag{3-15}$$

$$\dot{v}_i(t) = -\alpha_{ij}k_{ij}\cdot[\left(\tilde{r}_i(t)-\tilde{r}_j\left(t-\tau_{ij}(t)\right)\right)+\gamma_i\cdot\left(\tilde{v}_i(t)-\tilde{v}_j\left(t-\tau_{ij}(t)\right)\right)], \quad i,j\in\mathcal{H} \tag{3-16}$$

If we further define the dynamics of the vehicle in a compact form as

$$\tilde{r} = [\tilde{r}_1^T,\tilde{r}_2^T,\dots,\tilde{r}_i^T,\dots,\tilde{r}_n^T]^T \tag{3-17}$$

$$\tilde{v} = [\tilde{v}_1^T,\tilde{v}_2^T,\dots,\tilde{v}_i^T,\dots,\tilde{v}_n^T]^T \tag{3-18}$$

then the state vector can be defined as

$$\tilde{\chi} = [\tilde{r}^T\ \tilde{v}^T]^T \tag{3-19}$$

The double-integrator vehicle dynamics in equation eq. (3-11) and (3-12) can be further transformed into a compact form as

$$\dot{\tilde{\chi}}(t) = \Gamma_1\tilde{\chi}(t)+\Gamma_k\tilde{\chi}\big(t-\tau_k(t)\big) \tag{3-20}$$

$$\Gamma_1 = \begin{bmatrix}0_{n\times n} & I_{n\times n}\\ -\tilde{A} & -\gamma\tilde{A}\end{bmatrix}, \Gamma_k = \begin{bmatrix}0_{n\times n} & 0_{n\times n}\\ \tilde{A}_k & \gamma\tilde{A}_k\end{bmatrix} \tag{3-21}$$

$$\tilde{A} = \ \mathrm{diag}\{\alpha_{12},\alpha_{23},\dots,\alpha_{ij},\dots,\alpha_{(n-1)n}\} \tag{3-22}$$

where $\tau_k(t)$, $k = 1, 2, \dots, m$ with $m \leq n(n-1)$ is defined as an element of the time-varying communication delay $\tau_{ij}(t)$.

Given the Leibniz-Newton formula

$$\tilde{\chi}\big(t - \tau_k(t)\big) = \tilde{\chi}(t) - \int_{-\tau_k(t)}^{0} \dot{\tilde{\chi}}(t+s)ds$$

$$= \tilde{\chi}(t) - \Gamma_l \int_{-\tau_k(t)}^{0} \tilde{\chi}\big(t + s - \tau_l(t+s)\big)ds \tag{3-23}$$

where $l = 0, 1, 2, \dots, m$, and after substitution we have

$$\dot{\tilde{\chi}}(t) = B\tilde{\chi}(t) - \Gamma_k\Gamma_l \int_{-\tau_k(t)}^{0} \tilde{\chi}\big(t + s - \tau_l(t+s)\big)ds \tag{3-24}$$

$$B = \Gamma_1 + \Gamma_k = \begin{bmatrix} 0_{N\times N} & I_{N\times N} \\ -\bar{A} & -\gamma\bar{A} \end{bmatrix} \tag{3-25}$$

where $\bar{A} = -\tilde{A} + \tilde{A}_k$.

If there exists a directed spanning tree in the platoon information flow topology $\mathcal{G}$, and the control gain γ suffices

$$\gamma_i > \max_{\mu_i \in \eta(\bar{A})} \left\{ \frac{|\mathrm{Im}\{\mu_i\}|}{\sqrt{|\mathrm{Re}\{\mu_i\}|}\cdot|\mu_i|} \right\} \tag{3-26}$$

where μ_i is the ith eigenvalue of $\bar{A}$, and $\eta(\bar{A})$ is the set of all eigenvalues of $\bar{A}$, then there exists a constant $\tau_0 > 0$ such that when $0 \leq \tau_k \leq \tau_0$ ($k = 1, 2, \dots, m$), the vehicles in the same string can achieve consensus as defined in equation eq. (3-6) and (3-7).

String stability is a desirable characteristic for vehicle strings to attenuate either distance error, velocity or acceleration along upstream direction, and therefore guarantee the safety of the longitudinal control algorithm. If we consider vehicle i as a following vehicle j ($= i - 1$), then we can write eq. (3-12) in the Laplace domain with time-variant communication delay set to a constant value τ as

$$A_i(s) = -\alpha_{i(i-1)}k_{i(i-1)} \cdot \left[\left(R_i(s) - R_{(i-1)}(s)e^{-\tau s} + \frac{l_{i-1}}{s} + V_i(s)e^{-\tau s}\frac{\left(t^g_{i(i-1)}+\tau\right)}{s}\right) + \gamma_i(V_i(s) - V_{i-1}(s)e^{-\tau s})\right], i \in \mathcal{H} \quad (3\text{-}27)$$

After some algebraic manipulations when assuming low frequency condition, the following equation can be derived

$$\frac{A_i(s)}{A_{i-1}(s)} = \frac{\alpha_{i(i-1)}k_{i(i-1)} \cdot \left[e^{-\tau s} + se^{-\tau s}\left(t^g_{ij}+\tau\right)b_i + s\gamma_i e^{-\tau s}\right]}{s^2 + \gamma_i s + 1} \quad (3\text{-}28)$$

where the control gains k and γ in eq. (3-12) can be chosen to guarantee $\frac{A_i(s)}{A_{i-1}(s)} \leq 1$ and hence satisfy the string stability for all frequencies of interest.

3.2.3.3 Feedforward Control: Online Parameter Modeling Algorithm

As can be seen in the proposed consensus algorithm (3-12), there are two control gains k and γ. Although most existing literature proved convergence and string stability of their proposed consensus algorithms, whether they can satisfy real-world constraints during the implementation is not known. Since most works only adopt one initial condition of vehicles in the simulation study, one single set of well-defined control gains worked well under that condition. However, given different initial states of CAVs, the consensus algorithm tends to behave differently in terms of overshoot, convergence rate and maximum changing rate. A set of control gains working well under one initial condition does not necessarily mean working well under all other initial conditions. Finding the ideal value of control gains in real time when the initial conditions of vehicles are dynamically changing remains an unsolved problem.

In this section, we propose the feedforward control-based parameter modeling algorithms, aiming to find the ideal values of control gains in terms of different initial states of the leading vehicle and the following vehicle by building up a lookup table. Given the second-order dynamics of vehicles as equation (3-1) and (3-2), the initial condition of the following vehicle i and the leading vehicle j are $\left(r_i(t_0), v_i(t_0), a_i(t_0)\right)$ and $\Big(r_j\left(t_0 - \tau_{ij}(t_0)\right), v_j\left(t_0 - \tau_{ij}(t_0)\right), a_j\left(t_0 - \tau_{ij}(t_0)\right)\Big)$, where t_0 denotes the initial time step when the consensus algorithm is applied. Since the proposed double-integrator consensus algorithm (3-12) does not consider the acceleration of the leading vehicle, and the positions of vehicles are only calculated as their difference, the initial condition of the proposed consensus algorithm can be simplified to $\left(\Delta r_{ij}(t_0), v_i(t_0), v_j\left(t_0 - \tau_{ij}(t_0)\right)\right)$, where $\Delta r_{ij}(t_0) = r_j\left(t_0 - \tau_{ij}(t_0)\right) - r_i(t_0)$. The reason we cannot simplify the initial speed of two vehicles into one term is that the term $v_i(t_0)$ is also calculated in the position consensus term (3-6), so the value of each vehicle's speed matters to the consensus algorithm.

Every time the consensus algorithm (3-12) starts to run on the vehicle i, the value of control gains k_{ij} and γ can be set in real time with the initial condition of vehicles $\left(\Delta r_{ij}(t_0), v_i(t_0), v_j\left(t_0 - \tau_{ij}(t_0)\right)\right)$. The method is to build a 3-dimension lookup table ahead of time covering certain possible values of the initial conditions within certain sets, and the ideal values of control gains can be picked from certain sets of candidates. The

three major constraints we consider when choose the ideal control gains are: safety, efficiency, and comfort.

Constraint 1: Safety Constraint. The overshoot of the algorithm influences the safety of the longitudinal motion controller. Since the consensus algorithm is proposed to control the longitudinal motion of vehicles, overshoot of the longitudinal position might cause rear-end collision between two vehicles. Therefore, the following constraint should be satisfied to guarantee the safety of the longitudinal motion controller

$$r_j\left(t-\tau_{ij}(t)\right)-r_i(t)>l_j, t\in[t_0, t_{consensus}] \tag{3-29}$$

where $t_{consensus}$ denotes the time step when consensus is reached. If the headway between the leading vehicle and the following vehicle is no greater than the length of the leading vehicle, a rear-end collision happens. Control gains should be set to guarantee no overshoot of the headway.

Constraint 2: Efficiency Constraint. The convergence rate of the consensus algorithm influences the efficiency of the longitudinal motion controller. If the convergence process takes a relatively long time, the traffic mobility and roadway capacity are highly affected during this process. Specifically, if the consensus algorithm is applied to control the longitudinal motion of ramp merging vehicles, slow convergence rate also introduces safety issue since consensus must be reached before two vehicles merge with each other. Control gains should be set with the least time to consensus $\min t_{consensus}$ (they need to firstly satisfy constraint). Consensus is reached when the following constraints are satisfied

$$\left|r_j\left(t_{consensus}-\tau_{ij}(t_{consensus})\right)-r_i(t_{consensus})\right|\leq\eta_r\cdot\left[l_j+v_i(t_{consensus})\cdot\left(t_{ij}^{g}(t_{consensus})+\tau_{ij}(t_{consensus})\right)\right] \quad (3\text{-}30)$$

$$\left|v_j\left(t_{consensus}-\tau_{ij}(t_{consensus})\right)-v_i(t_{consensus})\right|\leq\eta_v\cdot v_j\left(t_{consensus}-\tau_{ij}(t_{consensus})\right) \quad (3\text{-}31)$$

$$|a_i(t_{consensus})|\leq\delta_a \quad (3\text{-}32)$$

$$|jerk_i(t_{consensus})|\leq\delta_{jerk} \quad (3\text{-}33)$$

where $jerk_i$ is the derivative of vehicle i's acceleration/deceleration, η_r and η_v are proportional thresholds of the headway consensus and speed consensus, respectively, δ_a and δ_{jerk} are differential thresholds of acceleration and jerk consensus, respectively.

Constraint 3: Comfort Constraint. The maximum changing rate of the consensus algorithm is defined as the maximum absolute value of acceleration/deceleration and jerk. This factor influences the ride comfort of the proposed longitudinal motion controller. A high maximum changing rate does not necessarily mean a high convergence rate, since algorithm (3-12) can either converge to consensus within a relatively short time but in a smooth manner, or converges to consensus within a relatively long time but change extremely fast at first. In this constraint, the maximum absolute value of acceleration/deceleration and jerk matter, since passengers on the vehicle would expect a comfort ride with acceleration/deceleration and jerk limited to certain intervals. The maximum changing rate of the consensus algorithm is evaluated by defining a parameter Ω as

$$\Omega_i = \omega_1 \cdot \max_{t\in[t_0,t_{consensus}]}(|a_i^{\max}(t)|, |d_i^{\max}(t)|) + \omega_2 \cdot$$

$$\max_{t\in[t_0,t_{consensus}]}\left(|jerk_i^{\max}(t)|, \left|jerk_i^{\min}(t)\right|\right), t \in [t_0, t_{consensus}] \quad (3\text{-}34)$$

where $a_i^{\max}$, $d_i^{\max}$, $jerk_i^{\max}$ and $jerk_i^{\min}$ denote the maximum acceleration, maximum deceleration, maximum jerk and minimum jerk of vehicle i, respectively, and ω_1 and ω_2 are weighting parameters. Control gains should be set with the minimum value of Ω in this constraint.

Upon proposing above three constraints, we propose Algorithm 1 to build the 3-dimension lookup table for choosing the control gains. The set of Δr_{ij} contains $\zeta 1$ elements, the set of v_i contains $\zeta 2$ elements, and the set of v_j contains $\zeta 3$ elements, therefore, the size of this lookup table is $\zeta 1 \times \zeta 2 \times \zeta 3$. These three sets $\Pi_{\Delta r_{ij}}, \Pi_{v_i}$ and Π_{v_j} are sorted set with ascending order. Each combination of these three parameters maps to an ideal value of k and an ideal value of γ, out of their sets Π_γ and Π_k. Note that some specific initial condition cannot satisfy Constraint 1, as shown on line 04-05 of Algorithm 1. In that case, no value of control gains is generated, considering algorithm (3-12) being not functional under that particular condition.

Once the lookup table has been generated, the initial condition of vehicles does not always match certain values while implementing algorithm (3-12)

$$\left(\Delta r_{ij}(t_0), v_i(t_0), v_j\left(t_0 - \tau_{ij}(t_0)\right)\right) \neq \left(\Delta r_{ij_{\xi 1}}, v_{i_{\xi 2}}, v_{j_{\xi 3}}\right) \quad (3\text{-}35)$$

Therefore, in order to find the ideal values of control gains given different initial conditions, the Algorithm 2 is proposed. If the initial states of vehicles fall out of the ranges, invalid values are returned as shown on line 02-03, meaning no values of γ and k could be

selected by the online parameter modeling protocol. In such rare cases, algorithm (3-12) cannot guarantee all three constraints and will not be applied to control the vehicle. The default car-following algorithm and lane changing algorithm equipped on the vehicle (whatever they are) will be applied to control the longitudinal and lateral vehicle motion, respectively.

Algorithm 1: Build feedforward lookup table

Input: $\Pi_{\Delta r_{ij}} = \left\{\Delta r_{ij_1}, \Delta r_{ij_2}, \dots, \Delta r_{ij_{\zeta 1}}\right\}$, $\Pi_{v_i} = \{v_{i_1}, v_{i_2}, \dots, v_{i_{\zeta 2}}\}$, $\Pi_{v_j} = \{v_{j_1}, v_{j_2}, \dots, v_{j_{\zeta 3}}\}$, $\Pi_\gamma = \{v_{\gamma_1}, v_{\gamma_2}, \dots, v_{\gamma_{\zeta 4}}\}$, $\Pi_k = \{v_{k_1}, v_{k_2}, \dots, v_{k_{\zeta 5}}\}$, $\zeta 1 = \left|\Pi_{\Delta r_{ij}}\right|$, $\zeta 2 = \left|\Pi_{v_i}\right|$, $\zeta 3 = \left|\Pi_{v_j}\right|$

Output: 3-dimension table with size $\zeta 1 \times \zeta 2 \times \zeta 3$

for $\xi 1 \in [1, \zeta 1], \xi 2 \in [1, \zeta 2], \xi 3 \in [1, \zeta 3], \Delta r_{ij_{\xi 1}} \in \Pi_{\Delta r_{ij}}$, $v_{i_{\xi 2}} \in \Pi_{v_i}, v_{j_{\xi 3}} \in \Pi_{v_j}$ **do**
  run algorithm (10) with $\Delta r_{ij_{\xi 1}}$, $v_{i_{\xi 2}}$ and $v_{j_{\xi 3}}$
  find $\Lambda_\gamma \subseteq \Pi_\gamma, \Lambda_k \subseteq \Pi_k$ satisfy *Constraint 1*
  if $\Lambda_\gamma = \emptyset \,||\, \Lambda_k = \emptyset$ **then**
    $\gamma_{(\xi 1, \xi 2, \xi 3)} = NaN,\ k_{(\xi 1, \xi 2, \xi 3)} = NaN$
  else
    find $\Psi_\gamma \subseteq \Lambda_\gamma, \Psi_k \subseteq \Lambda_k$ satisfy *Constraint 2*
    if $\left|\Psi_\gamma\right| == |\Psi_k| == 1$ **then**
      $\gamma_{(\xi 1, \xi 2, \xi 3)} \in \Psi_\gamma, k_{(\xi 1, \xi 2, \xi 3)} \in \Psi_k$
    else
      find $\Phi_\gamma \subseteq \Psi_\gamma, \Phi_k \subseteq \Phi_k$ satisfy *Constraint 3*
      if $\left|\Phi_\gamma\right| == |\Phi_k| == 1$ **then**
        $\gamma_{(\xi 1, \xi 2, \xi 3)} \in \Phi_\gamma, k_{(\xi 1, \xi 2, \xi 3)} \in \Phi_k$
      else
        $\gamma_{(\xi 1, \xi 2, \xi 3)} = \min_{\gamma \in \Phi_\gamma} \Phi_\gamma, k_{(\xi 1, \xi 2, \xi 3)} = \min_{k \in \Phi_k} \Phi_k$
      end if
    end if
  end if
end for

Algorithm 2: Search lookup table in real time

Input: $\left(\Delta r_{ij}(t_0), v_i(t_0), v_j\left(t_0 - \tau_{ij}(t_0)\right)\right)$, $(\zeta 1 \times \zeta 2 \times \zeta 3)$ size of lookup table

Output: values of control gains k and γ

for $\Delta r_{ij}(t_0), v_i(t_0), v_j\left(t_0 - \tau_{ij}(t_0)\right)$ **do**

  if $\Delta r_{ij}(t_0) < \Delta r_{ij_1} || \Delta r_{ij}(t_0) > \Delta r_{ij_{\zeta 1}} || v_i(t_0) < v_{i_1} || v_i(t_0) > v_{i_{\zeta 2}} || v_j\left(t_0 - \tau_{ij}(t_0)\right) < v_{j_1} || v_j\left(t_0 - \tau_{ij}(t_0)\right) > v_{j_{\zeta 3}}$ **then**

    return $\gamma = NaN,\ k = NaN$

  else

    find $\left(\Delta r_{ij_{\xi 1}} \middle| \min \left|\Delta r_{ij}(t_0) - \Delta r_{ij_{\xi 1}}\right|\right)$,
    $\left(v_{i_{\xi 2}} \middle| \min \left|v_i(t_0) - v_{i_{\xi 2}}\right|\right)$,
    $\left(v_{j_{\xi 3}} \middle| \min \left|v_j\left(t_0 - \tau_{ij}(t_0)\right) - v_{j_{\xi 3}}\right|\right)$

    return $\gamma = \gamma(\Delta r_{ij_{\xi 1}}, v_{i_{\xi 2}}, v_{j_{\xi 3}}), k = k\left(\Delta r_{ij_{\xi 1}}, v_{i_{\xi 2}}, v_{j_{\xi 3}}\right)$

  end if

end for

3.2.3.4 Simulation Results

In this section, we conduct numerical simulations to verify the effectiveness of the proposed longitudinal motion controller for CAV in car-following scenarios, which are based on the following four scenarios with different initial conditions of vehicles. These four scenarios stand for different typical initial conditions of vehicles, where $\Delta r_{ij}(t_0)$ can be either positive or negative, and $v_i(t_0)$ can be either larger or smaller than $v_j\left(t_0 - \tau_{ij}(t_0)\right)$. As shown in

Table **II**, the initial headway between the leading vehicle *j* and the following vehicle i is a negative value in scenario 3 and 4. Since the proposed longitudinal motion controller is not only for car-following cases on the same lane (e.g., platooning), where the following vehicle is physically behind the leading vehicle, it can also be applied to ramp merging or intersection crossing cases, where the leading vehicle can be projected on the same lane as the following vehicle. Therefore, the initial distance headway between them can be negative.

Table II Settings of Simulation Scenarios.

	$\Delta r_{ij}(t_0)$ (m)	$v_i(t_0)$ (m/s)	$v_j\left(t_0 - \tau_{ij}(t_0)\right)$ (m/s)
Scenario 1	50	28	14
Scenario 2	20	16	22
Scenario 3	-30	18	10
Scenario 4	-80	4	21

The parameters of the lookup table are set as: $\Pi_{\Delta r_{ij}} = \{-100, -90, \ldots, 100\}$(m), $\Pi_{v_i} = \{2,4, \ldots, 34\}$(m/s), $\Pi_{v_j} = \{2,4, \ldots, 34\}$ (m/s), $\Pi_{\gamma} = \{1,2, \ldots, 10\}$, $k = 0.1$, $\zeta 1 = 21$, $\zeta 2 = 17$, $\zeta 3 = 17$. The threshold parameters in Constraint 3 are set as $\eta_r = \eta_v = 0.05, \delta_a = 0.001, \delta_{jerk} = 0.005$. For the sake of simplicity while simulating algorithm (9), we assume the communication delay $\tau_{ij}(t)$ is a constant value of 60 ms [103]. The length of a vehicle is set as $l_j = 5$ m, and the desired time gap $t_{ij}^{g}(t)$ is set as a constant value of 0.7 s. We compare the proposed algorithm with respect to the widely cited CACC algorithm proposed by van Arem *et al.* [30], and also with the author's algorithm (3-12).

The speed trajectories of the leading vehicle and the following vehicle under different scenarios are shown in Figure 3-3, where each scenario has three different speed trajectories of the following vehicle's speed $v_i(t)$. The simulation results in terms of efficiency and comfort are shown in Table III. Since all three algorithms satisfy the safety constraint in these scenarios, the headway overshoot results are not shown here. Compared to the consensus algorithm the authors developed previously, the proposed algorithm in this dissertation intensively decreases convergence time and maximum jerk. When compared to the consensus algorithm proposed by van Arem et al., the convergence time is also reduced in all four scenarios. Although the proposed algorithm introduces a

relatively higher maximum jerk in scenario 2 and 4, they are still in the comfort zone of a human passenger, which is [-10 m/s3, 10 m/s3] [122].

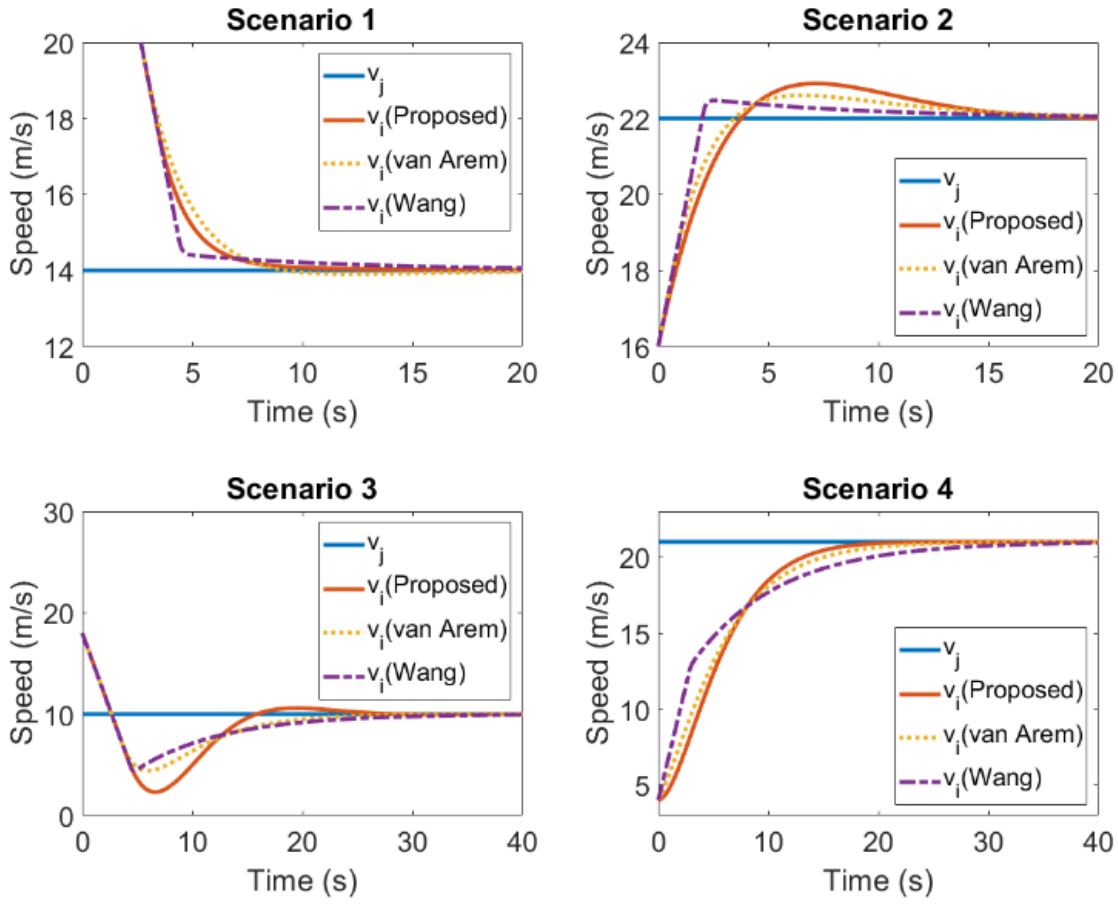

Figure 3-3. Speed trajectory of vehicles under different algorithms

Table III Simulation Results.

	Convergence time (s)				Maximum jerk (m/s³)			
Scenario	1	2	3	4	1	2	3	4
Wang	35.9	35.0	56.5	57.6	21.2	20.7	25.7	13.4
van Arem	29.3	32.1	41.8	40.1	1.5	1.6	2.3	0.7
Proposed	24.9	22.9	32.1	28.3	2.3	0.8	1.6	1.6

It should be noted that Constraint 2 has a higher priority than Constraint 3 in the proposed Algorithm 2, since the efficiency of the algorithm also relates to the ride safety

to some extent. For example, in scenario 2 and 4, the initial longitudinal position of the following vehicle is in front of the leading vehicle. If these two vehicles cannot converge to position consensus (i.e., the following vehicle is behind the leading vehicle) before they enter the conflict zone of a ramp merging or intersection crossing scenario, potential crash might occur. Therefore, the proposed algorithm outperforms the other two algorithms due to its reduction of convergence time in all these four scenarios.

3.2.4 CACC System for Heterogeneous Vehicles

3.2.4.1 Introduction

The development of CAV can help better manage traffic, thus improving traffic safety, mobility, and reliability without the cost of infrastructure buildout. One of the more promising CAV applications is Cooperative Adaptive Cruise Control (CACC), which extends Adaptive Cruise Control (ACC) with CAV technology (e.g., mainly via V2V communication) [91]. By sharing information among vehicles, a CACC system allows vehicles to form platoons and be driven at harmonized speeds with constant time headways between vehicles. The main advantages of a CACC system are: a) connected and automated driving is safer than human driving by minimizing driver distractions; b) roadway capacity is increased due to the reduction of inter-vehicle time gaps without compromising safety; c) fuel consumption and pollutant emissions are reduced due to the reductions of both unnecessary acceleration maneuvers and aerodynamic drag on the vehicles in the platoon [100].

The core of a CACC system is the vehicle-following control model, which depends on the vehicle information flow topology. The topology determines how all CAVs in a CACC system communicate with others, and it has been well studied by researchers. Zheng et al. [101] proposed some typical types of information flow topologies, including predecessor following, predecessor-leader following, and bidirectional. In our research, each vehicle in the CACC system only receives information from the predecessor (if it exists), which is exactly the predecessor following type. The vehicle-following controller efficiently describes the vehicle dynamics and cooperative maneuvers residing in the system. The performance and robustness of a CACC consensus algorithm were discussed in [102], where packet loss, network failures and beaconing frequencies were all taken into consideration when the simulation framework is built with the CACC controller developed by [103]. Bernardo et al. [104] designed a distributed control protocol to solve the platooning problem, which depends on a local action of the vehicle itself and a cooperative action received from the leader and neighboring vehicles. Lu et al. [105] used a nonlinear model to describe the vehicle longitudinal dynamics, where the engine power, gravity, road and tire resistance, and aerodynamics drag are all considered. However, since the complexity of such nonlinear models are problematic for system analysis, a linearized model is typically used for field deployment, such as the one in [106]. Amoozadeh et al. [107] developed a platoon management protocol for CACC vehicles, including CACC longitudinal control logic, platoon merge and split maneuvers, etc. In terms of inter-vehicle distance in motion (at relatively high speed), the existing vehicle-following models can be divided into two categories: one that regulates the spatial gap, where one vehicle follows

its predecessor with a fixed inter-vehicle distance [108]. The other is based on time gap or velocity dependent distance, where the inter-vehicle distance may vary with vehicle velocity and vehicle length by keeping a constant time headway. Our approach falls into the second category.

Stability is a basic requirement to ensure the safety of a CACC system. The control system should be capable to deal with various disturbances and uncertainties. Laumônier et al. [109] proposed a reinforcement learning approach to design the CACC system, where the system is modeled as a Markov Decision Process incorporated together with stochastic game theory. They showed that the system was capable of damping small disturbances throughout the platoon. The uncertainties in communication network and sensor information were modeled by a Gaussian distribution in [110], which was applied to calculate the minimal time headway for safety reasons. Qin et al. [111] studied the effects of stochastic delays on the dynamics of connected vehicles by analyzing the mean dynamics. Plant and string stability conditions were both derived, and the results showed stability domains shrink along with the increases of the packet drop ratio or the sampling time. In [112] propagation of motion signals was attenuated by adjusting the controller parameters in the system, which guaranteed the so-called string stability of the platoon. Since the inherent communication time delay and vehicle actuator delay significantly limit the minimum inter-vehicle distance in view of string stability requirements, Xing et al. [113] carried out Padé approximations of the vehicle actuator delay to arrive at a finite-dimensional model. It was shown in [114] that the standard constant time-gap spacing policy can guarantee string stability of the platoon as long as a sufficient large time gap is

maintained. In this dissertation, we also adopted the time-gap spacing policy, and selected time gap large enough to ensure the platoon's string stability. A simulation study of platoon restoration after disturbances is demonstrated to further prove the string stability of our system.

Communication plays a crucial role in the formation of a CACC system. The United States Department of Transportation (USDOT) developed a Connected Vehicle Reference Implementation Architecture (CVRIA) to provide the communication framework for different applications, including V2V and I2V communications [115]. IEEE 802.11p-based Dedicated Short-Range Communication (DSRC) has been developed by the automotive industry for use in V2V and I2V communication, considered as a promising wireless technology to improve both transportation safety and efficiency. Bai et al. [116] used a large set of empirical measurement data taken in various realistic driving environment to characterize communication properties of DSRC. Since the increase of CAVs in a certain coverage area may lead to a shortage of communication bandwidth, a distributed methodology is more advantageous for vehicular communication. In our study, the V2V communication is only conducted between predecessor and follower, making the proposed system more distributed.

Essentially, the proposed system is different from a conventional Adaptive Cruise Control (ACC) system for the following reasons: 1) In the proposed system, although some forward ranging sensing techniques such as camera, radar and LIDAR (Light Detection and Ranging) might be needed as supplementary methods, the core technique for CAVs to form platoon is V2V communication. CAVs send their absolute position and instantaneous

velocity information measured by equipped sensors (e.g., high-precision GPS, inertial measurement unit, and on-board diagnostic system) to their followers by V2V communication. However, for a conventional ACC system, V2V communication is not enabled, where vehicles need to use their forward ranging sensing equipment to obtain predecessors' information. 2) A conventional ACC system can only implement the function of vehicle following, however, the proposed CACC system allows individual vehicle to merge into the platoon by using V2V communication. "Ghost" vehicles are created as predecessors for following vehicles to follow, however, since they are virtual and only for V2V communication, it is impossible for forward ranging sensing techniques to sense them. 3) The measurement delay of forward ranging sensing techniques in a conventional ACC system is apparently different from the V2V communication delay of DSRC in the proposed system, which leads to different system behaviors in different scenarios, especially the one we talk about in the part 3.2 Platoon Restoration from Disturbances.

Despite the advantages of consensus-based platooning approach for the CACC system, several issues are still needed to be addressed to improve the reliability and practicality:

a) The primary V2V communication method being used nowadays is DSRC, which normally has a 300-meter transmission range [116]. As the transmission distance increases, the safety message reception probability dramatically decreases, and the relative signal strength index (RSSI) from DSRC antenna also decreases [117], [118]. However, many existing CACC systems such as [119] adopted predecessor-leader following information

flow topology, which required the leader of a platoon to communicate with all the vehicles in the broadcast mode. Therefore, when a platoon expands to a bigger size, the V2V communication between the leader with the last vehicle may introduce lower RSSI, or be impaired by obstructions along the platoon. In this dissertation, we adopt predecessor following information flow topology (i.e., "distributed"), where each vehicle in the platoon only communicates with its following vehicle to reach consensus of the whole platoon. Therefore, the platoon size is not limited by the DSRC transmission range, and the V2V communication has a higher safety message reception probability and a higher RSSI than in the predecessor-leader following topology.

b) Most existing CACC-related research has only considered vehicles in the system as homogenous point mass models. However, in reality, vehicles should be heterogeneous with different lengths and braking performances. Therefore, we consider the vehicle length together with the position of GPS antenna on vehicle in this dissertation. Moreover, according to different braking performances, we assign different braking factors to different types of vehicles in our system, allowing the inter-vehicle distances to be weighted based on these factors.

c) While the information flow topology and algorithm have been well studied, not many protocols have been developed to apply the theory to real-world transportation systems, especially for different traffic scenarios. In this dissertation, we design protocols for the normal platoon formation scenario, and merging and splitting scenario. Sensitivity analysis is also conducted to study the practical issues of the proposed CACC system, including the convergence rate of a platoon, the driving comfort for human passengers, and

the driving safety of the whole system. By optimizing the damping gain value of our algorithm, the proposed system is supposed to be efficient, comfortable, and safe.

3.2.4.2 Normal Platoon Formation Protocol

This protocol is designed for vehicles to form a platoon. For vehicle i in our CACC system, it needs to check whether there is a predecessor in a certain distance r after the platoon formation mode is activated.

a) If yes, then vehicle i will communicate with its predecessor and equation (3-12) will be applied, which enables vehicle i to be a following vehicle;

b) If no, then vehicle i may become a leading vehicle of a platoon (where $i = 1$) and cruise at a constant velocity. The driver can also take over the control to drive however he/she wants, but the vehicle may still potentially act as a leading vehicle of the platoon.

After the above procedure, vehicle i is in the distributed consensus-based CACC system, whether it plays the role of a following vehicle or a leading vehicle. However, the "following" and "leading" role for vehicle i may switch under the following conditions:

a) For a following vehicle i, if all of its predecessors move out of the distance r ahead of vehicle i, then vehicle i changes from a following vehicle to a leading vehicle, where $i = 1$;

b) For a leading vehicle i (i.e., $i = 1$), if one or more vehicles move into the distance r ahead of vehicle i, then vehicle i changes from a leading vehicle to a following vehicle, where $i = 2, \ldots, n$.

Figure 3-4 shows the flowchart of this protocol for the distributed consensus-based CACC system.

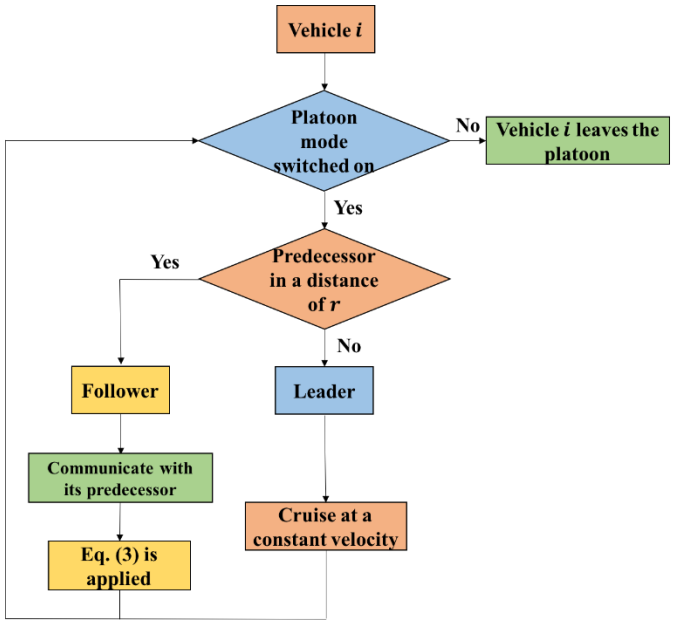

Figure 3-4. Normal platoon formation protocol

3.2.4.3 Merging and Splitting Maneuvers Protocol

Normal platoon formation protocol addresses the longitudinal maneuvers, while merging and splitting maneuvers protocol is aimed at handling the lateral maneuvers (i.e., lane change). It is introduced in [120] that there are four different cases for the lane change within the platoon maneuvers: 1) free-agent-to-free-agent lane change, 2) free-agent-to-platoon lane change, 3) platoon-to-free-agent lane change, and 4) platoon-to-platoon lane change. In this dissertation, we focus on the second and third cases. Since this part is about applying the proposed algorithm Eq. (3-12) to lane change scenarios, which is focused on gap creation and gap closure maneuvers implemented by V2V communication, the specific lane change behavior is considered as a manual driving behavior.

For the case where vehicle i (as a free agent) tries to merge into a platoon on the adjacent lane, after the merging mode is activated, vehicle i will communicate with the platoon leader and decide which position it will be in the platoon, as shown in Figure 3-5

(a). If it decides to be the jth vehicle of the platoon after merging maneuvers, then a "ghost" vehicle with respect to vehicle $j-1$ in the platoon will be created on the lane vehicle i is on, as shown in Figure 3-5 (b). This "ghost" vehicle has all the same parameters but the lateral position as vehicle $j-1$. Then, vehicle i will automatically adjust its absolute position and velocity with the "ghost" vehicle by Eq. (3-12). After that, vehicle i sends a merging signal to vehicle $j+1$ in the platoon, as shown in Figure 3-5 (c). Upon receiving the merging signal, a "ghost" vehicle with respect to vehicle i is created in front of vehicle $j+1$, and vehicle $j+1$ starts to adjust its absolute position and velocity to create a gap for vehicle i by Eq. (3-12), as shown in Figure 3-5 (d). After the gap is fully created, vehicle $j+1$ sends a confirmation signal to vehicle i, and vehicle i merges into the platoon, as shown in Figure 3-5 (e).

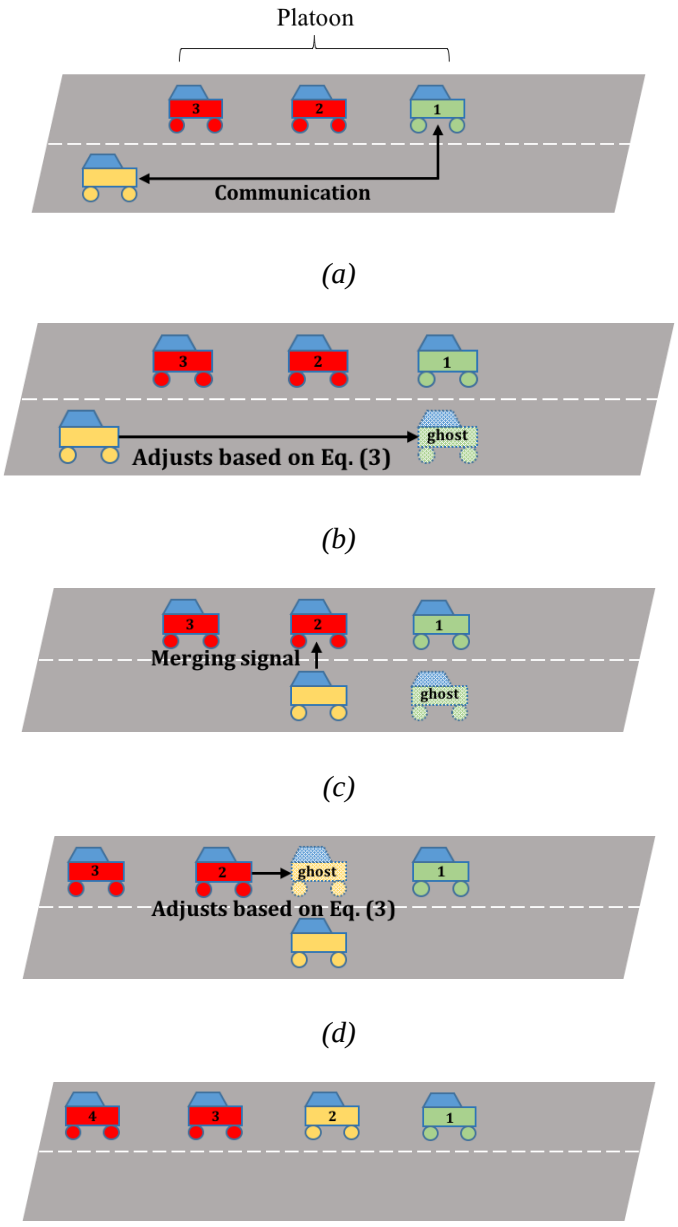

Figure 3-5 Merging maneuvers protocol (assuming merging into the 2nd position)

The case where vehicle *j* (in the platoon) tries to split from the platoon is easier. It is studied in [121] that there are two strategies for splitting maneuvers, or so-called CACC string dissolution. The most efficient action is for the departing driver to do a simple lane

change in the direction of the off-ramp. The other strategy is for the departing vehicle to deactivate the CACC function by tapping on the brakes before changing lanes, creating a split in the CACC string, and becoming the manually driver leader of the platoon until it moves out of the lane. In our system, we adopt the first strategy. After the splitting mode is activated, the driver can take over the lateral control of the vehicle and perform the lane change without adjusting the velocity longitudinally. After vehicle *j* completes the lane change, vehicle *j*+1 will be informed that its predecessor changes from vehicle j to vehicle $j-1$, and therefore adjusts its velocity to close the gap. A new platoon is formed, where vehicle $j+1$ becomes vehicle j, and vehicle $j+2$ becomes vehicle $j+1$, and so on.

3.2.4.4 Simulation Study and Results

In the first scenario, we assume that there are four CAVs of different types (i.e., 2 sedans, 1 SUV and 1 truck) driving at randomly varied velocities on the same lane of a highway. At a certain time ($t=0$), they all switch on the platoon mode. From then on, they adjust their absolute positions and velocities based on Eq. (3-12) as well as normal platoon formation protocol to reach consensus and form a platoon. The vehicle parameters of this distributed consensus-based CACC system are listed in Table IV.

Table IV Comparison Results between Cooperative Merging and Baseline.

Parameters	Vehicle 1	Vehicle 2	Vehicle 3	Vehicle 4
GPS antenna to front bumper l_{if}	3 m	3 m	3 m	6 m
GPS antenna to rear bumper l_{ir}	2 m	2 m	2 m	4 m
braking factor b_i	1	1	1.1	1.6
initial velocity $\dot{x}_{i0}$	30 m/s	33 m/s	36 m/s	39 m/s
desired velocity $\dot{x}_i$	30 m/s	30 m/s	30 m/s	30 m/s
initial time gap t_{ij0}^g	0.91 s	1.11 s	1.67 s	
initial weighted inter-vehicle distance d_{ij0}	30 m	40 m	65 m	
desired time gap t_{ij}^g	0.43 s	0.48 s	0.69 s	
desired time headway t_{ij}^h	0.6 s	0.64 s	0.86 s	
desired weighted inter-vehicle distance d_{ij}	13 m	14.3 m	20.8 m	
desired unweighted inter-vehicle distance d_{ij}/b_i	13 m	13 m	13 m	

As can be seen from Table IV, we assume vehicle 1 and 2 are sedans with vehicle lengths 5 m and braking factors 1, vehicle 3 is a SUV with a vehicle length 5 m and a braking factor 1.1, and vehicle 4 is a truck with a vehicle length 10 m and a braking factor 1.6. We further assume the GPS antenna is located at a point of vehicle satisfying $2l_{if} = 3l_{ir}$. The weighted inter-vehicle distances are used instead of time gaps to measure the consensus of vehicles' absolute positions in a more intuitive manner.

As a key parameter, the damping gain γ in Eq. (3-12) will affect the convergence rate of absolute positions and velocities of all the vehicles in the platoon. In this dissertation, $\gamma = 7$ is set to all three simulation scenarios. More detailed analysis on how the value of γ may affect the system performance (e.g., driving safety, driving comfort) is conducted in the next section. By implementing our distributed consensus-based strategy, the simulation results of our CACC system are shown in Figure 3-6 (a)-(c).

Figure 3-6 (a) shows that after the platoon mode is activated at $t = 0$, all of the three unweighted inter-vehicle distance converge to 13 m at around 35 seconds. This unweighted inter-vehicle distance can be considered as a "virtual" target value we set for

the system to achieve, not the “real” inter-vehicle distance. Figure 3-6 (b) shows the results for weighted inter-vehicle distance. By introducing the braking factor, the steady state of weighted inter-vehicle distance varies with different vehicle pairs. The weighted inter-vehicle distance indicates the “real” value for inter-vehicle distance in our CACC system. In this case, at the steady state of the system, vehicle 1 and vehicle 2 have a 13 m (0.43 s) gap, vehicle 2 and vehicle 3 have a 14.3 m (0.48 s) gap, and vehicle 3 and vehicle 4 have a 20.8 m (0.69 s) gap. It is shown in Figure 3-6 (c) that velocities of the four vehicles converge within around 35 seconds after the platoon mode is activated. After running the distributed consensus algorithms, they all converge to 30 m/s, which is the constant velocity of the leading vehicle, and also the desired velocity of this platoon.

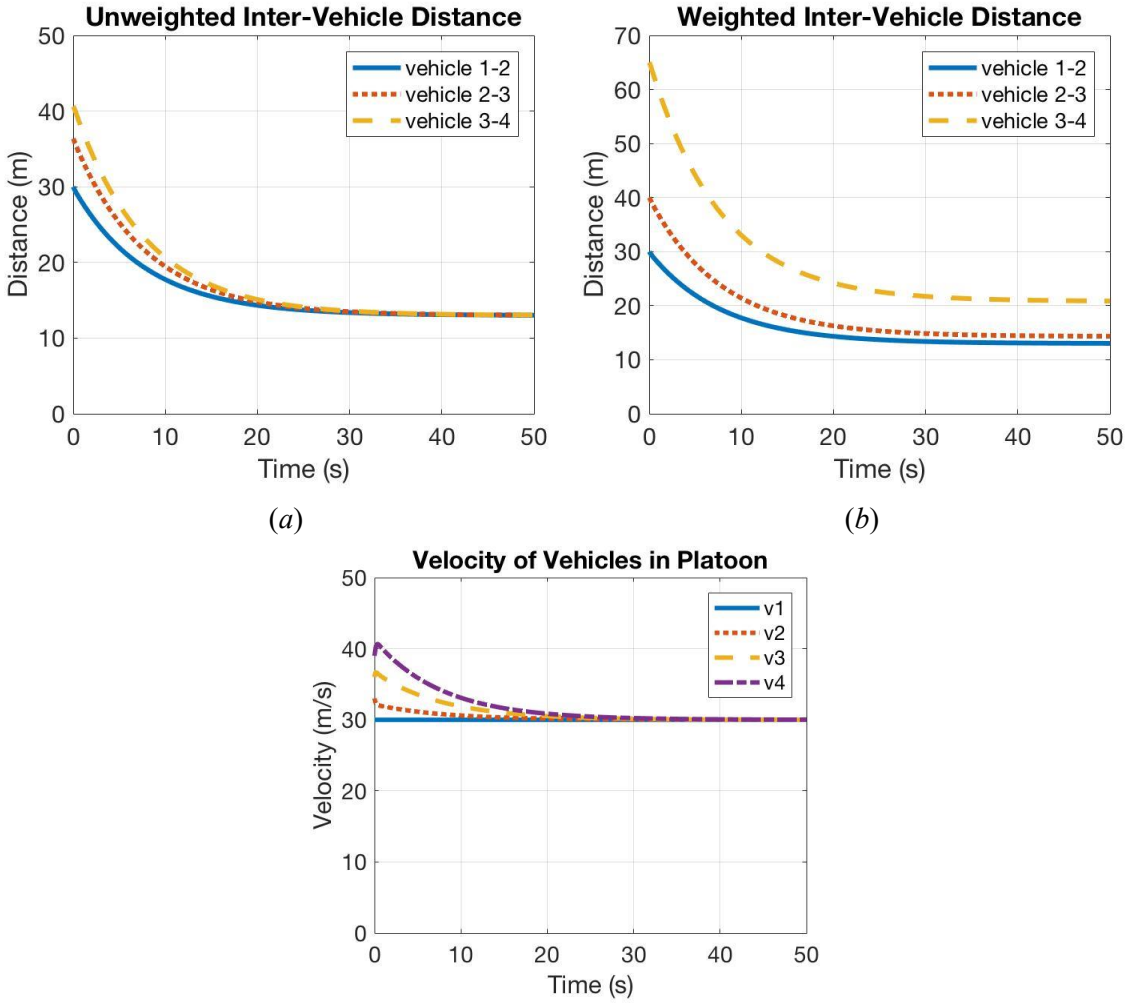

Figure 3-6 Simulation results of normal platoon formation

In the second scenario, a simulation test is conducted to demonstrate the string stability of our CACC system, where the distributed consensus algorithm has the capability to attenuate the impact of sudden disturbances. In the platoon mode of our distributed consensus-based CACC system, if one vehicle (e.g., leading vehicle) suddenly brakes and reduces its velocity due to emergency, then the following vehicles will decelerate accordingly to maintain certain weighted inter-vehicle distances.

For example, we assume all the parameters remain the same as the first scenario. At time $t = 45$ s, suppose the leading vehicle suddenly brakes due to a flat tire, and its velocity decreases from 30 m/s to 15 m/s. To simplify the scenario, we assume the brake happens only in a sudden ($\Delta t \approx 0$), i.e., a step change in leading vehicle's velocity.

The simulation results of sudden brake are shown in Figure 3-7 (a)-(c). Figure 3-7 (a) shows that the unweighted inter-vehicle distance between vehicle 1 and vehicle 2 suffers an approximately 4 m decrease at time $t = 45$ s. However, the unweighted inter-vehicle distance between vehicle 2 and vehicle 3 only suffers an approximately 0.7 m decrease, and the one between vehicle 3 and vehicle 4 is further smaller. This result implies that the sudden disturbance on the inter-vehicle distance is attenuated along the rest of the platoon.

The velocity of vehicles in platoon is shown in Figure 3-7 (c). The sudden brake originates from vehicle 1, and vehicle 2 tends to avoid the collision with vehicle 1 with a hard-braking event. The braking event of vehicle 3 is not as hard as vehicle 2 (the slope is smaller), and the braking of vehicle 4 is further smoother than vehicle 3. The smoother their braking is, the smaller the absolute value of their acceleration will be. After the braking event, the velocities of the three following vehicles slowly restore to the desired velocity. This result implies that the sudden disturbance on the vehicle acceleration is attenuated along the rest of the platoon.

Figure 3-7 (b) presents the results for weighted inter-vehicle distance, i.e., the unweighted inter-vehicle distance multiplies by the braking factor of different vehicles. Overall, the simulation results of this scenario indicate that our distributed consensus-based

CACC system is capable of attenuating sudden disturbances and restoring to normal conditions, i.e., this system is string stable.

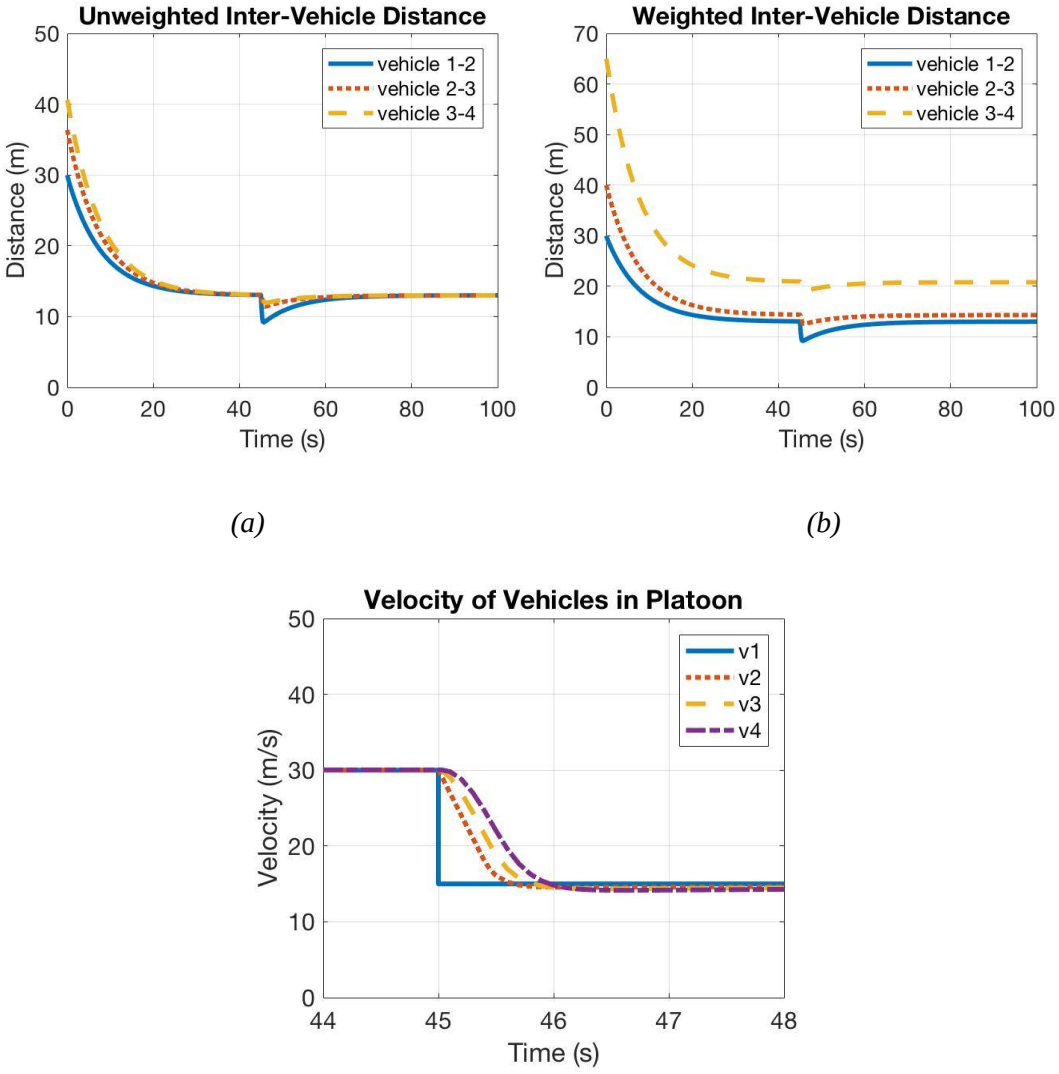

(a) *(b)*

(c)

Figure 3-7 Simulation results of platoon restoration from disturbances

In the third scenario, we show the effects when the proposed distributed consensus algorithm is performed together with the merging and splitting maneuvers protocol as presented in the previous subsection.

For merging maneuvers, assume at time $t = 0$, a three-vehicle platoon (same parameters as vehicle 1, 3 and 4 in the first scenario) is operating at the steady state (i.e., cruising at the velocity of 30 m/s). Another individual vehicle (same parameters as vehicle 2 in the first scenario) traveling at the velocity of 35 m/s on the adjacent lane plans to merge into the platoon, and the simulation result is shown in Figure 3-8 (a).

It can be observed from Figure 3-8 (a) that the individual vehicle switches on the merging mode at time $t = 5$ s. From then on, a "ghost" vehicle with respect to the first vehicle in the platoon is created, and the individual vehicle adjusts its velocity from 35 m/s to 30 m/s by Eq. (3-12). After that, the individual vehicle sends a merging signal to the second vehicle of the platoon. Then a "ghost" vehicle with respect to the merging vehicle is created in front of the second vehicle of the platoon. Based on Eq. (3-12), both the second and third vehicle of the platoon decelerate to create a gap, and the second vehicle sends a signal to the individual vehicle upon the completion of gap opening. Finally, the individual vehicle merges into the platoon, and the velocities of the other two following vehicles restore to consensus in around 8 s.

For splitting maneuvers, assume at time $t = 0$, a four-vehicle platoon (same parameters as vehicle 1, 2, 3 and 4 in the first scenario) is cruising at the velocity of 30 m/s. The second vehicle will split from the platoon, and the simulation result is shown in Figure 3-8 (b). The second vehicle of the platoon switches off the platoon mode and drives away (constantly accelerates from 30 m/s to 35 m/s) from platoon at time $t = 10$ s. After the second vehicle completes its lane change, the third vehicle confirms that its predecessor has changed to the first vehicle of the platoon. Then it adjusts its velocity based on Eq.

(3-12) to close the gap. The fourth vehicle accordingly adjusts its velocity to follow the movement of its predecessor. Therefore, the simulation results of the third scenario show that our distributed consensus-based CACC system is capable of carrying out merging and splitting maneuvers.

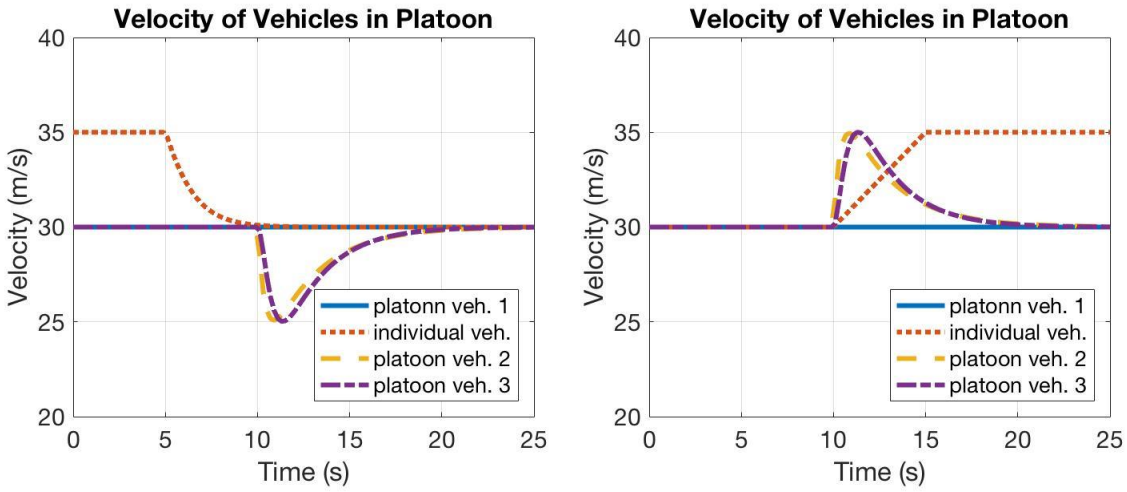

(*a*) (*b*)

Figure 3-8 Simulation results of merging and splitting maneuvers

3.2.4.5 Sensitivity Analysis

Firstly, we analyze the effect of γ on driving comfort. The change of vehicle velocity is related to vehicle acceleration and jerk, and it is studied in [122], [123] that a limitation of ± 2.5 m/s^2 and ± 10 m/s^3 for acceleration and jerk separately will be comfortable for human passengers. We measure the values of $arg\,max|a|$ and $arg\,max|jerk|$ through normal platoon formation process, and check under which value of γ will -2.5 m/$s^2 < a < 2.5$ m/s^2 and -10 m/$s^3 < jerk < 10$ m/s^3 be satisfied. If a and $jerk$ are both in the range, then driving is comfortable for human passengers.

Parameters of this analysis are set in Table V, which are exactly the same as the first two vehicles in aforementioned simulation scenarios. The result of the sensitivity analysis on driving comfort is shown in Figure 3-9. As can be seen from it, when $7 \leq \gamma \leq 7.8$, both the acceleration and the jerk are in the "comfort" ranges. Since a faster convergence rate is desired, a value of 7 can be chosen for γ.

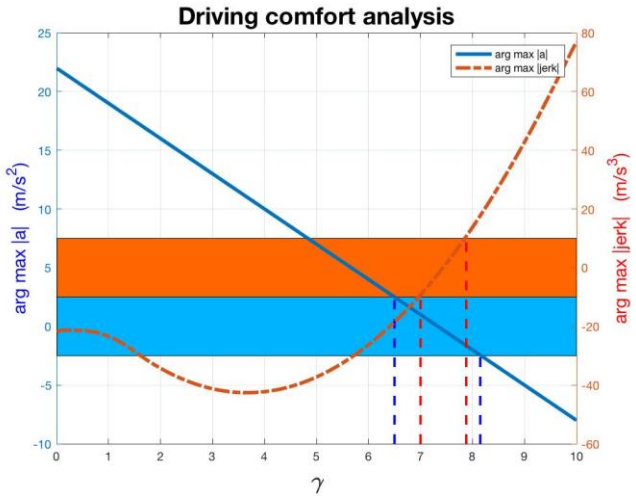

Figure 3-9 Driving comfort analysis

Table V Comparison Results between Cooperative Merging and Baseline.

Parameters	Vehicle 1	Vehicle 2
GPS antenna to front bumper l_{if}	3 m	3 m
GPS antenna to rear bumper l_{ir}	2 m	2 m
braking factor b_i	1	1
initial velocity $\dot{x}_{i0}$	30 m/s	33 m/s
desired velocity $\dot{x}_i$	30 m/s	30 m/s
initial weighted inter-vehicle distance d_{ij0}	30 m	
desired weighted inter-vehicle distance d_{ij}	13 m	

Secondly, we analyze the effect of γ on driving safety. We measure the value of minimum weighted inter-vehicle distance through normal platoon formation process, and

check whether it goes to negative. If it does, then a collision between the leading vehicle and the following vehicle occurs.

We first analyze how the changes of γ and the initial weighted inter-vehicle distance d_{ij0} will affect the minimum weighted inter-vehicle distance $\min(d_{ij})$. All parameters but the initial weighted inter-vehicle distance (d_{ij0} is a variable in this case) of this sensitivity analysis are set the same as in Table V. The result is shown in Figure 3-10.

As shown in the result, the areas indicating $\min(d_{ij}) < 0$ appear mostly when $d_{ij0} > 25$ m and meanwhile $\gamma < 1$. This is because when the absolute position difference is large and the damping gain of velocity consensus term is small, the system tends to put more weight on the absolute position consensus term, resulting in a large overshoot of the absolute position consensus. When the initial weighted inter-vehicle distance is sufficiently large ($d_{ij0} > 0.18$ m), we can avoid this by choosing the value of γ no smaller than 2. Also, there is a linear area indicating $\min(d_{ij}) < 0$ where d_{ij0} is small. A hypothesis is that at time $t = 0$, the following vehicle has a higher velocity and the weighted inter-vehicle distance is rather small, so there exists no γ to ensure the following vehicle to avoid the collision with the leading vehicle. If we fix the value of γ, it is found that the closer d_{ij0} approaches to d_{ij} (13 m), the larger $\min(d_{ij})$ is.

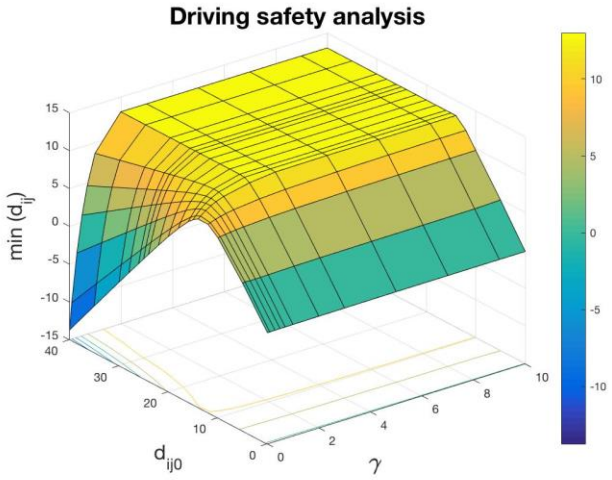

Figure 3-10 Driving safety regarding initial weighted inter-vehicle distance

We also analyze how the changes of γ and the initial velocity difference $\delta\dot{x}_{ij0}$ will affect the minimum weighted inter-vehicle distance $\min(d_{ij})$. All parameters but the initial velocity (the difference of $\dot{x}_{i0}$ and $\dot{x}_{j0}$ is a variable in this case) of this sensitivity analysis are set the same as in Table V. The result is shown in Figure 3-11.

As shown in the figures, collision only happens in the areas where γ is small. If we fix the value of γ, it is found that the closer $\delta\dot{x}_{ij0}$ approaches to 0 m/s, the larger $\min(d_{ij})$ is. A potential explanation is that although the weighted inter-vehicle distance will change regardless of the initial value, the change will be minimized when the initial velocity of the two vehicles are the same. When $\gamma \geq 2$, no matter how much the initial velocity difference is, the minimum weighted inter-vehicle distance will always be 13 m.

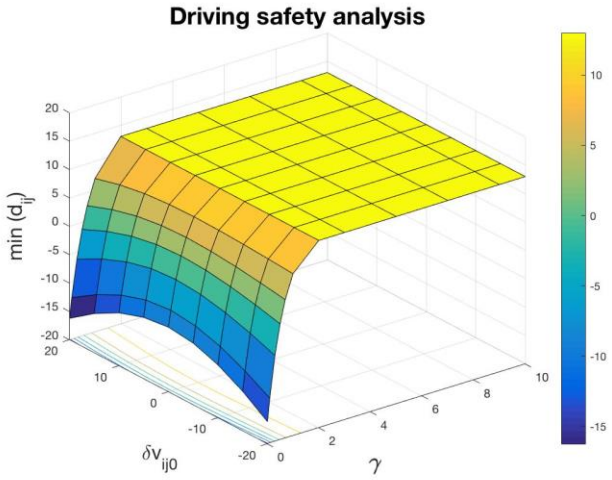

Figure 3-11 Driving safety regarding initial velocity difference

By analyzing the results of driving safety analysis, we know the preliminary value of γ ($\gamma = 7$) chosen for our CACC system is safe without any collision between two vehicles. When the parameter setting changes, the procedures of convergence rate analysis, driving comfort analysis and driving safety analysis can be applied to choose the best value of γ, which ensures the platoon in our CACC system to be efficient, comfortable and safe.

3.3 Distributed Optimal Control-Based CACC System

3.3.1 Problem Statement

Another primary motivation of developing the CACC system is to reduce energy consumption and pollutant emissions. Researchers have been investigating the main factors of high energy consumption levels and pollutant emissions generated by vehicles. Barth *et al.* [124] found that CO_2 emissions could be reduced by up to almost 20% through three different strategies: Congestion mitigation strategies that allow traffic to flow at better speeds, speed management techniques that reduce excessively high free-flow speeds to more moderate conditions, and shock wave suppression techniques that eliminate the

acceleration and deceleration events associated with the stop-and-go traffic. The CACC system allows vehicles to be driven in platoons with the same moderate speed and much shortened time gap (thus increasing the throughput), therefore the aforementioned three strategies are all realized to some extent. In addition, since all vehicles but the leading one in the CACC system follow their proceeding vehicles with a much shorter vehicle-following gap, the presence of the boundary layer along the platoon reduces air resistance, hence energy consumption is further decreased [125].

In this section, we propose a platoon-wide Eco-CACC system, developing different protocols for different stages of the CACC operation along freeway, i.e., platoon formation, platoon in-operation, and platoon dissolution. We develop an intra-platoon vehicle sequence optimization approach to further save energy of the eco-CACC system. The key protocols for the involved vehicle(s) at each stage may include sequence determination, gap closing and opening, platoon cruising with gap regulation, and platoon joining and splitting. Under each protocol, we assume all vehicles are CACC-enabled.

3.3.2 Platoon-Wide Eco-CACC System

3.3.2.1 Gap Closing and Opening

Generally speaking, there are two complementary protocols for a platoon to accommodate the weaving in and out maneuvers of a free-agent vehicle: gap closing and gap opening. The gap closing process happens when a following vehicle tries to catch up with its preceding vehicle from a certain distance. The following vehicle should first accelerate to gain a large speed difference with its preceding one, then cruise at this rather

high speed for a while to shorten the gap, and finally decelerate to the same speed as its preceding one.

In this dissertation, we propose a piecewise trigonometric function family to model the relationship between relative speed and relative distance of two consecutive vehicles to achieve higher energy efficiency for gap closing. It is noted that the similar idea has been proposed by the authors and extensively validated in the Eco-Approach and Departure (EAD) application at signalized intersections [27]. Given the relative speed and relative distance at time $t = 0$ (without loss of generality), we can determine the planned trajectory for the gap closing controller by solving the following optimization problem:

$$\min \Delta V_{h0} \tag{3-36}$$

subjects to

$$\Delta V(t) = \begin{cases} \frac{1}{2}(\Delta V_{h0} + \Delta V_0) - \frac{1}{2}(\Delta V_{h0} - \Delta V_0) \cdot \cos(m \cdot t), t \in [0, \frac{\pi}{m}) \\ \Delta V_{h0}, t \in [\frac{\pi}{m}, t_1) \\ \frac{1}{2}\Delta V_{h0} + \frac{1}{2}\Delta V_{h0} \cdot \cos[n \cdot (t - t_1)], t \in [t_1, t_1 + \frac{\pi}{n}) \end{cases} \tag{3-37}$$

$$\frac{\pi}{2m}(\Delta V_{h0} + \Delta V_0) + \Delta V_{h0}\left(t_1 - \frac{\pi}{m}\right) + \frac{\pi}{2n}\Delta V_{h0} = \Delta D_0 \tag{3-38}$$

$$\Delta V_0 \le \Delta V_{h0} \le \Delta V_{max,0} \text{ and } t_1 + \frac{\pi}{n} \le t_{th} \tag{3-39}$$

$$0 \le \frac{m}{2}(\Delta V_{h0} - \Delta V_0) \le a_{max} \text{ and } 0 \le \frac{n}{2}\Delta V_{h0} \le |a_{min}| \tag{3-40}$$

$$\frac{m^2}{2}(\Delta V_{h0} - \Delta V_0) \le Jerk_{max} \text{ and } \frac{n^2}{2}\Delta V_{h0} \le Jerk_{max} \tag{3-41}$$

where ΔD_0 is the difference between the initial gap and the desired gap of two consecutive vehicles; ΔV is the speed difference between two consecutive vehicles; ΔV_0 is the initial speed difference; ΔV_{h0} is the optimal speed difference peak calculated at time $t = 0$;

$\Delta V_{max,0}$ is the largest speed difference (at time $t = 0$) constrained by the speed limit posted on the roadway; m and n are the angular frequencies of trigonometric functions, respectively; t_{th} is the time threshold to complete the gap closing maneuver; a_{max}, a_{min} are the maximum and minimum acceleration, respectively; and $Jerk_{max}$ represents the maximum jerk (i.e., change rate of acceleration in time) to address driving comfort issue. In this dissertation, we choose a_{max} =2.5 m/s^2, a_{min} =-2.5 m/s^2, and $Jerk_{max}$ =10 m/s^3 [123]. Figure 3-12 illustrates an example of the proposed trajectory. As can be seen from the figure, after time $t = t_1 + \frac{\pi}{n}$, two consecutive vehicles should travel at the same speed, while maintaining a desired gap.

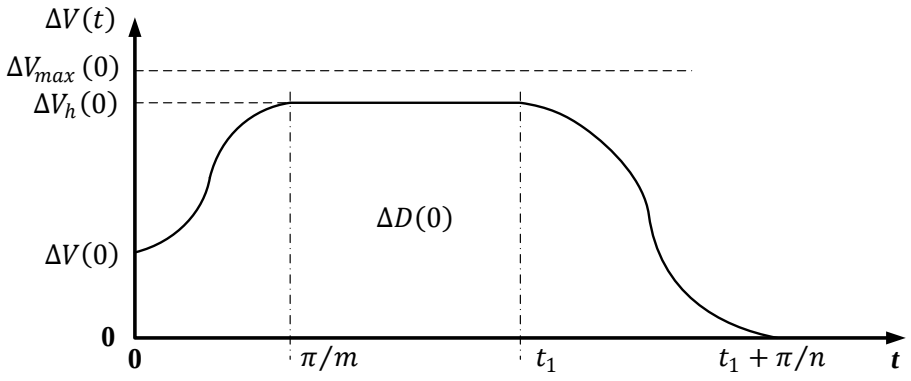

Figure 3-12 Trajectory planning for gap closing

The gap opening process happens when a following vehicle tries to create a larger gap with its preceding vehicle to allow other vehicles to join the platoon. Similar to the energy-efficient trajectory designed for gap closing, another optimization problem can be formulated with the constraints of another piecewise trigonometric function (see Figure 3-13) to model relative speed versus relative distance of two consecutive vehicles for gap opening.

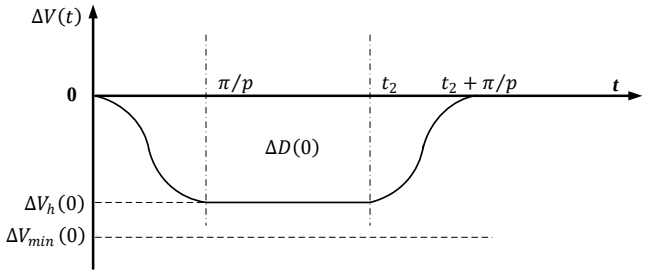

Figure 3-13 Trajectory planning for gap opening

3.3.2.2 Platoon Cruising with Gap Regulation

The cruising speed of a platoon is critical, since the optimal value leads to the minimization of energy consumption and pollutant emissions. Based on the authors' previous research [124], the estimated CO_2 emissions factor (in gram/mile) for light-duty vehicles on a flat road can be fitted as a convex function of cruising speed (e.g., the solid line in Figure 3-14), i.e., a fourth-order polynomial that can be expressed by

$$\ln(y) = b_0 + b_1 \cdot x + b_2 \cdot x^2 + b_3 \cdot x^3 + b_4 \cdot x^4 \qquad (3\text{-}42)$$

where y is the CO_2 emissions in g/mi ,and x is the cruising speed in mph. The coefficients for each fitted curve are given in TABLE I. In this dissertation, we choose the eco-cruising speed as 45 mph.

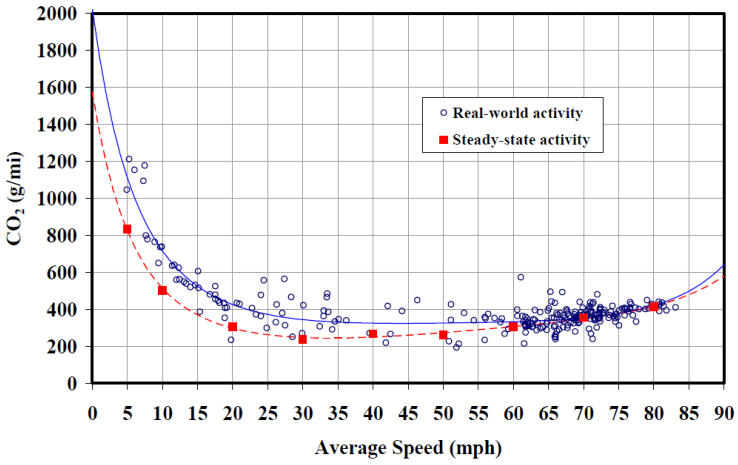

Figure 3-14 CO_2 emissions as a function of average speed [124]

Table VI Derived Line-Fit Parameters.

Parameters	Real-World	Steady-State
b_0	7.613534994965560	7.362867270508520
b_1	- 0.138565467462594	- 0.149814315838651
b_2	0.003915102063854	0.004214810510200
b_3	- 0.000049451361017	- 0.000049253951464
b_4	0.000000238630156	0.000000217166574

On the other hand, to guarantee the string stability [112], we design a gap regulation controller by following the recommendation in [21], which can be stated as

$$X_i(s) = \frac{D(s)+G(s)K_P(s)}{1+G(s)[K_P(s)P_P(s)+K_L(s)P_L(s)}X_{i-1}(s) \tag{3-43}$$

where $X_i(s)$ and $X_{i-1}(s)$ are the positions of two consecutive vehicles; $D(s)$ is the communication delay; $G(s)$ is the vehicle model; $K_P(s) = 0.45s + 0.25$ is the preceding gap error controller; $K_L(s) = 0.15s + 0.1$ is the leading gap error controller; $P_P(s)$ and $P_L(s)$ are preceding car-following policy and leading car-following policy, respectively, and can be defined as

$$P_P(s) = h_P(s) + 1 \tag{3-44}$$

$$P_L(s) = h_L(s) + 1 \tag{3-45}$$

with $h_P(s)$ and $h_L(s)$ being the time-gap target values with respect to the preceding and leading vehicles, respectively.

3.3.2.3 Preliminary Evaluation and Results

MATLAB/Simulink is used to conduct numerical simulation of the proposed Eco-CACC system under two different scenarios. All vehicles in our system are assumed to be connected vehicles with the ability to send and receive information among them. Results

of platoon-wide energy consumption and pollutant emissions are illustrated in different scenarios, and are also compared with the distributed consensus-based CACC system proposed in the previous subsection.

Firstly, a platoon formation scenario is analyzed where two vehicles on the same lane form a platoon by the proposed gap closing algorithm. The parameters of this scenario are listed in Table VII. More specifically, the proceeding vehicle always cruise at 45 mph. The following vehicle has an initial speed of 45 mph and a final target speed of 45 mph as well, but it may conduct potential acceleration and deceleration processes to close the $(7.58 - 0.9 =)$ 6.68 s inter-vehicle time gap difference. After the MOVES model has been adopted to perform the multiple scale analysis on the environmental impacts of the proposed Eco-CACC system together with the existing distributed consensus-based CACC system, the platoon-wide benefits of our system are demonstrated in Table VIII.

Table VII Vehicle Parameters of Platoon Formation Scenario.

Parameters	Value
Number of Vehicles	2
Length of Vehicles	16.4 feet
Length of Simulation Segment	1 mile
Initial Speed of Vehicles	45 mph
Final Speed of Vehicles	45 mph
Initial Inter-Vehicle Time Gap	7.58 s
Final Inter-Vehicle Time Gap	0.9 s

As can be seen from Table VIII, for the platoon formation scenario, the proposed system has an improvement of 1.45 % on energy consumption over the distributed

consensus-based CACC system. In addition, our system can also reduce the emissions of HC, NO_x, and CO_2, except for CO.

Table VIII Comparison of Platoon-Wide Energy Consumption and Pollutant Emissions on Platoon Formation.

	HC (g)	CO (g)	NO_x (g)	CO_2 (g)	Energy (kJ)
Consensus-CACC	0.146	4.68	0.758	684.2	9514.3
Eco-CACC	0.142	4.78	0.747	674.3	9376.6
Improved %	2.74	-2.14	1.45	1.45	1.45

Secondly, a platoon joining scenario is simulated where a free-agent vehicle tries to merge in a three-vehicle platoon. The parameters of this scenario are listed in Table IX.

Table IX Vehicle Parameters of Platoon Joining Scenario.

Parameters	Value
Number of Vehicles	4
Position of Free-Agent Vehicle in Platoon after Joining	2
Length of Vehicles	16.4 feet
Length of Simulation Segment	1 mile
Initial Speed of Free-Agent Vehicle	65 mph
Initial Speed of Platoon Vehicles	45 mph
Final Speed of Platoon Vehicles	45 mph
Initial Inter-Vehicle Time Gap Between Free-Agent Vehicle and Platoon Leading Vehicle	2.7 s
Final Inter-Vehicle Time Gap Between Free-Agent Vehicle and Platoon Leading Vehicle	0.9 s

Again, this scenario is simulated along a one-mile segment. We assume that based on the propose sequence determination protocol, the free-agent vehicle on the adjacent lane of the platoon has been decided to be the second vehicle in the platoon after the joining maneuver. The initial speed of the free-agent vehicle is $(65 - 45 =)$ 20 mph higher than

the speed of the platoon. Initially, the free-agent vehicle has a 2.7 s inter-vehicle time gap with the leading vehicle of the platoon, while this decreases to 0.9 s after the free-agent vehicle joins the platoon. After adopting the MOVES model, the platoon-wide benefits of the proposed Eco-CACC system over the existing distributed consensus-based CACC system are demonstrated in Table X. As can be seen from the results, our system has better performances on all the indices. For energy efficiency, the proposed Eco-CACC system has an improvement of 2.17 % over the distributed consensus-based CACC system. For pollutant emissions, our system can effectively reduce the emissions of HC, CO, NOx, and CO2 by 6.7%, 17.0%, 3.0% and 2.2%, respectively.

Table X Comparison of Platoon-Wide Energy Consumption and Pollutant Emissions on Platoon Joining.

	HC (g)	CO (g)	NO_x (g)	CO_2 (g)	Energy (kJ)
Consensus-CACC	0.312	10.14	1.425	1327.8	18462.7
Eco-CACC	0.291	8.42	1.382	1298.9	18061.6
Improved %	6.67	16.96	3.02	2.18	2.17

3.3.3 Intra-Platoon Vehicle Sequence Optimization

3.3.3.1 Vehicle Sequence Optimization

As a follow-up effort of the previously proposed platoon-wide eco-CACC system, a protocol for intra-platoon vehicle sequence optimization is introduced in this section. A bi-level integer programing model is developed to investigate the most energy-efficient intra-platoon position when each vehicle joins the platoon to minimize the total of all acceleration, deceleration and cruising maneuvers from gap opening and closing.

In this subsection we develop a model to synthetically consider the impact of the disturbances when each single vehicle joins and splits from the platoon and optimize the energy consumption. We assume the time order of the event when each vehicle joins or leaves the platoon is pre-determined before the platoon is formulated, i.e. all vehicles shares their origins and destinations information before they join the platoon. For an Eco-CACC system associated with *M* vehicles, there are *2M* platoon joining and splitting events in total. For vehicle *i*, the event IDs of the joining event and leaving event are defined as A_i and B_i respectively (A_i<B_i). Accordingly, for event *k*, the corresponding vehicle ID is defined as V_k and the event type is defined as an integer variable S_k, where S_k is 1 for joining event and -1 for leaving event. Then N_k, the number of vehicles in the platoon (or platoon length) right after event k is calculated as

$$N_k = \sum_{l=1}^{k} S_l \tag{3-46}$$

As the time order of joining and leaving events are pre-determined, the variables stated above, i.e. A_i, B_i, V_k, S_k, N_k, can be considered as constants for a certain Eco-CACC system.

In the proposed optimization problem, we aim to find the optimal sequence (*i.e.* position in the platoon) when each vehicle joins the platoon to minimize the total energy consumption of all acceleration and deceleration maneuvers of the entire platoon. For vehicle *i*, we define the position when joining and leaving the platoon as *xi* ($1 \le x_i \le N_{A_i}$) and *yi* ($1 \le y_i \le N_{B_i} + 1$) respectively. Note that N_{B_i} is the platoon length right after event Bi and *yi* is the vehicle position before event B_i, so y_i may be equal to $N_{B_i} + 1$ if the ith vehicle is at the end of the platoon. For the joining maneuver, a gap is created to allow

vehicle i to join a platoon of size N_{A_i} at position x_i. This can be accomplished either by following vehicles after a deceleration-cruising-acceleration gap opening process, or by leading vehicles after an acceleration-cruising-deceleration process. Corresponding to the most energy-efficient way to open a gap, the minimum incremental energy consumption for vehicle i to join the platoon at position x_i is defined as $F(x_i)$. Similarly, the minimum incremental energy consumption for vehicle i at position y_i to leave a platoon is defined as $G(y_i)$. The objective of the optimal sequence problem is then formulated as follows:

$$\min_{\{x_i\},\{y_i\}} z = \sum_{i=1}^{M} F(x_i) + \sum_{i=1}^{M} G(y_i) \tag{3-47}$$

In (3-47), $\{y_i\}$ can be considered as a function of $\{x_i\}$. To prove that, we define the position of vehicle i right after event k ($A_i \leq k < B_i$) as $R_i(k)$, which is calculated and updated iteratively as follows:

1. Right after event A_i, $R_i(A_i)$ is initialized as x_i,

2.1. Right after event k ($A_i < k < B_i$), if $S_k = 1$, vehicle V_k joins the platoon at position x_{V_k}.

$$R_i(k) = \begin{cases} R_i(k-1) + 1 & if\, x_{V_k} \leq R_i(k-1) \\ R_i(k-1) & otherwise \end{cases} \tag{3-48}$$

2.2. Right after event k ($A_i < k < B_i$), if $S_k = -1$, vehicle V_k at position y_{V_k} leaves the platoon.

$$R_i(k) = \begin{cases} R_i(k-1) - 1 & if\, y_{V_k} \leq R_i(k-1) \\ R_i(k-1) & otherwise \end{cases} \tag{3-49}$$

3. Right after event B_i, vehicle i leaves the platoon. The final position right before splitting is $y_i = R_i(B_i - 1)$. Therefore y_i is determined by x_i after above iterations.

Therefore y_i, the position of vehicle *i* when leaving is formulated as follows

$$y_i = x_i + \sum_{k=A_i}^{B_i-1} \xi_k^i S_k, \tag{3-50}$$

where ξ_k is a binary parameter that describes whether the event vehicle V_k is in front of vehicle i in event *k*.

Based on (3-47) and (3-50), we can formulate the complete form of the optimal sequence problem:

$$\min_{\{x_i\},\{y_i\}} z = \sum_{i=1}^{M} F(x_i) + \sum_{i=1}^{M} G(y_i) \tag{3-51}$$

$$\text{s.t. } 1 \le x_i \le N_{A_i}, i = 1,2,3 \dots M \tag{3-52}$$

$$1 \le y_i \le N_{B_i} + 1, \ i = 1,2,3 \dots M \tag{3-53}$$

$$y_i = x_i + \sum_{k=A_i}^{B_i-1} \xi_k^i S_k \,, i = 1,2,3 \dots M \tag{3-54}$$

The optimal sequence problem above is a bi-level optimization problem. Variable sets $\{x_i\}$ and $\{y_i\}$ are first applied to the sub-problems for platoon joining and splitting to figure out minimal incremental gap opening/closing energy consumption $F(x_i)$ and $G(y_i)$. Then we calculate the objective values according to each variable set pair $\{x_i\}$ and $\{y_i\}$ and search for the optimal solution that to minimize the total energy consumption of all acceleration and deceleration maneuvers of the entire Eco-CACC system.

3.3.3.2 Gap Closing and Opening Strategies

The optimization goal of the integer programing problem (3-51)- (3-54) is to minimize the incremental energy consumption of all gap closing and opening maneuvers due to the joining and leaving of vehicles. We therefore need to identify $F(x_i)$ and $G(y_i)$

in (3-51)- (3-54), the minimum incremental energy consumption per gap opening/closing.

There are two approaches to create a gap. If vehicle *i* plans to join the platoon at position *xi*, following vehicles (from the $x_i{}^{\text{th}}$ vehicle to the NAi^{th} vehicle in the existing platoon) can open a gap after a deceleration-cruising-acceleration process. The incremental energy consumption during this process is computed as $\sum_{j=x_i}^{N_{A_i}}(E_j^D - E_j^C)$, where E_j^D is the energy consumption for vehicle *j* to make a designed deceleration-cruising-acceleration trajectory and E_j^C is the energy consumption for vehicle *j* if it keeps the current speed during the same time period. Symmetrically, leading vehicles (from the 1st vehicle to $(x_i - 1)^{\text{th}}$ vehicle in the existing platoon) may also make an acceleration-cruising-deceleration maneuvers to create the gap. The incremental energy consumption during this process is $\sum_{j=1}^{x_i-1}(E_j^A - E_j^C)$, where E_j^A is the energy consumption for vehicle *j* to make a designed acceleration-cruising-deceleration trajectory.

The optimal strategy to open a gap is then the one with less incremental energy consumption, so the minimum incremental energy consumption for vehicle *i* to join the platoon at position x_i is

$$F(x_i) = \min\left\{\sum_{j=x_i}^{N_{A_i}}(E_j^D - E_j^C), \sum_{j=1}^{x_i-1}(E_j^A - E_j^C)\right\} \quad (3\text{-}55)$$

For gap closing process, after vehicle *i* at position y_i leaves the platoon, there are also two approaches-an acceleration-cruising-deceleration gap closing process acted by following vehicles, or a deceleration-cruising-acceleration process acted by leading vehicles. Then the incremental energy consumption for each approach is $\sum_{j=y_i}^{N_{B_i}-1}(E_j^A -$

E_j^C) and $\sum_{j=1}^{y_i-1}(E_j^D - E_j^C)$, respectively. The minimum incremental energy consumption for vehicle *i* at position *yi* leave the platoon is

$$G(y_i) = \min\left\{\sum_{j=y_i}^{N_{B_i}-1}(E_j^A - E_j^C), \sum_{j=1}^{y_i-1}(E_j^D - E_j^C)\right\} \quad (3\text{-}56)$$

In this paper, we estimate energy consumption E_j^A, E_j^D and E_j^C using MOVES model developed by U.S. Environmental Protection Agency [99]. In MOVES, the vehicle operating modes (OpMode) are grouped into 23 categories with vehicle-specific power (VSP) as its primary metric. As VSP is a function of speed, acceleration, mass, road grade, and vehicle-specific coefficients, the energy consumption is mainly decided by planed trajectory and type (e.g. light-duty or heavy duty) of each vehicle in the platoon. As the sequence optimization is conducted before the actual gap opening or closing maneuvers are performed, it is reasonable to assume each vehicle follows a well-calibrated standard deceleration-cruising-acceleration or acceleration-cruising-deceleration trajectory during the process. For certain vehicle type *n*, we use Δ_n^D to represent the incremental energy consumption for deceleration-cruising-acceleration, and Δ_n^A to represent that for acceleration-cruising-deceleration process. Then (3-49) and (3-50) could be reformulated as

$$F(x_i) = \min\left\{\sum_{j=x_i}^{N_{A_i}} \Delta_{n(j)}^D, \sum_{j=1}^{x_i-1} \Delta_{n(j)}^A\right\}, \text{ and} \quad (3\text{-}57)$$

$$G(x_i) = \min\left\{\sum_{j=y_i}^{N_{B_i}-1} \Delta_{n(j)}^A), \sum_{j=1}^{y_i-1} \Delta_{n(j)}^D\right\}, \quad (3\text{-}58)$$

where $n(j)$ denotes the vehicle type of vehicle *j*. In particular, if all vehicles in the platoon are under the same vehicle type (say *n**), the objective function (3-51) is reduced into the following form.

$$\min_{\{x_i\},\{y_i\}} z = \sum_{i=1}^{M} (\min\{x_i \Delta_{n^*}^{A}, (N_{A_i} - x_i + 1)\Delta_{n^*}^{D}\} + \min\{y_i \Delta_{n^*}^{D}, (N_{B_i} - y_i)\Delta_{n^*}^{A}\}) \quad (3\text{-}59)$$

3.3.3.3 Solution Method and Model Extension

The integer programing problem (3-51)-(3-54) is difficult to be solved exactly if the size of the platoon is large. Since each vehicle have N_{A_i} candidate position when joining the platoon, it is computational expensive if all possible combinations ($\prod_{i=1}^{M} N_{A_i}$ in total) are enumerated. The complexity of the problem grows explosively as the number of vehicles increases, e.g. consider a platoon with 20 vehicles, there are 20! = 2.43×1018 possible combination outcomes. To avoid enumerating all possible outcomes, the problem is solved using a global optimization algorithm called tabu search. Tabu search applies local search procedure to move from one potential solution to another enhanced solution. A memory structure named tabu list is introduced to avoid poor-scoring areas that may trap conventional local search methods. The solution procedure is briefly summarized in Figure 3-15.

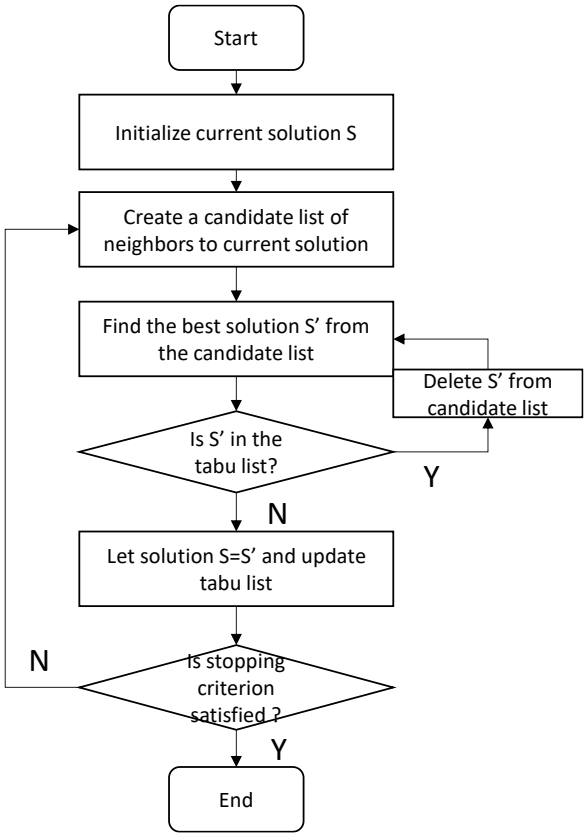

Figure 3-15 Flow chart of TABU search algorithm

The proposed model can be extended to the scenarios that multiple vehicles would make cooperative plan to join or leave the platoon simultaneously. In this situation, in an Eco-CACC system associated with *M* vehicles, *2M* events are grouped into Mc event clusters. Each cluster consists of joining/leaving events that are planned to be acted cooperatively at the same time. For the nth cluster, we define the position set of all joining vehicles as $\{x_i^n\}$ and the position set of all leaving vehicles as $\{y_i^n\}$. Then a bi-level optimization problem can be formulated to estimate the optimal $\{x_i^n\}$ and $\{y_i^n\}$ at each event cluster. Similar as the basic model in (3-51)-(3-54), in the lower-level, we investigate the most energy-efficient approach to open and close multiple gaps for a certain

set of $\{x_i^n\}$ and $\{y_i^n\}$ at each event cluster. For example, if two vehicles plan to join an Eco-CACC platoon at the 2nd and the 9th position respectively as shown in Figure 3-16, the existing platoon have three strategies to make two gaps to accommodate the newcomers: (1) the 1st vehicle makes an acceleration-cruising-deceleration maneuver to move two gaps forward in relative to its presumed location under operation speed, and the 2nd ~ 6th vehicle in the existing platoon move one gap forward; (2) the 1st vehicle moves one gap forward and the 7th ~ 8th vehicles move one gap backward; and (3) the 7th ~ 8th vehicles move one gap backward, and the 2nd ~ 6th vehicle move one gap backward. The MOVES based energy consumption estimation method is then applied to identify the optimal strategy corresponding to certain pair of $\{x_i^n\}$ and $\{y_i^n\}$.

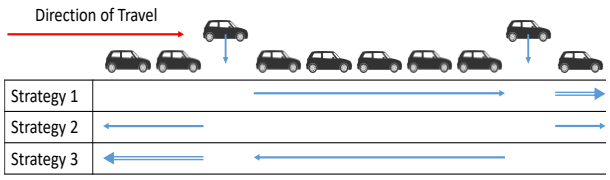

Figure 3-16 Three strategies to accommodate the newcomers to the existing platoon

In the upper-level of the event cluster-based optimization problem, we explore the optimal combination of Mc event clusters that minimize the incremental energy consumption from all gap opening and closing behaviors. A tabu search method can be developed to solve this problem efficiently.

Another extension to (3-51)-(3-54) is to include the incremental energy that the new vehicle consumed when catching up the platoon and join it. To achieve the designed optimal sequence, the new joining vehicle may spend additional energy cost to find the pre-determined location and merge into the platoon. In this paper, we assume the single

vehicle is well coordinated and synchronized with the platoon so that it can meet the platoon at the pre-determined location from the optimal solution at beginning. However, if the relative location information is provided and the energy consumption of the new joining vehicle before merging is calibrated, a new energy consumption term can be included to the objective function (3-51) to address the energy consumption of the new vehicles when they join the platoon.

3.3.3.4 Preliminary Evaluation and Results

In order to calibrate the sequence optimization model, sample vehicle trajectories for gap opening and closing are required as the input of energy consumption estimation in (3-55) and (3-56). As shown in Figure 3-17, we collect vehicle speed profile data from the simulated gap opening and closing maneuvers in a proposed distributed consensus algorithm based CACC system from MATLAB/Simulink simulation. As discussed in the previous subsection, the acceleration-cruising-deceleration profile (represented by solid curve) corresponds to the typical behavior of following vehicles in gap closing and that of leading vehicles in gap opening. The deceleration-cruising-acceleration profile (represented by dashed curve) corresponds to the typical behavior of leading vehicles in gap closing and following vehicles in gap opening.

Based on the sample vehicle trajectories, the second-by-second VSP are calculated using following equation,

$$VSP = v\left[a(1+\varepsilon_i) + g\phi + \frac{9.80665}{W}(A + Bv + Cv^2)\right] \quad (3\text{-}60)$$

where v is the velocity (m/s), a is the acceleration rate (m/s^2), g is the acceleration of gravity (m/s^2), and W is the vehicle test weight (kg). Parameters *A, B, C* are dynamometer

road load coefficients, and ε_i, the "mass factor", is the equivalent translational mass of the rotating components (wheels, gears, shafts, etc.) of the powertrain. Based on VSP, speed, acceleration and vehicle type information, we can identify the OpMode for specific vehicle at each time step, and calculate the incremental energy consumption for both maneuvers using MOVES [99]. In the following part of the numerical experiment sections, we assume all vehicles that associate with the Eco-CACC system are under passenger truck category, i.e. Category 31, so the incremental energy consumption is 172 kJ for the acceleration-cruising-deceleration process and 373 kJ for the deceleration-cruising-acceleration process.

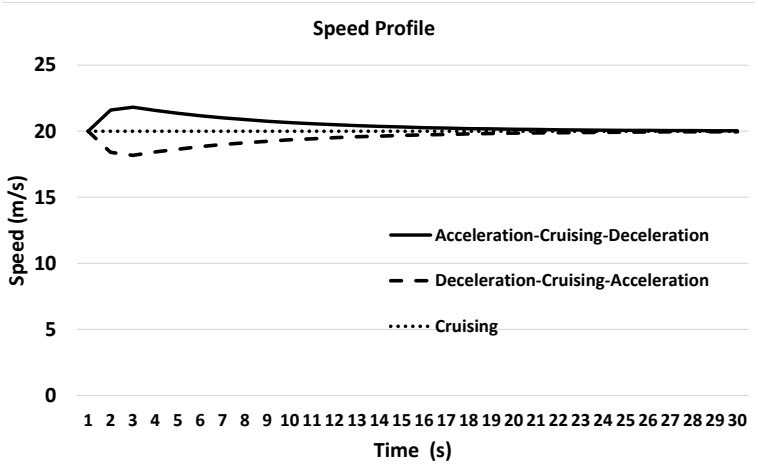

Figure 3-17 Sample vehicle trajectories during gap opening and closing

Table XI Results of the numerical simulation.

Platoon Size	Mean Incremental Energy (KJ)			Saving (%)
	To front	To back	Optimal	
8	738	748	196	73.8
9	942	965	229	76.3
10	1269	1220	339	72.2
11	1472	1488	442	70.3
12	2054	2077	716	65.5
13	2384	2362	838	64.5
14	2886	2830	1084	61.7
15	3287	3182	1314	58.7
16	3666	3779	1591	57.9
17	4432	4358	1921	55.9
18	5006	5059	2214	56.2
19	5623	5652	2786	50.7
20	6171	6322	3053	51.7

We then evaluate the performance of the proposed model using numerical simulation in MATLAB. Two baseline strategies are introduced for comparison. For “To front” strategy, each new vehicle becomes the first vehicle of the platoon. For “To back” strategy, each new vehicle is attached to the end of platoon. For different sizes of platoon (i.e. number of vehicles that associates with the CACC system), we make 100 runs with random event sequences. The numerical results are summarized in Table XI. As listed in the table, the incremental energy consumption from gap opening/closing are reduced significantly by implementing the optimal strategy. The percentage improvement of the optimal solution in relative to the “To back” strategy decreases from 74% to 52% when the platoon size increases from 8 to 20. That means, more than 50% of gap opening/closing related acceleration and deceleration maneuvers can be reduced by smartly organize the in-platoon vehicle sequence during the lifecycle of platoon.

To further validate the proposed VSO algorithms, MATLAB/Simulink is adopted to conduct a simulation on a CACC system of 10 vehicles. All vehicles in the platoon are assumed to be capable to send and receive velocity and position information among them. We further assume they adopt distributed consensus based CACC algorithm to conduct gap opening and closing maneuvers, which was proposed earlier as (3-12).

MATLAB/Simulink simulation is then conducted to evaluate three different join strategies: “To front”, “To back”, and optimal. The parameters of the simulation are listed in Table XII and the vehicle speed trajectory results of the three strategies are shown below.

Table XII Parameters of MATLAB/Simulink simulation.

Parameters	Value
Number of Vehicles	10
Length of Each Vehicle	5 m
Initial Velocity of Vehicles	20 m/s
Desired Velocity of Vehicles	20 m/s
Final Inter-Vehicle Gap Between Vehicles in the Platoon	10 m

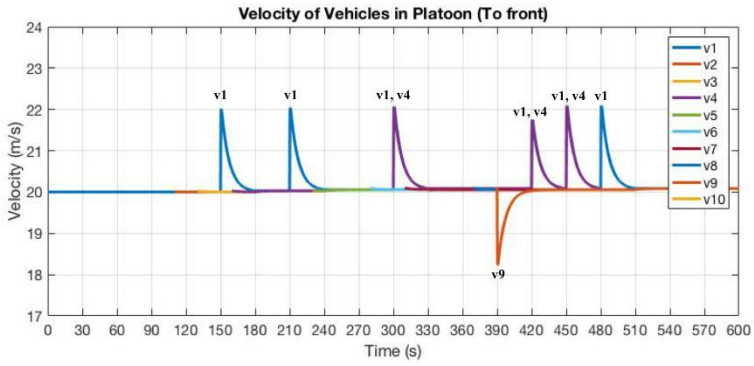

(a)

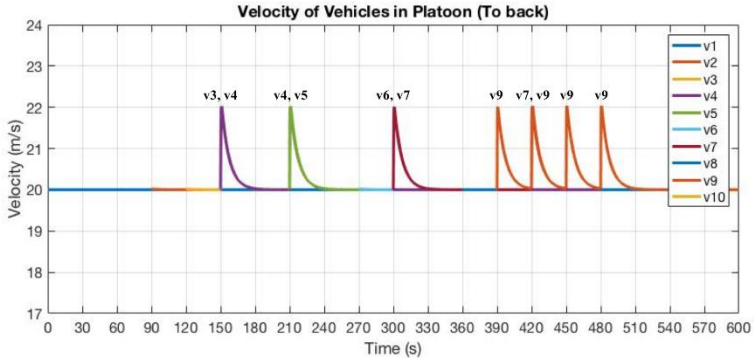

(b)

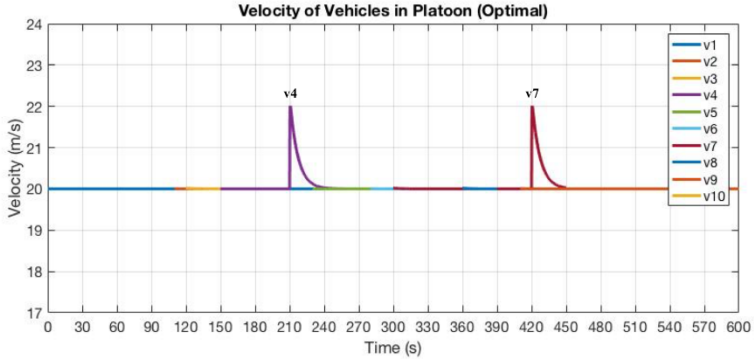

(c)

Figure 3-18 Vehicle trajectories under different optimal strategies

Since we only analyze the gap opening and closing maneuvers of the platoon, we filter out the free vehicle catching-up process, which is the first 30-second trajectory of

each vehicle. As can be seen from the Figure 3-18*(a)*, “To front” strategy has nine acceleration-cruising-deceleration profiles (six of them are overlapped in pairs) and one deceleration-cruising-acceleration profile, “To back” strategy also has nine acceleration-cruising-deceleration profiles (six of them are overlapped in pairs). In Figure 3-18*(c)*, the optimal strategy only has two acceleration-cruising-deceleration profiles, which shows the ability of the proposed vehicle sequence optimization methodology to reach higher energy-efficiency during the lifecycle of a platoon.

We further analyze the emissions and energy consumption of three strategies, and results are shown in Table XIII. For the entire trips which include all CACC cruising and merging/splitting processes, the proposed optimal solution have the best performance in emissions and energy consumption, saving 1.6% energy from the “To back” strategies and 1.6%~23.8% air pollutant emissions. If we concentrate on the incremental emissions and energy consumption made from gap opening and closing, the advantage is more explicit – about 74% saving on emissions and energy consumption.

Table XIII Results from MATLAB/Simulink simulation.

Total Emissions and Energy Consumption						
Strategy	HC (g/s)	CO (g/s)	NOx (g/s)	CO2 (g/s)	Energy (KJ/s)	PM2.5 (g/s)
Optimal	1.11	28.36	4.71	5067	70462	0.074
To front	1.32	40.09	6.17	5989	83280	0.109
To back	1.14	30.94	4.83	5149	71601	0.097
Saving (%)	3.2	8.3	2.6	1.6	1.6	23.8
Incremental Emissions and Energy Consumption						
Strategy	HC (g/s)	CO (g/s)	NOx (g/s)	CO2 (g/s)	Energy (KJ/s)	PM2.5 (g/s)
Optimal	-0.03	0.98	-0.02	28	396	0.074
To front	0.18	12.71	1.45	950	13214	0.109
To back	0.002	3.56	0.11	110	1534	0.097
Saving (%)	-	73	-	74	74	24

4 DISTRIBUTED COOPERATIVE SYSTEMS WITH V2V and I2V COMMUNICATION

4.1 Problem Statement

In addition to V2V communication, I2V communication also plays an important role in CAV technology. Information measured or stored in the infrastructure can be sent or broadcasted to CAVs with I2V communication, so each CAV can plan its movement based on the information received, and potentially also collaborate with other CAVs simultaneously with V2V communication. Such information could include SPaT, vehicle sequence, downstream traffic flow, and etc. In this section, we develop several distributed consensus-based approaches and optimal control-based approaches for two major traffic scenarios that utilize both V2V and I2V communication: Eco-driving at signalized intersections and cooperative merging at highway on-ramps.

4.2 Cooperative Eco-Driving at Signalized Intersections

4.2.1 Introduction and Background

In recent years, increased transportation activity continues to have significant impacts on the above measures and raises awareness and concerns from the general public. In terms of traffic mobility, drivers in the U.S. spent an average of 41 hours a year in traffic during peak hours in 2017, costing nearly $305 billion in total, which equals to $1,445 per driver [126]. In terms of traffic safety, it is estimated that 37,461 people died in accidents in the U.S. involving motor vehicles in 2016, which endured a 6 percent rise from the year before [127]. And in terms of environmental sustainability, the transportation sector was

the second largest producer of GHG nationwide, accounting for approximately 27% of total U.S. emissions in 2013 [128].

In recent years, there has been a significant amount of research interest on how to improve the mobility, safety and sustainability of signalized intersections. Specifically, CAV technology has been widely studied to improve the sustainability of transportation systems, where a CAV can be driven by itself with the help of its on-board perception sensors, and also communicate with the driver, other vehicles on the road (through V2V communications), roadside infrastructure (through I2V communications), and the "Cloud". Such applications are often categorized as eco-driving at signalized intersections, with specific names such as GLOSA (Green Light Optimized Speed Advisory (GLOSA) or EAD.

Most of the existing EAD system are designed from an ego-vehicle perspective (Ego-EAD), considering the interaction with other traffic in a passive manner. This may result in negative impacts, e.g., queue spillback, on the upstream traffic along a corridor with short blocks due to the "pushing-back" effects of Ego-EAD algorithms. To overcome this issue while preserving the benefits from EAD, we combine the ideas of EAD and CACC to propose a CACC-Enabled EAD application and a cluster-wise cooperative EAD (Coop-EAD) application, enabling CAVs to cooperate with each other to form clusters and travel through the signalized intersection with smaller time headways in an energy efficient manner. The proposed system not only reduces energy consumption and pollutant emissions, but also improves system efficiency (e.g. traffic throughput) and safety.

4.2.2 CACC-Enabled Eco-Approach and Departure

4.2.2.1 Problem Statement

The objective of this dissertation is to develop a cooperative eco-driving (CED) system by CAV technology to improve the energy efficiency along a corridor with signalized intersections. To study the effect of penetration rate of CAVs, we define two different types of vehicles in the system as conventional vehicles and CED vehicles. Different role transition protocols and longitudinal control models are proposed for different vehicles based on their degrees of connectivity and automation. In this dissertation, a microscopic traffic simulation network is modeled in VISSIM, where different vehicle longitudinal control models and their relevant logic (e.g., role transition) are integrated into simulation network to simulate vehicles' behavior, and an energy/emission model is implemented to analyze the environmental impacts of proposed methodologies.

Note that our study mainly focuses on designing an integrated traffic system with proposed control protocol, so some reasonable specifications and assumptions are made as follows to quantify the potential benefits while modelling the system:

- All CED vehicles in the proposed system are equipped with appropriate on-board sensors (e.g., OBD, camera, radar, LIDAR, etc.), and their measurements and calculations are precise without error.
- All CED vehicles are V2V-enabled, which are equipped with wireless communication devices such as Dedicated Short Range Communications (DSRC) on-board units (OBUs), to transmit vehicle information among each other, and also

I2V-enabled, which can receive MAP and SPaT (Signal Phase and Timing) information from intersections.

- All intersections in the system are equipped with DSRC roadside units (RSU) to broadcast their MAP and SPaT message, and all signals are fixed-timing control.
- We focus on the development of longitudinal control strategies and application in the simulation study. The lateral maneuvers rely on the default lane change model of VISSIM.

The general framework of the proposed system can be seen in Figure 4-1.

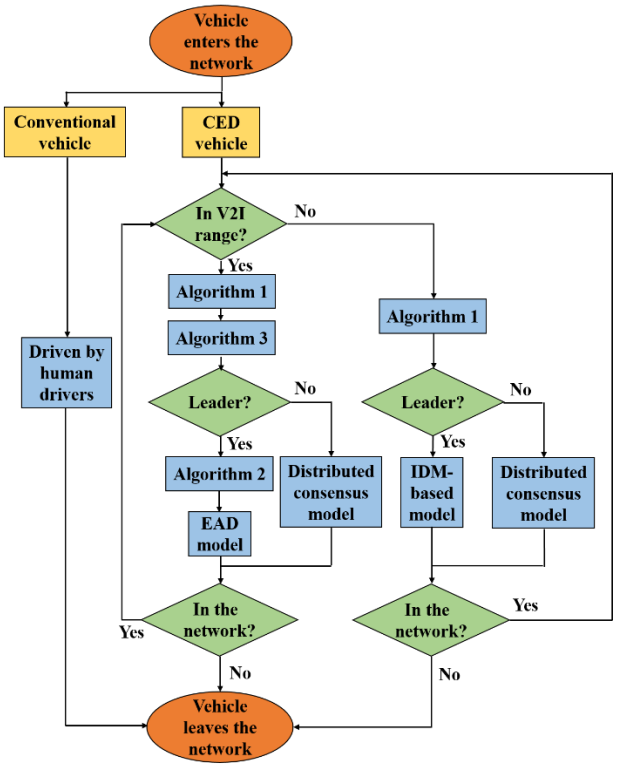

Figure 4-1. General framework of the proposed eco-driving system

Compared to similar existing studies in this research area, such as [129], [130], [131], our system has the following improvements:

- Most current works assume 100% penetration rate of CAVs in the systems, which are unrealistic for real-world implementations. Further, we not only consider two different types of vehicles, but also model the interactions between different vehicle types. For example, we study how a CED vehicle will response when a conventional vehicle suddenly moves in front of it.
- Different from most literatures that consider CAVs as different individual system that conducts eco-driving maneuver by itself, this dissertation proposes a cooperative eco-driving system, where different CAVs are categorized by different roles. Generally, leaders conduct eco-driving maneuver with respect to signals through I2V communication, while followers follow leaders' maneuvers through V2V communications. Therefore, less conflicts will be generated among different CAVs due to their collaborations.
- Instead of studying the eco-approaching maneuver on only one direction of one isolated signalized intersection, we model a corridor with two signalized intersections and all four directions, so both eco-approach and eco-departure maneuvers are developed and analyzed. The proposed algorithms allow CED vehicles to reset their parameters once passing the current intersection, and update parameters again while entering the I2V communication range of the next intersection.
- Rather than just numerical simulations, we conduct microscopic traffic simulation based on the University Avenue corridor in Riverside, CA, with real-world traffic flow and signal timing data provided by the government. Therefore, the results of

implementing the proposed CAV technology on the current transportation system would be more realistic and convincing.

4.2.2.2 Vehicle Role Transition Protocol

In the proposed system, there are generally two types of passenger vehicles: conventional vehicles and CED vehicles. Conventional vehicles are assumed to be driven by human drivers with no degree of connection and automation. CED vehicles are assumed to be CAVs with appropriate on-board sensors to conduct automated driving, and OBUs to transmit information among vehicles and receive information from the infrastructure. A vehicle role transition protocol is proposed for V2X-enabled vehicles as Algorithm 1, since a CED vehicle can transit from a leader to a follower in a vehicle string, or vice versa.

Algorithm 1: Role Transition of CED Vehicles

Input: inter-vehicle distance d_{gap}, distance to the intersection d_1, time-to-arrival of the ego vehicle t^{arr}, time-to-arrival of the preceding vehicle t_{pre}^{arr}, time-to-collision with respect to the preceding vehicle $t^{collision}$
Output: vehicle role

```
for all CED vehicles do
    if d_gap < V2V range then
        if d_gap > d_1 then
            ego vehicle is a CED leader
        else
            if preceding is a CED vehicle then
                if (t^arr − t_pre^arr) ≥ threshold then
                    ego vehicle is a CED leader
                else
                    ego vehicle is a CED follower
                end if
            else
                if (t^collision) < threshold then
                    ego vehicle is a CED follower
                else
                    ego vehicle is a CED leader
                end if
            end if
        end if
    else
        ego vehicle is a CED leader
    end if
end for
```

A CED vehicle continuously checks whether there is a preceding vehicle on the same lane, and within the V2V communication range. If no, then it is a leader of a string. If yes, then it compares the distance to the preceding CED vehicle with the distance to the intersection. If the preceding vehicle already passes the intersection, then the ego-vehicle is a CED leader. If not, then it furtherly checks the time-to-collision value (if the preceding vehicle is a conventional vehicle), or checks the estimated time-to-arrival at the intersection (if the preceding vehicle is also a CED vehicle).

If the preceding vehicle is a conventional vehicle and the time-to-collision value is lower than a certain threshold, it means the CED vehicle has a high chance to get a front-bumper-to-rear-bumper collision with its preceding conventional vehicle, so the CED vehicle will be a follower to follow its preceding conventional vehicle's movement.

If the preceding vehicle is also a CED vehicle and the difference between two consecutive CED vehicles' time-to-arrival is larger than a certain threshold (normally the total length of an amber phase and a red phase), then the following CED vehicle may be considered as the "string breaker" scenario and becomes a CED leader. The method to calculate estimated time-to-arrival can be found in Algorithm 2 and Algorithm 3.

Essentially, the "string breaker" scenario happens when two consecutive CED vehicles' time-to-arrival fall into two different green windows. Since we take green windows into account when calculating the time-to-arrival values, it is possible that the preceding one of two neighboring CED vehicles estimates to reach the intersection at the end of the preceding green window, but the following vehicle estimates to arrive at the start of the following green window. Therefore, a "string breaker" scenario is created, where the

following CED vehicle becomes a CED leader, and conducts its own EAD movement through the intersection.

4.2.2.3 Longitudinal Control Model

In the proposed system, conventional vehicles are assumed to be driven by human drivers, which are not equipped with any on-board sensor or OBU. Therefore, the car-following model originally proposed by Rainer Wiedemann in 1974 (i.e., Wiedemann 74) is used to model the longitudinal behaviors of conventional vehicles.

The safety clearance is defined in Wiedemann 74 as

$$d = a \cdot x + (b \cdot x_{add} + b \cdot x_{mult} \cdot z) \cdot \sqrt{v} \tag{4-1}$$

where $a \cdot x$ denotes the average standstill distance; $b \cdot x_{add}$ is the additive part of safety distance; $b \cdot x_{mult}$ is the multiplicative part of safety distance; v is the speed of vehicle; z is a value of range $[0, 1]$. The tolerance of $a \cdot x$ lies between ± 0.1 m which is normally distributed at around 0 m, with a standard deviation of 0.3 m. Both $b \cdot x_{add}$ and $b \cdot x_{mult}$ allow to adjust the time requirement values.

For modeling purposes, a CED vehicle can be separated into two different components: the CED vehicle longitudinal control model that delivers reference values of vehicle acceleration, and a vehicle powertrain model that transforms reference acceleration values into realized throttle or brake values. In this part, we mainly focus on the longitudinal control model, which generates the acceleration reference demand and then feeds it into the powertrain model.

When the CED leader is running out of the I2V communication range of the intersection, it follows its desired speed while there is no preceding conventional vehicle

in a certain range, or follows the preceding conventional vehicle while there is one. In the proposed system, the Intelligent Driver Model (IDM)-based longitudinal control strategy is applied to the longitudinal movement of the CED leader when out of I2V range of intersections.

IDM was proposed by Treiber *et al.* [132] and has been widely studied in many research work. In this dissertation, we develop a longitudinal control model for the CED leader (in the case of outside the I2V communication range) based upon IDM, which can be given as

$$a_{ref} = a_{max} \cdot \left[1 - \left(\frac{v_{ego}}{v_{des}}\right)^{\delta} - \Sigma\right] \tag{4-2}$$

where $\Sigma = \left(\frac{d_{safe} + v_{ego} \cdot t_{gap} + \frac{v_{ego} \cdot (v_{ego} - v_{pre})}{2 \cdot \sqrt{a_{max}{}^2}}}{d_{gap}}\right)^2$ is the correlation term with the front vehicle, which has a value when there is a conventional vehicle gets in front of the CED leader, and equals to 0 when no other vehicle is in front. a_{max} is a preset constant which denotes the maximum changing rate of speed; v_{ego} denotes the current speed of the ego vehicle; v_{pre} denotes the current speed of its preceding vehicle; v_{des} is a preset constant which denotes the desired speed of the ego vehicles; d_{safe} is a preset constant which denotes the minimum allowed inter-vehicle distance; t_{gap} is a preset constant which denotes the desired time gap; d_{gap} denotes the measured inter-vehicle distance between the ego vehicle and its preceding vehicle. The free acceleration exponent δ is defined based upon IDM, which characterizes how the acceleration of the ego vehicle decreases with speed (e.g., $\delta = 1$ corresponds to a linear decrease, and $\delta \to \infty$ leads to a constant acceleration).

Different from the case when running out of the I2V communication range of the intersection, the CED leader can receive MAP and SPaT information from upcoming intersections while it is in the I2V range, and is able to conduct EAD movement through intersections accordingly. In the proposed system, we develop a piecewise trigonometric-linear EAD algorithm based upon our previous work to control the longitudinal movements of the CED leader when in the I2V range. Similar to previous segments, we mainly focus on the longitudinal control model that generates the acceleration reference demand and then feeds it into the dynamics model.

We define four different EAD scenarios for a CED leader when it is in the I2V communication range of the intersection, which are accelerate scenario, cruise scenario, decelerate scenario, and stop scenario. Once the CED leader receives the SPaT information from the intersection and combines that with the MAP information, it calculates the following variables to decide which scenario it should be in:

$$t_c = \frac{d_1}{v_1} \tag{4-3}$$

$$t_e = \frac{d_1 - v_1 \cdot \frac{\pi}{2\alpha}}{v_{lim}} + \frac{\pi}{2\alpha} \tag{4-4}$$

$$t_l = \frac{d_1 - v_1 \cdot \frac{\pi}{2\beta}}{v_{coast}} + \frac{\pi}{2\beta} \tag{4-5}$$

$$\alpha = \min\left\{\frac{2 \cdot a_{max}}{v_{lim} - v_1}, \sqrt{\frac{2 \cdot jerk_{max}}{v_{lim} - v_1}}\right\} \tag{4-6}$$

$$\beta = \min\left\{\frac{2 \cdot a_{max}}{v_1 - v_{coast}}, \sqrt{\frac{2 \cdot jerk_{max}}{v_1 - v_{coast}}}\right\} \tag{4-7}$$

where t_c, t_e and t_l stand for cruising time-to-arrival, earliest time-to-arrival, and latest time-to-arrival, respectively; α and β are variables to calculate t_e and t_l, respectively; d_1 denotes the current distance to the intersection; v_1 denotes the current speed of vehicle; $jerk_{max}$ is a preset constant which denotes the maximum changing rate of acceleration or deceleration; v_{lim} is a preset constant which denotes the speed limit of the current roadway; v_{coast} is a preset constant which denotes the coasting speed. If the current signal phase is green, then we can define the available green window as $T = [0, t_{curr\_e}) \cup [t_{next\_s}, t_{next\_e})$; If the current signal phase is red, then $T = [t_{next\_s}, t_{next\_e})$. Note t_{curr_e} denotes time-to-the-end-of-current-green-window, t_{next_s} and t_{next_e} denote time to-the-start-of-next-green-window and time-to-the-end-of-next-green-window, respectively. Then the EAD scenario identification protocol can be demonstrated as Algorithm 2.

Algorithm 2: EAD Scenario Identification of the CED Leader When in the I2V Range

Input: available green window T, cruising time-to-arrival t_c, earliest time-to-arrival t_e, latest time-to-arrival t_l
Output: EAD scenario, estimated time-to-arrival t_{arr}

for *all CED leaders in the I2V range* **do**
  if $t_c \in T$ **then**
    cruise scenario, $t_{arr} = t_c$
  else if $[t_e, t_c] \cap T \neq \emptyset$ **then**
    accelerate scenario, $t_{arr} = \min[t_e, t_c] \cap T$
  else if $[t_c, t_l] \cap T \neq \emptyset$ **then**
    decelerate scenario, $t_{arr} = \min[t_c, t_l] \cap T$
  else
    stop scenario, $t_{arr} = t_{next\_s}$
  end if
end for

Once the EAD scenario of the CED leader is identified by Algorithm 2, the CED leader will adopt different longitudinal control models with respect to different scenarios.

If the CED leader is categorized into the cruise scenario, it means this vehicle can travel through the intersection during the green phase without any speed change. Therefore, the reference longitudinal acceleration of this vehicle is zero.

If the CED leader is categorized into the accelerate or decelerate scenario, the vehicle needs to firstly accelerate or decelerate to a certain speed while approaching the intersection. This takes a half period of the trigonometric algorithm, where the reference acceleration of the CED leader during the first quarter period $t \in \left[0, \frac{\pi}{2j_1}\right)$ is

$$a_{ref} = v_{d1} \cdot j_1 \cdot \sin(j_1 t) \tag{4-8}$$

followed by the second quarter period $t \in \left[\frac{\pi}{2j_1}, \frac{\pi}{2j_1} + \frac{\pi}{2k_1}\right)$

$$a_{ref} = v_{d1} \cdot j_1 \cdot \sin\left[k_1 \cdot \left(t + \frac{\pi}{k_1} - t_1\right)\right] \tag{4-9}$$

Upon finishing the first half of the trigonometric algorithm, the CED leader maintains a constant speed and approaches the intersection. When the CED leader departs the intersection, it decelerates or accelerates to the target speed (if $v_h \neq v_{tar}$), which takes the other half period of this trigonometric algorithm. The reference acceleration during the third quarter period $t \in \left[t_{depart}, t_{depart} + \frac{\pi}{2k_2}\right)$ is

$$a_{ref} = v_{d2} \cdot j_2 \cdot \sin\left[k_2 \cdot \left(t + \frac{\pi}{k_2} - t_{depart}\right)\right] \tag{4-10}$$

followed by the last quarter period $t \in \left[t_{depart} + \frac{\pi}{2k_2}, t_{depart} + \frac{\pi}{2j_2} + \frac{\pi}{2k_2}\right)$

$$a_{ref} = v_{d2} \cdot j_2 \cdot \sin\left[j_2 \cdot \left(t - t_{depart} - \frac{\pi}{2j_2} - \frac{\pi}{2k_2}\right)\right] \tag{4-11}$$

In above equations, $v_h = \frac{d_1}{t^{arr}}$, $v_{d1} = v_h - v_1$, $v_{d2} = v_h - v_{tar}$, where v_{tar} is a preset constant that denotes the target speed while departing the intersection;$t_{depart} = \frac{d_2}{v_h}$ denotes time-to-departure; d_2 is a preset constant that denotes the departure distance; k_i and j_i are gains to control the changing rate of acceleration or deceleration, which can be obtained by solving the following optimization problem.

$$\max_{i=1,2} k_i \tag{4-12}$$

subject to

$$\begin{gathered} |k_i \cdot v_{di}| \le a_{max} \\ |{k_i}^2 \cdot v_{di}| \le jerk_{max} \\ k_i \ge \left(\frac{\pi}{2} - 1\right) \cdot \frac{v_h}{d_i} \end{gathered} \tag{4-13}$$

since the vehicle dynamics should subject to the hard constraint of vehicle powertrain's ability, and ride comfort of human passengers. Once k_i is solved, j_i can be calculated by

$$j_i = \frac{-\frac{\pi}{2}k_i - \sqrt{\left(\frac{\pi}{2}k_i\right)^2 - 4{k_i}^2 \cdot \left[\left(\frac{\pi}{2}-1\right) - \frac{d_i}{v_h} \cdot k_i\right]}}{2\left[\left(\frac{\pi}{2}-1\right) - \frac{d_i}{v_h} \cdot k_i\right]}, (i = 1, 2) \tag{4-14}$$

If the CED leader is categorized into the stop scenario, it means the vehicle cannot avoid the red phase by either accelerating or decelerating. The vehicle needs to firstly decelerate all the way to full stop while approaching the intersection, and then accelerate to the target speed while departing. The reference acceleration of the CED leader in this scenario is also calculated by equations (4-8)-(4-11), with

$$t_{depart} = t_{next\_s} \tag{4-15}$$

$$v_h = \frac{v_1}{2} \tag{4-16}$$

$$k_i = j_i = \frac{v_h}{d_i} \cdot \pi \tag{4-17}$$

It should be noted that while the CED leader is in the I2V range and is conducting the EAD maneuver, it also continuously runs Algorithm 1 to check whether potential role transition is needed. There are chances that other vehicles cut in front of the CED leader, so the CED leader will transform into a CED follower and will no longer adopt the piecewise trigonometric-linear EAD algorithm to control its longitudinal movement. If the role of the CED leader stays unchanged, it will still apply EAD algorithm.

When the CED follower is out of the I2V communication range of the intersection, the distributed consensus algorithm is proposed to control its longitudinal movement, which is based upon the distance difference and the speed difference between the ego vehicle and the preceding vehicle. The reference acceleration of the ego vehicle is calculated by the second-order consensus algorithm as

$$a_{ref} = \beta \cdot \left(d_{gap} - d_{ref}\right) + \gamma \cdot (v_{pre} - v_{ego}) \tag{4-18}$$

where β and γ are damping gains; d_{ref} denotes the reference inter-vehicle distance, which can be calculated as

$$d_{ref} = min(d_{gap}, d_{safe}) \tag{4-19}$$

where d_{gap} denotes a time gap-based inter-vehicle distance, which is calculated by the product of ego vehicle's current speed and desired time gap, stated as

$$d_{gap} = v_{ego} \cdot t_{gap} \tag{4-20}$$

When ego vehicle's speed is very low (e.g., $v_{ego} \rightarrow 0$), the reference inter-vehicle distance returned by d_{time} is also very low, which might lead to front-to-rear collision.

Therefore, a minimum allowed inter-vehicle distance d_{safe} is defined to ensure the reference inter-vehicle distance is always higher than a threshold value.

When the CED follower is in the I2V range, it needs to continuously calculate its estimated time-to-arrival based on Algorithm 3. While running Algorithm 3, the CED follower also runs Algorithm 1 with the updated estimated time-to-arrival calculated from Algorithm 3. Some certain outcomes of Algorithm 3 will trigger a role transition in Algorithm 1, which was mentioned earlier in section III as the "string breaker" scenario. In that case, the CED follower will transform into a CED leader and will no longer adopt the distributed consensus algorithm to control its longitudinal movement. If the role of the CED follower stays unchanged, it will still apply the distributed consensus algorithm.

Algorithm 3: Estimated Time-to-Arrival of the CED Follower

Input: available green window T, CED leader's estimated time-to-arrival t_{arr_l}, preceding vehicle's estimated time-to-arrival t_{arr_p}, position of the ego CED follower in the string n, length of a red phase t_{red}, length of an amber phase t_{amber}, desired time headway $t_{headway}$

Output: estimated time-to-arrival t_{arr}

```
for all CED followers in the I2V range do
    t_arr_temp = t_arr_l + n · t_headway
    if t_arr_temp ∈ T then
        t_arr = t_arr_temp
    else
        if t_arr_p ∈ T then
            t_arr = t_arr_p + t_amber + t_red
        else
            t_arr = t_arr_p + t_headway
        end if
    end if
end for
```

4.2.2.4 Simulation and Discussion

We conduct a simulation study on the proposed CED system and evaluate its system-wide impacts. The simulation network is built based upon the six-mile University

Avenue corridor in Riverside, California. We focus on the intersections of University & Cranford, and University & Iowa, where the specific road segments modeled in this simulation study can be illustrated in Figure 4-2. The particular segments of roads that lie between two ends of each black brace are built in traffic simulation environment, where University Avenue has a length of 1084 m, Cranford Avenue has a length of 367 m, and Iowa Avenue has a length of 352 m. The data of signal timing and traffic count on these two intersections are provided by the City of Riverside. Specifically, we use the data collected during 7:00-8:00 AM on Thursday, June. 2nd, 2016 to calibrate the inputs of our simulation network. We select this period since we want to simulate a morning-peak traffic network in a typical weekday. The signal timing data are shown in Table XIV and Table XV, and the traffic count data are shown in Table XVI.

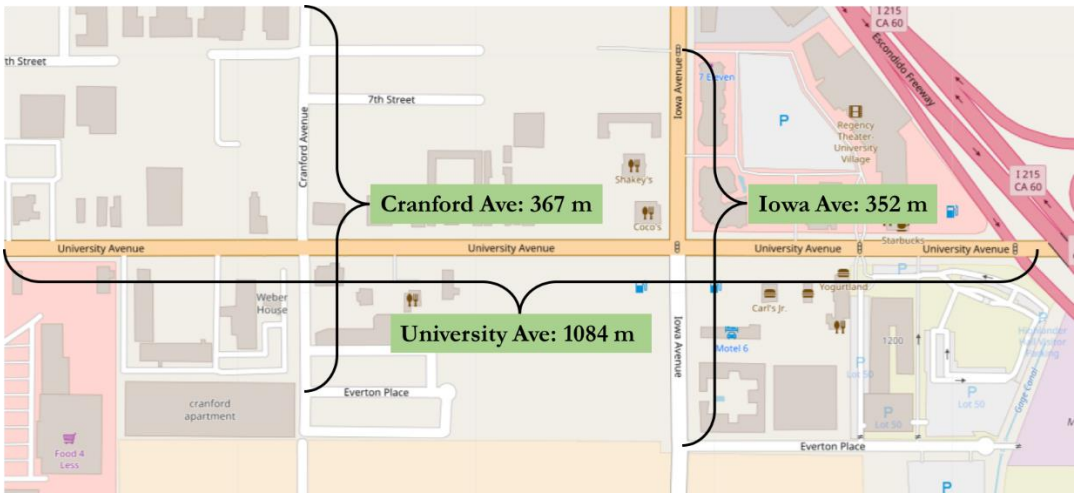

Figure 4-2. Road segments in Riverside, CA that are modeled in this simulation study

Table XIV Signal Timing Data of Cranford Avenue & University Avenue Intersection.

Intersection	Direction	Signal Phase (denoted by color) and Timing (in second)											
Cranford Avenue & University Avenue	North Through	0~23				23~60			60~64	64~100			
	South Through												
	East Left	0~5	5~18	18~22	22~100								
	East Through	0~4	4~80										80~100
	West Left	0~65									65~75	75~79	79~100
	West Through	0~4	4~65								65~100		

Table XV Signal Timing Data of Iowa Avenue & University Avenue Intersection.

Intersection	Direction	Signal Phase (denoted by color) and Timing (in second)											
Iowa Avenue & University Avenue	North Through	0~39						39~68		68~72	72~100		
	South Through												
	North Left	0~21				21~34		34~38		38~100			
	South Left												
	East Left	0~5	5~16	16~20	20~100								
	East Through	0~16		16~20	20~87								87~100
	West Left	0~73									73~82	82~86	86~100
	West Through	0~4	4~73								73~100		

Table XVI Traffic Count Data of University & Cranford Intersection and University & Iowa Intersection.

Intersection	University & Cranford Intersection											
Direction	Northbound			Southbound			Eastbound			Westbound		
	Left	Through	Right	Left	Through	Right	Left	Through	Right	Left	Through	Right
Number of Lanes	0	1	0	0	1	0	1	2	1	1	2	0
Total Volumes	8	4	22	32	5	46	41	367	9	4	282	29
Intersection	**University & Iowa Intersection**											
Direction	Northbound			Southbound			Eastbound			Westbound		
	Left	Through	Right	Left	Through	Right	Left	Through	Right	Left	Through	Right
Number of Lanes	1	2	1	1	2	0	2	2	1	1	2	1
Total Volumes	56	502	54	113	214	102	138	246	31	49	163	91

We adopt PTV VISSIM, a microscopic multi-modal traffic flow simulation software, to build the simulation network of the proposed CED system [81]. Specifically, VISSIM Application Programmer's Interface (API) package enables users to integrate external applications to take influence on the traffic simulation. In this research, we implement the proposed role transition and longitudinal models in the DriverModel.DLL, which can be assigned to specific vehicle types in VISSIM and overwrite the standard driving behavior. Additionally, the EmissionsModel.DLL is provided by VISSIM to add

user-defined emission models, where we implement the U.S. Environmental Protection Agency's MOVES-based model to perform analysis on the environmental impacts of the system [99]. The overall architecture of this simulation study can be illustrated as Figure 4-3.

The simulation traffic network built in VISSIM can be partially illustrated as Figure 4-4 (2D mode) and Figure 4-5 (3D mode). We use light green color for conventional vehicles, and several different colors for CED vehicles based on their scenarios (mainly for debugging and demonstration purposes). All signal controllers in the network are designed based on Table XIV and Table XV, and vehicle volumes are set by Table XVI. Parameters of the traffic network and vehicles in this simulation study are listed in Table XVII.

The microscopic traffic simulation results are shown in Table XVIII, with two baseline scenarios (1) and (2) and ten CED scenarios (3)-(12). Specifically, we also include EAD-Only vehicles in scenario (2), which conduct EAD maneuvers in an ego manner. For EAD-only vehicles, only I2V communications are enabled where they can plan their speed trajectories based on the information received from the infrastructure. V2V communications are not enabled for them, which means they cannot cooperate with each other like CED vehicles. Note baseline scenario (2) already outperforms (1) in terms of all environmental measurements, as shown in Table XVIII.

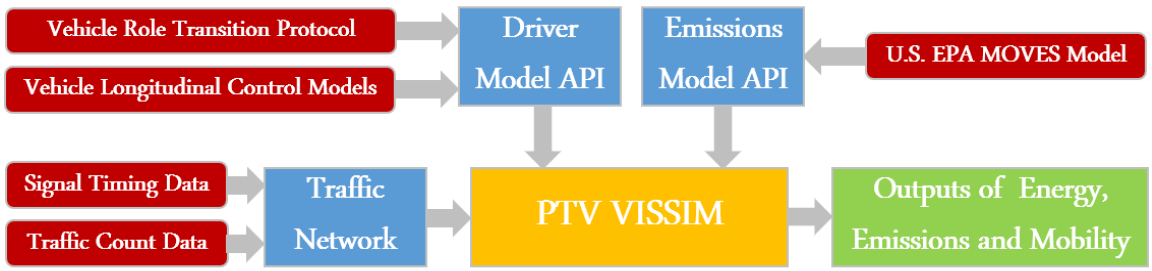

Figure 4-3. System architecture of the simulation study in VISSIM

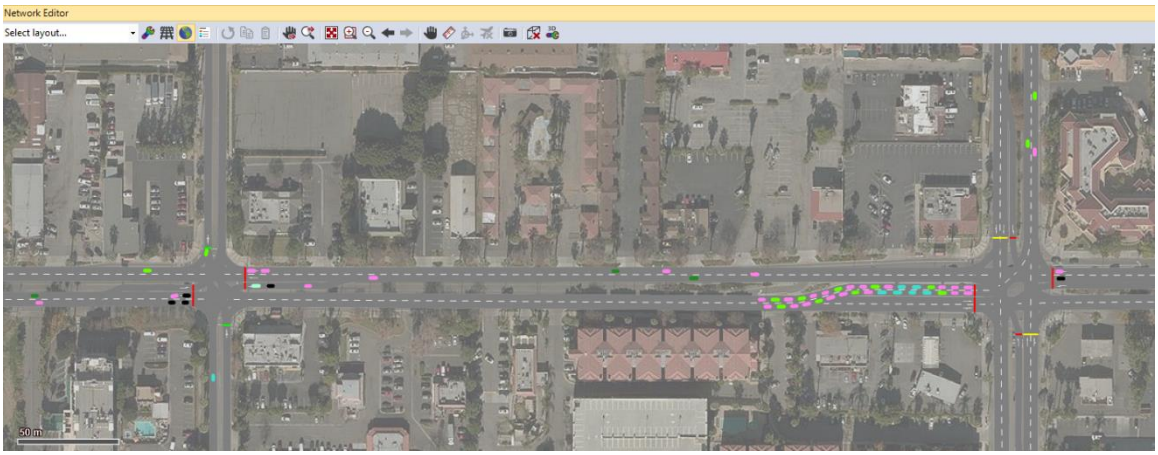

Figure 4-4. University Avenue network built in VISSIM

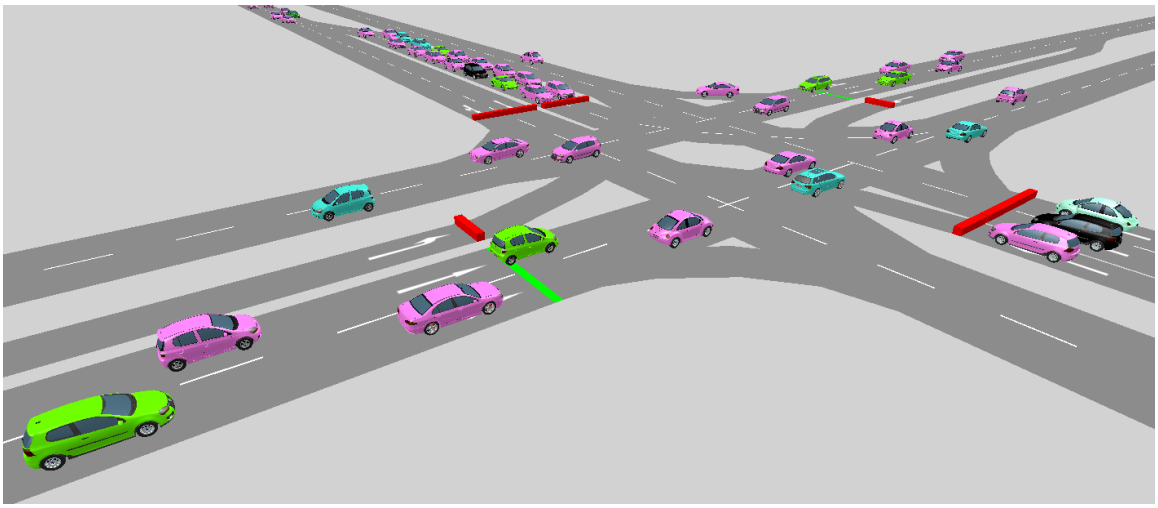

Figure 4-5. Simulation is running in VISSIM with 3D mode

Table XVII Parameters of the Simulation Traffic Network and Vehicles.

Parameters	Value	Parameters	Value
Simulation Date	June 2nd, 2016	Desired Speed of Vehicles v_{des}	20 m/s
Simulation Period	7:00 – 8:00 AM	Free Acceleration Exponent δ	4
Simulation Resolution	10 time steps/second	Damping Gain β	0.58
V2V Communication Range	100 m	Damping Gain γ	1
V2I Communication Range	300 m	Desired Time Gap t_{gap}	0.5 s
Average Standstill Distance $a \cdot x$	2 m	Minimum Allowed Inter-Vehicle Distance d_{safe}	3 m
Additive Part of Safety Distance $b \cdot x_{add}$	2 m	Maximum Allowed Jerk $jerk_{max}$	10 m/s^3
Multiplicative Part of Safety Distance $b \cdot x_{mult}$	3 m	Maximum Allowed Acceleration a_{max}	1.5 m/s^2
Coefficient z	0.5	Maximum Allowed Deceleration d_{max}	-2.5 m/s^2

Table XVIII Simulation Results of Energy Consumption and Pollutant Emissions.

Scenario	Vehicle Composition	Energy		NO_X		HC		CO		CO_2	
(1)	0% CED & 100% Conventional	3924.2 kJ/km		0.051 g/km		0.015 g/km		1.394 g/km		284.9 g/km	
(2)	0% CED & 100% EAD-Only	3737.5 kJ/km		0.044 g/km		0.013 g/km		1.254 g/km		271.3 g/km	
	Reductions ratio with respect to	Sce.(1)	Sce.(2)	Sce.(1)	Sce.(2)	Sce.(1)	Sce.(2)	Sce.(1)	Sce.(2)	Sce.(1)	Sce.(2)
(3)	10% CED & 90% Conventional	-0.3%	-5.4%	7.3%	0.0%	7.8%	-1.2%	7.9%	6.1%	-0.3%	-5.4%
(4)	20% CED & 80% Conventional	-3.1%	-8.2%	14.6%	7.9%	15.4%	7.1%	16.0%	6.1%	-3.1%	-8.2%
(5)	30% CED & 70% Conventional	-4.0%	-9.2%	20.7%	14.5%	21.8%	14.2%	22.5%	-2.3%	-4.0%	-9.2%
(6)	40% CED & 60% Conventional	-12.0%	-17.6%	25.6%	19.7%	26.2%	19.0%	27.8%	6.7%	-12.0%	-17.6%
(7)	50% CED & 50% Conventional	-6.5%	-11.8%	33.3%	28.1%	34.4%	28.0%	35.5%	13.9%	-6.5%	-11.8%
(8)	60% CED & 40% Conventional	-3.1%	-8.2%	37.9%	33.0%	39.6%	33.8%	40.9%	19.8%	-3.1%	-8.2%
(9)	70% CED & 30% Conventional	-0.9%	-5.9%	42.5%	38.0%	44.3%	38.9%	45.2%	28.3%	-0.9%	-5.9%
(10)	80% CED & 20% Conventional	3.9%	-0.9%	46.9%	42.8%	49.2%	44.3%	49.8%	34.3%	3.9%	-0.9%
(11)	90% CED & 10% Conventional	6.5%	1.8%	49.9%	46.0%	51.0%	46.2%	54.5%	39.1%	6.5%	1.8%
(12)	100% CED	7.1%	2.5%	54.6%	51.1%	56.7%	52.5%	59.0%	44.3%	7.1%	2.5%

With respect to CED scenarios, positive impacts on NOx, HC and CO can be observed at any penetration rate of CED vehicles in the traffic system. However, when there are less than 70% CED vehicles in the traffic system, negative impacts on energy and CO2 can be observed compared to these two baseline scenarios. Especially, as can be seen from Table XXIV, the worst scenario in terms of energy consumption and CO2 emission is with 40% CED vehicles in the traffic network. There are basically two reasons for this behavior:

The introduction of CED vehicles brings about conservative driving behaviors to the traffic network: When they know they can travel through the intersection during the green window with current speed, they approach the intersection by cruising instead of accelerating. When they depart the intersection after a full stop during the red window, they conduct an eco-departure maneuver with low acceleration process to save energy.

Such conservative driving behaviors surely impede the movements of conventional vehicles, which always try to travel through the intersection as fast as possible. A very good example of this can be observed in Figure 4-4, specifically at the right intersection (Iowa Avenue & University Avenue). As can been seen from Table XVI, the volume of eastbound left-turn vehicles at that intersection during that one hour is 138, however, there is only an 11-second green window during a 100-second signal cycle on that direction (derived from Table XV). Therefore, the relatively slow departure rate of CED vehicles introduces a long queue along the upstream of eastbound University Avenue, so many through vehicles have to make unnecessary speed changes/full stops and consume more energy.

Since the proposed cooperative eco-driving methodology focus on collaborations among different CED vehicles, when the penetration rate of CED vehicles in the traffic network is lower than some certain threshold, it is difficult for CED vehicles to connect with each other and conduct collaborative maneuvers, and therefore brings about negative impacts on energy consumption. Based on the simulation results, 40% is the threshold when CED vehicles are not enough in the traffic network to conduct cooperative eco-driving maneuver, so the energy consumption comes out as the worst-case scenario. When the penetration rate of CED vehicles is higher than 40%, it starts to compensate the negative impacts on conventional vehicles, so the energy consumption becomes better.

As can be seen from Table XVIII, when there are enough CED vehicles in the traffic system, positive environmental impacts are shown. Specifically, compared to baseline scenario (1), 3.9% reduction on energy consumption can be observed when there are 80%

CED vehicles. When all vehicles are CED vehicles, 7.1% and 2.5% reduction on energy consumption can be observed compared to baseline scenario (1) and (2), respectively. These results indicate that, only when the penetration rate of CED vehicles in the traffic system is high enough, the proposed CED system can work efficiently with more CED followers, instead of conventional vehicles, follow the movements of CED leaders and conduct eco-driving in a cooperative manner. It shall also be noted that CACC maneuver introduces energy savings for string followers since the reduction of their aerodynamic drag, but this factor is not included in the MOVES-based model. Therefore, if we consider aerodynamic drag of vehicle in the energy consumption model, the proposed system will get further reductions of energy consumption and pollutant emissions.

4.2.3 Cluster-Wise Eco-Approach and Departure

4.2.3.1 Methodology

The difference of this cluster-wise EAD with aforementioned CACC-enabled EAD lies on the information flow topology of CAVs. In the former approach, different CACC strings operate in an isolated manner, with role transitions happened only within a certain vehicle string. However, this cluster-wise approach enables the collaborations among different string by allowing string leaders to communicate with each other. The information flow topology of this approach is shown as Figure 4-6.

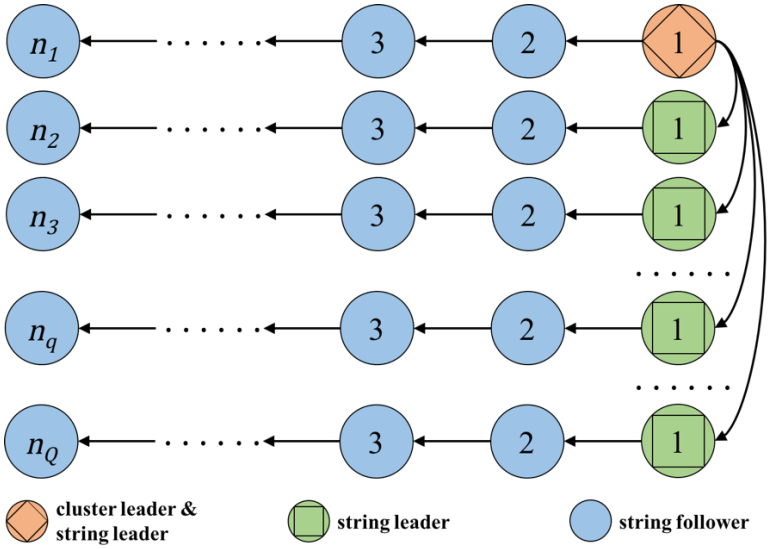

Figure 4-6. Information flow topology of cluster-wise EAD

The information flow topology shows that the number of strings and the number of vehicles in one string are both not constrained by the topology. In the cluster network, the cluster leader also works as a string leader. It not only needs to send information to the other string leaders as a cluster leader, but also sends information to its string follower as a string leader. The previously proposed consensus algorithm (3-12) is applied to all vehicles in the cluster except for the cluster leader, since the cluster leader does not have a predecessor to follow. For each string follower, it adjusts its longitudinal speed and relative longitudinal position with respect to its predecessor by equation (3-12). For each string leader (cluster leader excluded), it adjusts its longitudinal speed and relative longitudinal position with respect to the cluster leader, which works as a "predecessor" for all these string leaders. Since each string leader (cluster leader excluded) is on a different lane from the one the cluster leader is on, the relative longitudinal position between a string leader

and the cluster leader might be zero (but not necessarily), i.e., they are driven parallel to each other on adjacent lanes.

4.2.3.2 Simulation and Discussion

A MATLAB/Simulink model has been set up and used to conduct numerical simulation of the proposed Coop-EAD application, and the U.S. Environmental Protection Agency's MOVES model has been adopted to perform analysis on the environmental impacts of the proposed application. The results are also compared to the Ego-EAD application along urban signalized arterials, where vehicles conduct EAD maneuvers with respect to intersections in an ego way.

The general parameters of this simulation are set in Table XIX. To get a more explicit result, we assume all vehicles in this simulation to be identical, i.e., they have the same vehicle length, GPS antenna location on the vehicle, and braking factor. The starting time of this simulation is 0 s, and the order of the signal phase is set to be red-green-yellow-red-green-yellow. These 16 vehicles are distributed on these two lanes (a and b) with different initial speeds and initial distances to the intersection, as listed in Table XX.

Table XIX Values of Simulation Parameters.

Parameter	*Value*
Number of Cars (N)	16
Number of Lanes (J)	2
Simulation Time Step	0.1 s
Actuator and Communication Delay (τ)	60 ms
Roadway Speed Limit (v_{lim})	17.88 m/s
Maximum Acceleration (a_i^{max})	3.5 m/s^2
Maximum Deceleration (d_i^{max})	-3.5 m/s^2
GPS Antenna to Front Bumper (l_{if})	3 m
GPS Antenna to Rear Bumper (l_{jr})	2 m
Braking Factor (b_i)	1
Desired Time Headway (t_{ij}^h) for Ego-EAD	2 s
Desired Time Headway (t_{ij}^h) for Coop-EAD	1 s
Minimum Inter-Vehicle Gap (d_{safe})	2 m
Red Window (not allowed to travel through)	27 s
Green Window (allowed to travel through)	8 s
Yellow Window (not allowed to travel through)	2 s

Table XX Values of Vehicle Parameters.

Vehicle Index	*Lane/Sequence Index*	*Initial Speed*	*Initial Distance to Intersection*
1	*a*/1	13.41 m/s	300 m
2	*a*/2	14.32 m/s	344 m
3	*a*/3	14.42 m/s	374 m
4	*b*/1	14.10 m/s	321 m
5	*b*/2	12.39 m/s	372 m
6	*a*/4	13.09 m/s	428 m
7	*b*/3	13.12 m/s	417 m
8	*a*/5	12.44 m/s	452 m
9	*a*/6	12.77 m/s	494 m
10	*b*/4	13.88 m/s	470 m
11	*b*/5	13.29 m/s	529 m
12	*b*/6	12.67 m/s	552 m
13	*a*/7	12.64 m/s	530 m
14	*b*/7	13.08 m/s	588 m
15	*a*/8	13.22 m/s	584 m
16	*a*/9	13.30 m/s	700 m

For the Ego-EAD application, based on the desired time headway and SPaT information, these 16 vehicles can be assigned into two clusters stated in Table XXI. On the other hand, for the Coop-EAD application. A and B, vehicles can be assigned into two clusters with adjusted sequences inside each cluster, which is demonstrated in Table XXII. Then we can apply the Ego-EAD algorithm to vehicles in the Ego-EAD application, and apply the proposed operating modes to vehicles in the Coop-EAD application, respectively. The trajectories of all vehicles on lane a and lane b of both applications are illustrated in

Figure 4-7 and Figure 4-8. The y axis of both figures denote vehicle's distance to intersection. That is to say, the intersection is located at 0 m of the y axis.

Table XXI Ego-EAD Vehicle Clusters and Sequences.

Sequence	*Lane a*	*Lane b*	*Cluster*
1	Vehicle 1	Vehicle 4	Cluster 1:
2	Vehicle 2	Vehicle 5	Travel through the intersection
3	Vehicle 3	Vehicle 7	in the first green window
4	Vehicle 6	Vehicle 10	(27 s – 35 s)
5	Vehicle 8	Vehicle 11	
6	Vehicle 9	Vehicle 12	Cluster 2:
7	Vehicle 13	Vehicle 14	Travel through the intersection
8	Vehicle 15		in the second green window
9	Vehicle 16		(64 s – 72 s)

Table XXII Coop-EAD Vehicle Clusters and Sequences.

Sequence	*Lane a*	*Lane b*	*Cluster*
1	Vehicle 1	Vehicle 4	
2	Vehicle 2	Vehicle 5	
3	Vehicle 3	Vehicle 7	Cluster 1:
4	Vehicle 6	Vehicle 8	Travel through the intersection
5	Vehicle 10	Vehicle 9	in the first green window
6	Vehicle 11	Vehicle 13	(27 s – 35 s)
7	Vehicle 12	Vehicle 15	
8	Vehicle 14		
9	Vehicle 16		Cluster 2:
			Travel through the intersection
			in the second green window
			(64 s – 72 s)

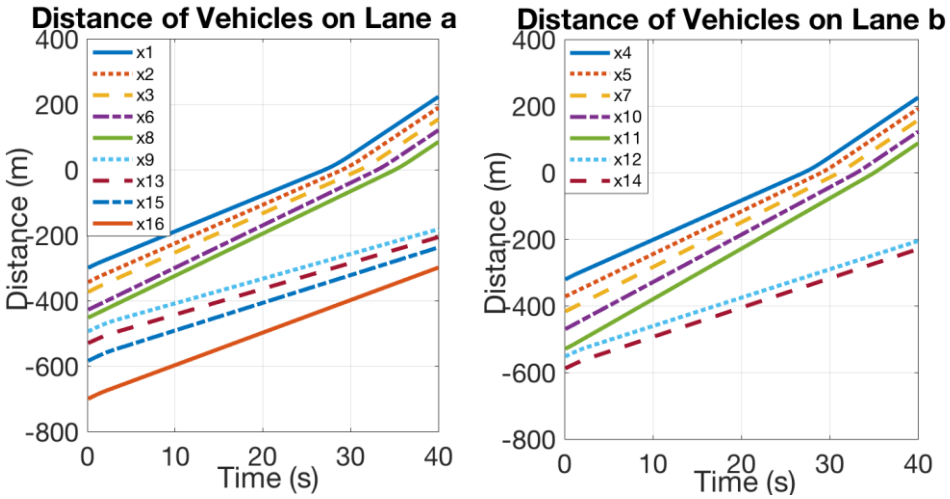

Figure 4-7. Vehicle trajectories of Ego-EAD

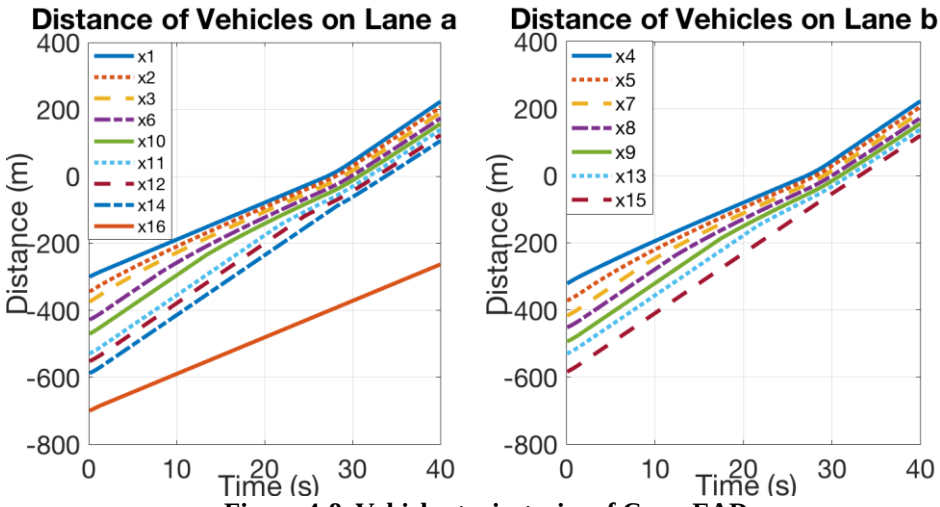

Figure 4-8. Vehicles trajectories of Coop-EAD

Since Coop-EAD application takes advantage of V2V communication, CAVs are allowed to follow others with shorter time headways compared to Ego-EAD application. Namely speaking, more CAVs can be squeezed into one green phase to pass the intersection. As shown in the figures, in the Ego-EAD application, only 5 vehicles on lane a and 5 vehicles on lane b can travel through the intersection during the first green window, respectively. However, in the Coop-EAD application, all vehicles but vehicle 16 on lane a and all vehicles on lane b travel through the intersection during the first green window, respectively. Specifically, vehicle 16 on lane a cannot catch up with the cluster due to the roadway speed limit, i.e., even if it travels with the speed v_{lim}, it cannot shorten the time headway to 1 s with its preceding vehicle. Based on the results, we can conclude that by adopting the proposed Coop-EAD application, an ((15–10)/10=) 50% increase on traffic throughput can be achieved in this scenario.

In this dissertation, the MOVES model is adopted to perform the multiple scale analysis on the environmental impacts of the proposed application. The MOVES model is capable of estimating tailpipe emissions from mobile sources, which covers a wide

spectrum of pollutants including carbon monoxide (CO), hydrocarbons (HC), and oxides of nitrogen (NOX). During the modeling process, a quantity of information is required as the system inputs, including vehicle type, driving cycle, acceleration and deceleration, and road grade. This model preforms a range of calculations based upon predefined look-up tables (which are developed to precisely characterize vehicle operating process), and then provides estimates of system-wise energy consumption and pollutant emissions.

After the MOVES model is adopted to analyze the environmental impacts of these two applications, a comparison result of the average energy consumption and pollutant emissions per vehicle per trip are shown in Table XXIV. As can be seen from the results, the proposed Coop-EAD application can further reduce energy consumption by 11% in this simulation, when compared to Ego-EAD application. Regarding to pollutant emissions, the proposed Coop-EAD application can further reduce up to 18% PM2.5, when compared to the Ego-EAD application. The decreases of energy consumption and pollutant emissions are introduced by the Coop-EAD application based on the following reasons:

- Vehicles originally cannot pass the intersection during the first green window can now catch up with their predecessors and pass the intersection (due to shorter inter-vehicle gap). Therefore, unnecessary full stop at the intersection can be avoided by those vehicles.
- Instead of vehicles are driven in an ego manner, vehicles in the Coop-EAD application can be driven cooperatively with V2V communication, where unnecessary speed fluctuations can be avoided.

It should be noted that although our vehicle dynamics model takes aerodynamic drag into account, in our simulation, the benefit from shorter inter-vehicle gap is not integrated to calculate the aerodynamic drag. Otherwise, greater decreases of energy consumption and pollutant emissions can be expected in the results.

Table XXIII Comparison of Energy Consumption and Pollutant Emissions of Ego-EAD and Coop-EAD.

	HC (g)	*CO (g)*	*NO_X (g)*	*CO_2 (g)*	*PM2.5 (g)*	*Energy (KJ)*
Ego-EAD	0.041	1.398	0.144	159.8	0.011	2222.94
Coop-EAD	0.037	1.161	0.141	142.3	0.009	1978.15
Decrease%	9.76	16.95	2.08	10.95	18.18	11.01

4.3 Cooperative Merging at Highway On-Ramps

4.3.1 Introduction and Background

Researchers around the world have been developing various CAV applications to address traffic-related issues and improve efficiency and safety in specific traffic scenarios such as highway on-ramp merging. A literature review on the coordination of CAVs merging at highway on-ramps was conducted by Rios-Torres et al., which summarized the developments and research trends in this research topic [43]. It can be noted that the optimal control approach has been adopted by many of the recent on-ramp merging works. However, the approaches proposed in those previous works have one or more of the following limitations: 1) Some of the methods are not always suitable for real-time implementation due to the difficulty in finding an optimal solution; 2) A vehicle is considered in a single form, making it difficult to extend to a vehicle string; 3) Benefits of

energy efficiency and pollutant emissions are not typical considered. The cooperative ramp merging system proposed in this paper is aimed at addressing these limitations.

4.3.2 Distributed Consensus-Based Cooperative On-Ramp Merging

4.3.2.1 Vehicle Sequencing Protocol

The vehicle sequencing protocol is designed to arrange vehicles with a predefined sequence, so they can cooperate with each other before merging, avoiding high risks of collisions and excessive energy consumption and pollutant emissions upon reaching the merging point. This protocol can be broken down into three procedures: a) Calculation of the maximum reachable speed of on-ramp vehicles; b) Calculation of the estimated arrival time; c) Assignment of vehicle sequence identification.

Parameters used in this protocol are defined in two groups below. Parameters in the first group are directly measurable by vehicles or infrastructures, therefore are assumed to be known:

s_h — Distance on the rightmost lane of highway from the I2V communication starting point to the merging point;

s_r — Distance on the on-ramp from the I2V communication starting point to the merging point;

v_{lim} — Highway speed limit;

v_{hs_i} — Speed of vehicle i when reaching the I2V communication starting point on the rightmost lane of highway;

v_{hs_avg} — Average speed of vehicles when reaching the I2V communication starting point on the rightmost lane of highway during the past time window $[0, t_{window}]$;

v_{rs_j} — Speed of vehicle j when reaching the I2V communication starting point on the on-ramp;

v_{rs_avg} — Average speed of vehicles when reaching the I2V communication starting point on the on-ramp during the past time window $[0, t_{window}]$;

a_{max} — Maximum acceleration of vehicles without compromising safety and comfort.

When vehicles reach the I2V communication starting point on both the rightmost lane of highway and the on-ramp, they send their speed information to the RSU-equipped infrastructure. Therefore, the infrastructure can calculate average speeds of vehicles reaching both points (v_{hs_avg}, v_{rs_avg}) during the past time window $[0, t_{window}]$, which reflect recent traffic conditions on both lanes.

Parameters in the second group are not directly measurable by vehicles or infrastructures, and they can be calculated by the methods demonstrated later in this section:

t_{acc} — Minimum time spent by on-ramp vehicles accelerating from v_{rs_avg} to v_{lim};

s_{acc} — Distance travelled by on-ramp vehicles accelerating from v_{rs_avg} to v_{lim};

v_{rm_max} — Maximum reachable speed of on-ramp vehicles when reaching the merging point;

t_{r_min} — Minimum reachable time spent by vehicles on the on-ramp;

t_{h_i} — Estimated time spent by vehicle i travelling the distance of s_h;

t_{r_j} — Estimated time spent by vehicle j travelling the distance of s_r;

t_{head_safe} — Safety time headway;

t_{head_V2V} — V2V connection time headway;

v_m — Estimated merging speed.

Vehicles coming from arterials to highways are most likely to accelerate while travelling through the on-ramp, therefore we want to calculate the maximum reachable speed of on-ramp vehicles based on known parameters. Since the highway speed limit v_{lim} is assumed to be known, we can calculate the minimum reachable time spent by on-ramp vehicles accelerating from v_{rs-avg} to v_{lim} as

$$t_{acc} = \frac{v_{lim} - v_{rs-avg}}{a_{max}} \tag{4-21}$$

Therefore, this accelerating distance is

$$S_{acc} = \frac{(v_{rs-avg} + v_{lim}) t_{acc}}{2} = \frac{{v_{lim}}^2 - {v_{rs-avg}}^2}{2a_{max}} \tag{4-22}$$

The on-ramp calculation process can then be divided into two different cases based on this acceleration process. The first case is $s_r < s_{acc}$, which means that on-ramp vehicles cannot accelerate to highway speed limit v_{lim} before merging, which most likely to happen when the on-ramp is short. We can calculate the maximum reachable speed based on Figure 4-9.

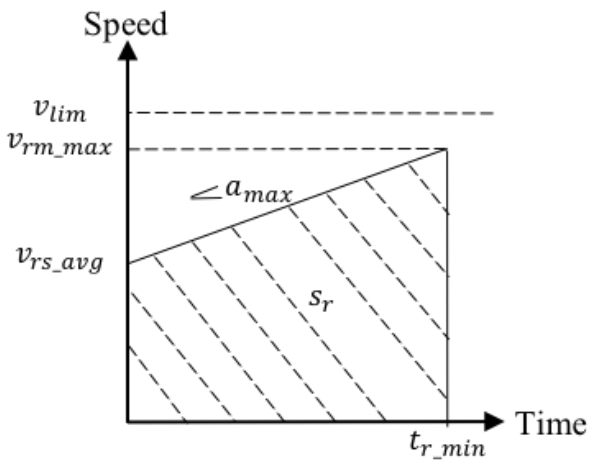

Figure 4-9 Maximum reachable speed of on-ramp vehicles when reaching the merging point without accelerating to highway speed limit

The maximum reachable speed of on-ramp vehicles when reaching the merging point can be derived as

$$v_{rm\_max} = v_{rs\_avg} + a_{max} t_{r\_min} \tag{4-23}$$

And based on Figure 4-9, we can get the following equation

$$s_r = \frac{(v_{rs\_avg} + v_{rm\_max}) t_{r\_min}}{2} \tag{4-24}$$

Therefore, combining above equations, the following variables can be derived as

$$t_{r\_min} = \frac{-v_{rs\_avg} + \sqrt{{v_{rs\_avg}}^2 + 2 a_{max} s_r}}{a_{max}} \tag{4-25}$$

$$v_{rm\_max} = \sqrt{{v_{rs\_avg}}^2 + 2 a_{max} s_r} \tag{4-26}$$

For the case that $s_r > s_{acc}$, on-ramp vehicles can accelerate to highway speed limit v_{lim} before merging. The vehicle speed trajectory can be illustrated by Figure 4-10. In this case, the maximum reachable speed of on-ramp vehicles is

$$v_{rm\_max} = v_{lim} \tag{4-27}$$

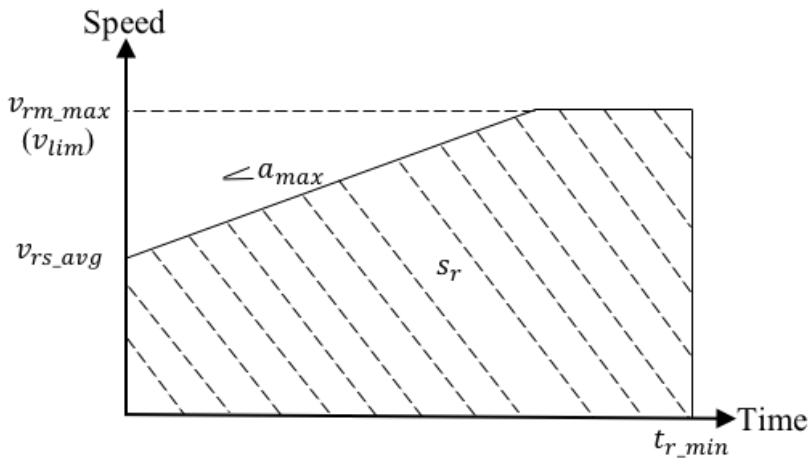

Figure 4-10 Maximum reachable speed of on-ramp vehicles when reaching the merging point with highway speed limit

The estimated arrival time is calculated to assign SID to each vehicle in the system. Since it is estimated before a vehicle actually travels to the merging point, the result may vary from the actual arrival time. However, since the actual arrival time of vehicles usually vary by relatively large values based on the errors we introduce, the estimated values we calculate are already effective enough to be sorted in order of time.

Since the values of v_{rm_max} can be calculated by known parameters for both cases above, we can categorize the calculation of vehicle estimated arrival time into two scenarios, and set the estimated merging speed v_m to be the lower one of v_{hs_avg} and v_{rm_max}. The reason we consider the average speed of highway vehicles but the maximum reachable speed of on-ramp vehicles is that on-ramp vehicles are supposed to accelerate on the on-ramp, but highway vehicles are more likely to maintain rather stable speeds in a short segment.

For the first case that, if $v_{hs\_avg} \leq v_{rm\_max}$, then $v_m = v_{hs\_avg}$. Since the merging speed is set to v_{hs_avg}, we can derive the estimated time spent by vehicle i traveling the distance of s_h on the rightmost lane of highway by

$$t_{h\_i} = \frac{s_h}{v_{hs\_i}} \tag{4-28}$$

In this case, since on-ramp vehicles reach v_{hs_avg} before merging, the speed trajectory of vehicle j has the same shape as in Figure 4-10 (though parameters in the figure are different). We can derive estimated time spent by vehicle j travelling the distance of s_r on the on-ramp by

$$t_{r\_j} = \frac{2a_{max}s_r + (v_{hs\_avg} - v_{rs\_j})^2}{2a_{max}v_{hs\_avg}} \tag{4-29}$$

For the second case that, if $v_{hs-avg} > v_{rm-max}$, then $v_m = v_{rm-max}$. Since the merging speed is set to v_{rm-max}, based on Figure 4-11 we can derive the estimated time spent by vehicle i travelling the distance of s_h on the rightmost lane of highway by

$$t_{h\_i} = \frac{2a_{max}(s_h - s_r) - (v_{hs\_i}{}^2 + v_{rs_{avg}}{}^2) + 2v_{hs\_i}\sqrt{v_{rs\_avg}{}^2 + 2a_{max}s_r}}{2a_{max}\sqrt{v_{rs\_avg}{}^2 + 2a_{max}s_r}} \tag{4-30}$$

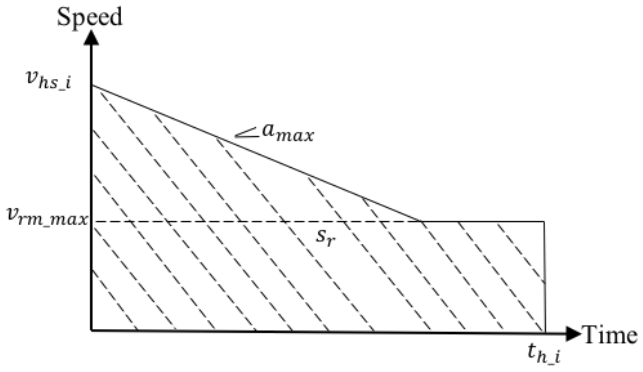

Figure 4-11 Deceleration process of vehicle i travelling the distance of s_h on the rightmost lane of highway

In this case, since on-ramp vehicles do not reach v_{hs_avg} before merging, the speed trajectory of vehicle j has the same shape as in Figure 4-9 (though parameters in the figure are different). Since the merging speed is set to be the same as v_{rm-max}, we can derive estimated time spent by vehicle j travelling the distance of s_r on the on-ramp by

$$t_{r\_j} = \frac{-v_{rs\_j} + \sqrt{{v_{rs\_j}}^2 + 2a_{max}s_r}}{a_{max}} \tag{4-31}$$

Once the estimated time spent by each vehicle travelling through the I2V communication area is calculated, the estimated arrival time at the merging point can be easily get by adding the estimated spending time (t_{h_i} or t_{r_j}) to the current time while vehicle i or vehicle j reaches the I2V communication starting point. Different from estimated spending time, which is a time segment (e.g., 10.5 s), the estimated arrival time is the time of day (e.g., 15:08:10:5).

Since the estimated arrival time is calculated based on different vehicles' speeds when reaching the I2V communication starting point (v_{hs_i} and v_{rs_j}), it is possible that the estimated arrival time of a follower is earlier than its predecessor on the same lane. In that case, the estimated arrival time of the follower is defined as t_{head_safe} later than the estimated arrival time of the predecessor. If a highway vehicle and an on-ramp vehicle have the same estimated arrival time, then the estimated arrival time of the on-ramp vehicle is defined as t_{head_safe} later than that of the highway vehicle. Upon receiving the estimated arrival time of every vehicle in the I2V communication area, the infrastructure sorts vehicles in the network in order of time, and assign them with consecutive SIDs.

Once vehicles are assigned with different SIDs, they are allowed to connect with others through V2V communications, and then apply the distributed consensus algorithm to merge in a cooperative manner. The algorithm we adopt for this cooperative merging scenario is already presented as (3-11) and (3-12), so we will not cover it in this section.

4.3.2.2 Agent-Based Modeling using Unity

A vehicle is modeled as a game object in Unity, which always includes a rigid body and its associated colliders. By applying forces or torque to the vehicle's rigid body, the vehicle will start to move. Forces such as gravity, friction, drag and angular drag also have effects on the movement of a vehicle. Compared to real world environment, time in Unity is discrete (default simulation time step is 0.02 s), so the accumulative force acts on the vehicle's rigid body at the start of each simulation time step, and resets to zero before the start of the next simulation time step.

Colliders are components defined by Unity to simulate physical collisions between two rigid bodies. Since colliders are the major physical parts of game objects, they also define the shapes and sizes of game objects in the simulation. Wheel colliders, specifically, are colliders of game objects that interact with the simulation environment in Unity. In our cooperative on-ramp merging case study, we adopt two different vehicle models with realistic dimensions in the real world, which are shown in Figure 4-12 (a) and (b).

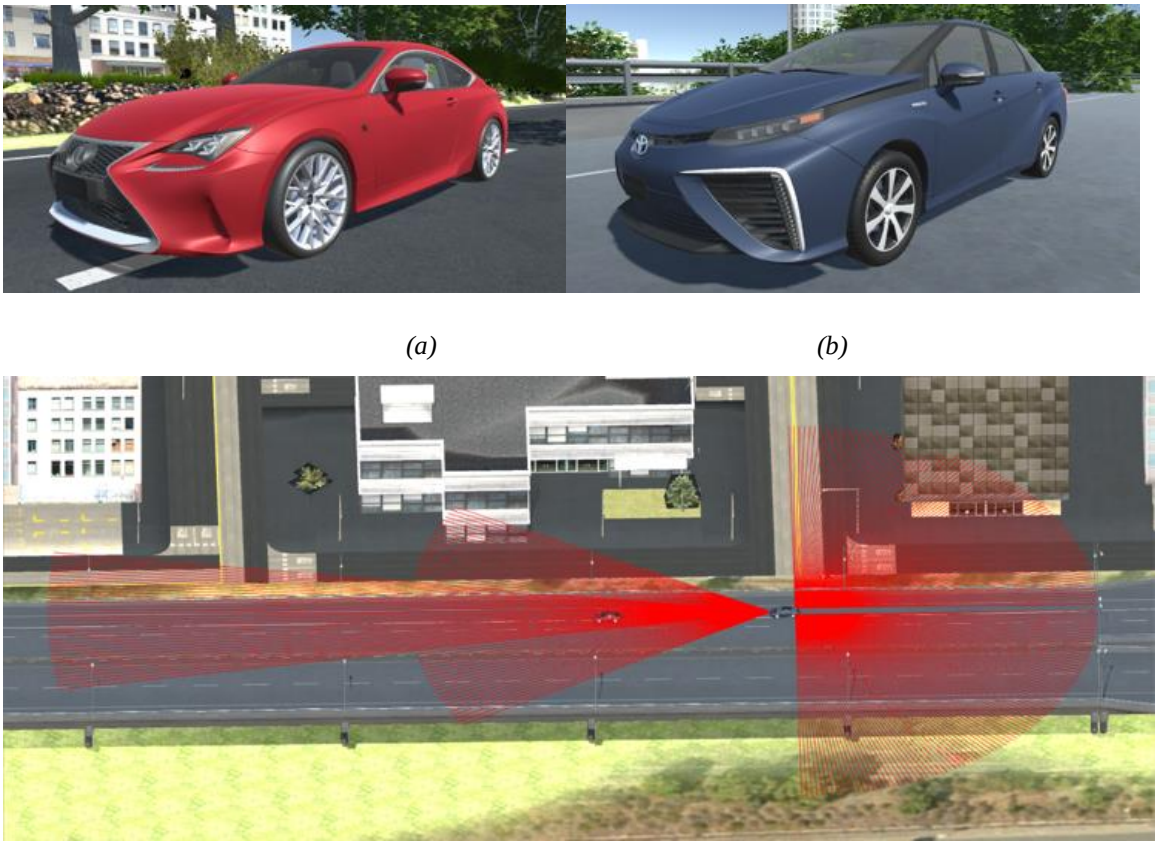

(a) *(b)*

(c)

Figure 4-12. Vehicle models (a, b) and radar illustration (c) built in Unity

In order to enable vehicles with CAV technology in Unity, scripts with cooperation protocol are attached to enable their connectivity, and sensors are integrated to enable their autonomy. Specifically, a script written in Unity's C#-based Mono Scripting API is attached to all merging vehicles, which allows those CAVs to retrieve information from the infrastructure and other vehicles through V2X communications. This script also controls CAV's longitudinal movements by the proposed online feedforward/feedback longitudinal control algorithm. Since we mainly focus on the longitudinal control of CAVs in this case study, the Simple Waypoint System is adopted, where a vehicle can track the preset trajectory with a user-defined longitudinal speed [98]. Additionally, four radar

sensors, including long/short-range front radars and left/right blind spot radars, are equipped on each CAV. As shown in Figure 4-12 (c), the long-range front radar has a relative narrow angle and long detection distance, so it is appropriate to be considered the primary front sensing approach. In order to prevent any rear-end collisions, the long-range front radar and the short-range front radar (redundant sensor) continuously check the distance to the physical preceding vehicle on the same lane.

(a)

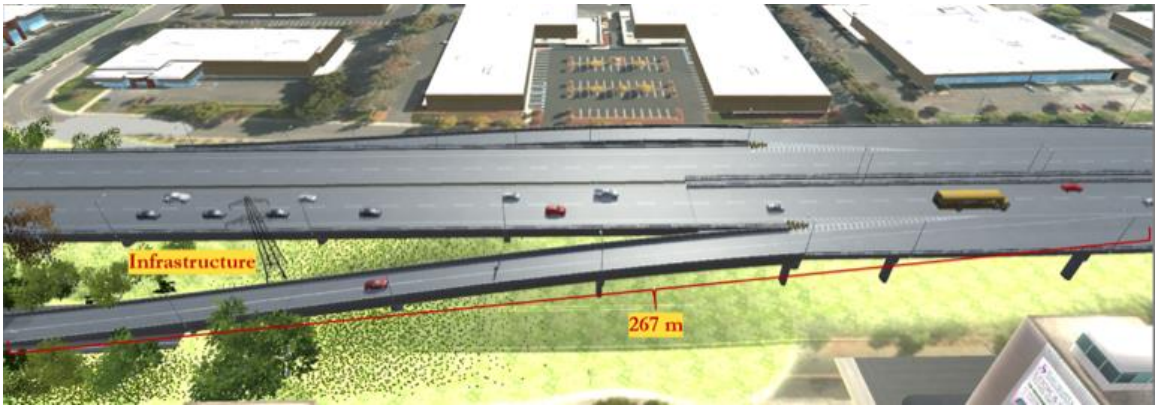

(b)

Figure 4-13. Game environment of Mountain View, California (A) and infrastructure (b) built in Unity

In order to conduct ABMS for CAVs, we build a simulation environment in Unity partially based on the city of Mountain View, California as shown in Figure 4-13 (a). California State Route 237 (CA-237) is the major corridor in this environment, with several on-ramps and off-ramps connecting it with urban arterial roads. In this dissertation, we conduct the case study based on the on-ramp which connects E Middlefield Rd and CA-237 westbound. As shown in Figure 4-13 (b), this on-ramp has a length of 267 meter, with a roadside unit-equipped infrastructure positioned between the on-ramp and main line. There is also an elevation difference between the on-ramp and main line, which means the vision of the on-ramp vehicle's driver is obstructed for a long period before merging.

In this simulation environment, a game object associated with a sphere collider is used to simulate the I2V-enabled infrastructure. Essentially, the center of the sphere collider is positioned at this game object (which is represented by a power tower in Figure 4-13 (b)), and the sphere collider's radius can be set as the I2V communication range. The 'isTrigger" function of the sphere collider is enabled to prevent any collisions with incoming vehicles, otherwise vehicles cannot enter the volume of this collider. After setting this sphere collider to "isTrigger", when a vehicle enters and exits its volume, it sends "OnTriggerEnter" and "OnTriggerExit" messages. Then we can attach a configuration script to this game object to call these functions, and integrate the aforementioned vehicle sequencing protocol into the script. Namely, when a vehicle enters the radius of this sphere collider (i.e., enters the I2V communication range of the infrastructure), the "OnTriggerEnter" function is called, and the infrastructure retrieve information from the vehicle through "GetComponent" function. The infrastructure then processes this

information along with other information retrieved from all other entering vehicles during a certain time window, and sends the sequence identification number back to each vehicle at the next time step of sorting process. Once a vehicle exits the radius of this sphere collider, the "OnTriggerExit" function is called, and the infrastructure clear all stored information of this vehicle.

The information sent from a vehicle to the infrastructure includes its longitudinal speed, acceleration, and the global position. Since the distance to the merging point of a vehicle is needed to calculate its estimated arrival time, we also come up with a map matching system to convert the global position of a vehicle into its distance to the merging point. Since the road segment is neither straight nor flat, we cannot simply calculate the distance between the vehicle's position and the merging point's position. Instead, we build paths with multiple waypoints along the lanes of both main line and on-ramp. Whenever the infrastructure gets the global position of a vehicle, it firstly compares the position with all waypoints' positions on that path to figure out which path segment this vehicle is currently on and what the next waypoint is. Once finished, the distance to the merging point of this vehicle is the sum of its distance to the next waypoint and the path length from the next waypoint to the merging point.

It should be noted that building such a CAV simulation environment which conforms to various test criteria requires huge efforts from developers. Test criteria are oftentimes decided by different OEMs, CAV features to be tested, and the level of confidence obtained from previous tests. In order to construct similar realistic test

environment in the virtual simulation in an automatic manner, one needs to come up with some test case generation protocol, which is discussed in the reference [89].

4.3.2.3 Agent-Based Simulation and Results

In this dissertation, we study the case where one on-ramp vehicle tries to merge with a six-vehicle string traveling in the mainline. The proposed cooperative on-ramp merging protocol is applied to all these seven vehicles. There are other vehicles on the on-ramp and in the mainline, but they are all conventional vehicles and are running with a cruise speed of 20 m/s in their own lanes, so they will not affect the cooperative merging process. Hence, they are not considered when we analyze simulation results. The on-ramp vehicle is discharged from the starting point of the on-ramp at an initial speed of 5 m/s. The mainline vehicles are discharged from the upstream of the mainline (which is outside the I2V communication range of the infrastructure) with random initial speeds and longitudinal positions. Before they reach the I2V communication starting point, they are driven in a vehicle string at a desired speed of 20 m/s and with a desired time-gap of 0.5 s. Upon the mainline vehicles arriving at the I2V communication starting point, the vehicle string has already been formed with a stable state.

(a)

(b)

(c)

Figure 4-14. Cooperative on-ramp merging process

Figure 4-14 illustrates the cooperative on-ramp merging process in this simulation. Figure 4-14 (a) shows the state when the mainline vehicles have already formed the vehicle string, but have not entered the I2V communication range yet. Figure 4-14 (b) shows that the on-ramp vehicle and all mainline vehicles are already inside of the I2V communication range, and a sequence identification number of "2" is assigned to the on-ramp vehicle. Therefore, the mainline vehicle with a sequence identification number of "3" is decelerating to create a gap for the on-ramp vehicle to merge. When the on-ramp vehicle

is about to merge, as shown in Figure 4-14 (c), the gap has already been created and no further longitudinal speed adjustments are needed.

Human-in-the-Loop Simulation with Driver Simulator Platform. After running the simulation with all the vehicles controlled by the proposed online feedforward/feedback longitudinal controller, we also conduct human-in-the-loop simulations where the merging vehicle is controlled by a human driver on a driving simulator as shown in Figure 4-15. In this scenario, the on-ramp vehicle is a conventional vehicle with no connectivity and autonomy, while all six mainline vehicles are still CAVs. A mainline vehicle can sense the on-ramp vehicle by its long-range front radar once the on-ramp vehicle cuts in front.

Figure 4-15. Driving simulator platform

Given the fact that Unity allows users to change user input in its graphical user interface (GUI) very easily, the Logitech driving simulator (or potentially any other plug-in-and-play driving simulators) can be connected to Unity by simply plugging in the USB

cable. A car user control script and a car controller script work together to allow a human driver to control the longitudinal and lateral movements of the vehicle on the driving simulator platform. The car user control script receives horizontal input from the driving simulator's steering wheel, and vertical input from the driving simulator's throttle and brake pedals. Then it calls the move function of the car controller script with the horizontal and vertical inputs. Wheel colliders of the vehicle will then be controlled based on these inputs, and the vehicle can be set in motion. In order to reduce any system biases on the results of human-in-the-loop simulation, we recruit four different drivers to drive the on-ramp vehicle, each for five times. The drivers drive the vehicle on the driving simulator based on their own preferences, namely, there is no requirement for them to drive aggressively or cautiously. We categorize their driving behaviors only after the speed trajectories are generated by their simulation runs. It should be also noted that, a scene view of the game is displayed on the left-hand side of the driver's view, which is slightly different with the view shown in Figure 4-15. The scene view works as the rearview mirrors to allow the driver of the vehicle to observe its surrounding traffic.

The vehicle speed profiles and distances to the merging point from the cooperative merging scenario and the human-in-the-loop scenario are compared in Figure 4-16 and Figure 4-17, respectively. Both cooperative merging simulation and human-in-the-loop simulation are run with a frequency of 50 FPS. It should be noted that, we only show five of the twenty simulation runs from the human-in-the-loop scenario, and categorize them into "cautious driver" and "aggressive driver" cases based on the average changing rate of

vehicle speed, but all twenty simulation runs are included when calculating the results shown in Table XXIV.

Also note that in the cooperative merging simulation, ramp vehicle merges to the second place of the vehicle string. However, in the human-in-the-loop simulation, there is no requirement for the human driver to follow. All he/she needs to do while conducting the human-in-the-loop simulation is to drive the ramp vehicle from on-ramp to the main lane, but the ramp vehicle can either merge into the 6-vehicle string, or attach to the from/end of the vehicle string.

Simulation results are shown by Figure 4-16 and Figure 4-17, where Figure 4-16 shows the longitudinal speed profiles of CAVs, while Figure 4-17 shows the longitudinal position of CAVs, respectively, for different simulation cases. Note that the longitudinal positions of CAVs on different lanes (main line and on-ramp) are calculated by their distances to the merging point, which is also the way we apply our online feedforward/feedback longitudinal controller.

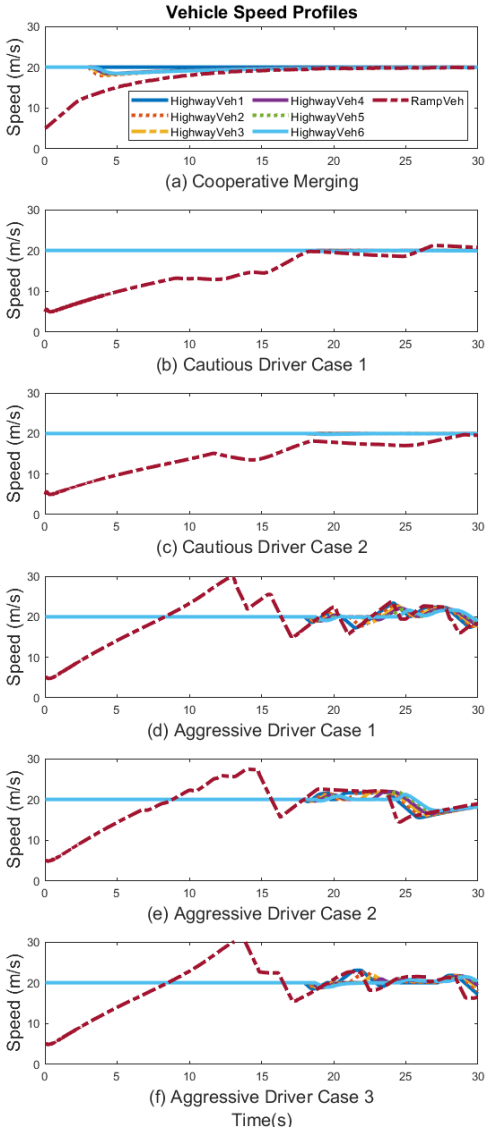

Figure 4-16. Speed profiles of vehicles driven in different scenarios

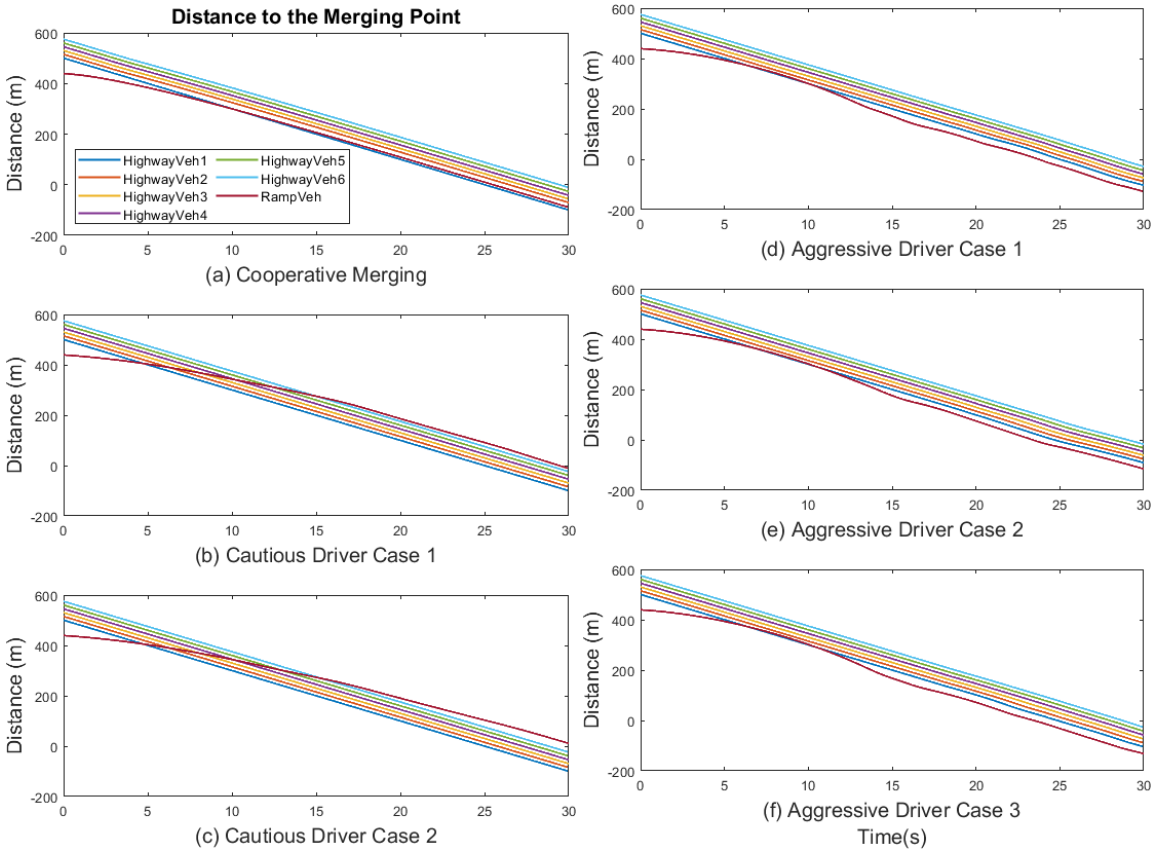

Figure 4-17. Distance profiles of vehicles driven in different scenarios

Figure 4-16 (a) shows the speed profiles generated from the proposed cooperative merging scenario, where mainline Vehicle 2 reaches the I2V communication starting point at around 3 s, and is assigned a sequence identification number of 3, which means it needs to follow the movement of the on-ramp vehicle. When Vehicle 2 starts to decelerate to adjust its speed and longitudinal position with respect to the on-ramp vehicle, its followers (mainline Vehicles 3, 4, 5, and 6) also decelerate accordingly since they are still in a vehicle string. Meanwhile, the on-ramp vehicle gradually adjusts its speed and longitudinal position with respect to mainline Vehicle 1. Therefore, when the merging happens at

around 18 s, there is no speed change of any vehicle. As shown in Figure 4-17, different vehicles' distances to the merging point further explain aforementioned descriptions.

For the cautious driver cases shown in Figure 4-16 (b) and (c), the on-ramp vehicle speeds up with a relatively small acceleration while it is on the on-ramp. Upon approaching the merging point, the on-ramp vehicle is already behind all mainline vehicles. So, it attaches to the end of the mainline vehicle string, and there is no speed change of any mainline vehicle. The distance to the merging point plots shown in Figure 4-17 (b) and (c) are also straightforward.

For the aggressive driver cases shown in Figure 4-16 (d), (e) and (f), the on-ramp vehicle speeds up with a relatively large acceleration at first since the driver's line of sight is obstructed and the driver does not know the traffic condition in the mainline at that time. Once the driver observes the traffic condition at around 14 s, the vehicle begins to slow down to avoid the rear-end collision with downstream traffic (which all travel at a speed of 20 m/s). Although the aggressive drivers already decide to overpass the whole six-vehicle string, they also need to adjust their speed to merge into the gap between the string leader and its downstream vehicle (but the time gap is larger than 0.5 s so it is possible to merge in). Upon attaching to the front of the mainline vehicle string, all the six followers in that string change speed accordingly to prevent any rear-end collisions, and there are also some speed fluctuations afterwards due to the relatively poor speed control of the aggressive drivers.

Table XXIV Comparison results between cooperative merging and baseline.

	Travel Time (s)	Energy (KJ)	HC (g)	CO (g)	CO2 (g)	NOx (g)
Cooperative Merging	218.14	9154.0	0.0094	1.1737	651.29	0.0440
Human-in-the-loop	233.58	9930.6	0.0200	2.8192	706.54	0.0759
Reduction Percentage	6.6%	7.8%	53.0%	58.4%	7.8%	42.0%

We also compare the system performance of the cooperative merging scenario with that of the human-in-the-loop scenario, in terms of travel time, energy consumption, and pollutant emissions. The number shown in each cell of Table XXIV is the sum of all seven vehicles' results over the same traveling distance. The results for the human-in-the-loop scenario are the average of all twenty simulation runs. Specifically, travel time is used to represent the mobility benefit of the proposed cooperative on-ramp merging protocol, and it is calculated as the average time spent by all seven vehicles to travel the same distance. It is shown in TABLE 1 that a reduction in travel time of 6.6% can be achieved by applying the protocol. Energy consumption and pollutant emissions are calculated by the U.S. Environmental Protection Agency's MOVES [99]. Compared to the human-in-the-loop scenario, the cooperative merging protocol provides 7.8% savings on energy consumption, and up to 58.4% reduction on pollutant emissions, respectively.

5 Conclusions and Future Work

5.1 Conclusions

In this dissertation, an agent-based distributed cooperative vehicle-infrastructure system framework has been developed in the CAV environment, where different CAV applications are designed based on V2V and/or I2V communication, and different motion control algorithms are proposed and evaluated in numerical simulations, microscopic traffic simulations, game engine simulations, as well as field implementations. Specifically, our dissertation is formed in a high-to-low-level structure, with the following achievement:

- We demonstrated how agent-based distributed cooperative vehicle-infrastructure systems work in from a high-level architecture point of view. System architecture of such vehicle-infrastructure systems was analyzed by disaggregating them into subsystems and their hardware/software components.
- We proposed applications of agent-based distributed cooperative vehicle-infrastructure systems in the CAV environment, presenting where it could be implemented in the transportation system. Upon demonstrating how the agent-based distributed cooperative vehicle-infrastructure systems work, I am also interested in where it could work. Therefore, different CAV applications were developed under V2V and/or I2V communication, with each of them bringing one or more benefits to the transportation system.
- We developed motion control algorithms to realize the desired movements of CAVs in the proposed CAV applications. The algorithms were not only analyzed

qualitatively and quantitatively, but were also evaluated by various simulation approaches.

5.2 Selected Publications Resulting from This Research

[1] Ziran Wang, Guoyuan Wu, Kanok Boriboonsomsin, Matthew J. Barth, Kyungtae Han, BaekGyu Kim, and Prashant Tiwari, "Cooperative Ramp Merging System: Agent-Based Modeling and Simulation Using Game Engine", *SAE International Journal of Connected and Automated Vehicles*, vol. 2, no. 2, May 2019

[2] Ziran Wang, Guoyuan Wu, and Matthew J. Barth, "Cooperative Eco-Driving along Multiple Signalized Intersections in a Partially Connected and Automated Vehicle Environment", *IEEE Transactions on Intelligent Transportation Systems*, Early Access

[3] Ziran Wang, Guoyuan Wu, and Matthew J. Barth, "Cluster-Wise Cooperative Eco-Approach and Departure Application for Connected and Automated Vehicles along Signalized Arterials," *IEEE Transactions on Intelligent Vehicles*, vol. 3, no. 4, Dec. 2018, pp. 404–413

[4] Ziran Wang, Guoyuan Wu, and Matthew J. Barth, "Developing a Distributed Consensus-Based Cooperative Adaptive Cruise Control (CACC) System for Heterogeneous Vehicles with Predecessor Following Topology," *Journal of Advanced Transportation*, vol. 2017, Article ID 1023654, Aug. 2017

[5] Ziran Wang, Kyungtae Han, BaekGyu Kim, Guoyuan Wu, and Matthew J. Barth, "Lookup Table-Based Consensus Algorithm for Real-Time Longitudinal Motion

Control of Connected and Automated Vehicles," *2019 American Control Conference,* Philadelphia, PA, Jul. 2019

[6] Ziran Wang, BaekGyu Kim, Hiromitsu Kobayashi, Guoyuan Wu, and Matthew J. Barth, "Agent-Based Modeling and Simulation of Connected and Automated Vehicles Using Game Engine: A Cooperative On-Ramp Merging Study," *Transportation Research Board 98th Annual Meeting,* Washington D.C., Jan. 2019

[7] Guoyuan Wu, Peng Hao, Ziran Wang, Kanok Boriboonsomsin, and Matthew J. Barth, "Eco-Approach and Departure along Signalized Corridors," *Transportation Research Board 98th Annual Meeting*, Washington D.C., Jan. 2019

[8] Ziran Wang, Guoyuan Wu, and Matthew J. Barth, "A Review on Cooperative Adaptive Cruise Control (CACC) Systems: Architectures, Controls, and Applications," *IEEE 21st International Conference on Intelligent Transportation Systems*, Maui, Hawaii, Nov. 2018

[9] Ziran Wang, Guoyuan Wu, and Matthew J. Barth, "Distributed Consensus-Based Cooperative Highway On-Ramp Merging Using V2X Communications," *SAE Technical Paper*, 2018-01-1177, Apr. 2018

[10] Ziran Wang, Guoyuan Wu, and Matthew J. Barth, "Cluster-Wise Cooperative Eco-Approach and Departure Application along Signalized Arterials," *IEEE 20th International Conference on Intelligent Transportation Systems*, Yokohama, Japan, Oct. 2017

[11] Peng Hao, Ziran Wang, Guoyuan Wu, Kanok Boriboonsomsin, and Matthew J. Barth, "Intra-Platoon Vehicle Sequence Optimization for Eco-Cooperative Adaptive Cruise Control," *IEEE 20th International Conference on Intelligent Transportation Systems*, Yokohama, Japan, Oct. 2017

[12] Ziran Wang, Guoyuan Wu, Peng Hao, Kanok Boriboonsomsin, and Matthew J. Barth, "Developing a Platoon-Wide Eco-Cooperative Adaptive Cruise Control (CACC) System," *2017 IEEE Intelligent Vehicles Symposium*, Redondo Beach, CA, Jun. 2017

[13] Ziran Wang, Guoyuan Wu, and Matthew J. Barth, "Developing a Distributed Consensus-Based Cooperative Adaptive Cruise Control (CACC) System," *Transportation Research Board 96th Annual Meeting*, Washington D.C., Jan. 2017

5.3 Future Work

Although many positive results have been achieved in this dissertation, there are still some open questions that need to be addressed in future work related to the agent-based distributed cooperative vehicle-infrastructure systems, especially in the development of CAV applications:

- How to build a more reliable architecture for CAV systems? Unlike most theoretically proposed CAV systems that assume a static setting, a more realistic traffic network would introduce a highly dynamic environment. For example, the cooperative longitudinal motion control of multiple CAVs is heavily based on V2V communication, which are vulnerable to communication impairments such as latency and packet loss. Also, cyberattacks such as jamming, V2X data injection,

and vehicle sensor manipulation can also impair the performance of CAV systems. In the future development of the agent-based distributed cooperative vehicle-infrastructure systems, the resilience against system impairments or attacks should also be considered and studied. How to conduct fault detection and isolation regarding communication impairments or cyberattacks, how to temporarily but smoothly switch to degraded modes of control that are less dependent on the communicated data, and how to maintain string stability under those situations could be some interesting topics to study and test.

- How can we identify and close the gap between theoretical research and experimental implementation? It is true that many advanced methodologies have been proposed and analyzed in theory, however, the gap between theoretically functional and practically functional needs to be identified and closed. For example, the theoretical studies of string stability in most cases ignored the destabilizing effect of communication latency. CAV applications that would appear to be stable based on the theoretical analyses are not always stable in practical implementations due to unavoidable latencies in communications. Therefore, stability analyses need to include realistic quantifications of communication latency in order to compensate for this gap between theory and practice. Theoretical research results need to be tested under various realistic conditions to identify this gap, but that could be both labor-intensive and time-consuming.
- How can we develop more ready-to-market cooperative vehicle-infrastructure systems with mixed traffic environment? Most of the CAV applications developed

in this dissertation made a strong assumption that all involved vehicles are CAVs. However, it is obvious that we will endure a long period during which the traffic environment is mixed with different types of vehicles: CAVs, connected vehicles, automated vehicles, and conventional vehicles. Cooperative longitudinal motion controllers that work for a pure CAV environment do not necessarily work for a mixed traffic environment, given the uncertainties introduced by other vehicle types in the environment. In order to facilitate more ready-to-market CAV applications, the future development of agent-based distributed cooperative vehicle-infrastructure systems might take advantage of advanced sensing and communication technology to deal with mixed traffic environment.

BIBLIOGRAPHY

[1] D. Jia, K. Lu, J. Wang, X. Zhang, and X. Shen, "A survey on platoon-based vehicular cyber-physical systems," IEEE Communications Surveys Tutorials, vol. 18, no. 1, pp. 263–284, 2016.

[2] USDOT. (2016) Traffice safety factsresearch note. [Online]. Available: https://crashstats.nhtsa.dot.gov/Api/Public/ViewPublication/812318

[3] INRIX. (2017) Los angeles tops inrix global congestion ranking. [Online]. Available: http://inrix.com/press-releases/scorecard-2017/

[4] USDOE. (2015) Fuel wasted in traffic congestion. [Online]. Available: https://www.energy.gov/eere/vehicles/fact-897-november-2-2015-fuel-wasted-traffic-congestion

[5] Engaged IT for the CIO. (2011) The future of intelligent transportation systems (ITS). [Online]. Available: https://mubbisherahmed.wordpress.com/2011/11/29/the-future-of-intelligent-transport-systems-its/

[6] S. E. Shladover, C. Nowakowski, X.-Y. Lu, and R. Ferlis, "Cooperative adaptive cruise control: Definitions and operating concepts," Transportation Research Record, vol. 2489, pp. 145–152, 2015.

[7] K. C. Dey, L. Yan, X. Wang, Y. Wang, H. Shen, M. Chowdhury, L. Yu, C. Qiu, and V. Soundararaj, "A review of communication, driver characteristics, and controls aspects of cooperative adaptive cruise control (CACC)," IEEE Transactions on Intelligent Transportation Systems, vol. 17, no. 2, pp. 491–509, Feb. 2016.

[8] Federal Communications Commission. (2003) Dedicated short range communications (DSRC) service. [Online]. Available: https://www.fcc.gov/wireless/bureau-divisions/mobility-division/ dedicated-short-range-communications-dsrc-service

[9] J. B. Kenney, "Dedicated short-range communications (dsrc) standards in the united states," Proceedings of the IEEE, vol. 99, no. 7, pp. 1162– 1182, July 2011.

[10] F. Bai, D. D. Stancil, and H. Krishnan, "Toward understanding characteristics of dedicated short range communications (dsrc) from a perspective of vehicular network engineers," in Proceedings of the Sixteenth Annual International Conference on Mobile Computing and Networking, ser. MobiCom '10. New York, NY, USA: ACM, 2010, pp. 329–340. [Online]. Available: http: //doi.acm.org/10.1145/1859995.1860033

[11] S. Lee and A. Lim, "An empirical study on ad hoc performance of dsrc and wi-fi vehicular communications," International Journal of Distributed Sensor Networks, vol. 9, no. 11, p. 482695, 2013. [Online]. Available: https://doi.org/10.1155/2013/482695

[12] S. Chen, J. Hu, Y. Shi, Y. Peng, J. Fang, R. Zhao, and L. Zhao, "Vehicle-to-everything (v2x) services supported by lte-based systems and 5g," IEEE Communications Standards Magazine, vol. 1, no. 2, pp. 70–76, 2017.

[13] Z. Xu, X. Li, X. Zhao, M. H. Zhang, and Z. Wang, "DSRC versus 4G-LTE for connected vehicle applications: A study on field experiments of vehicular communication performance," Journal of Advanced Transportation, vol. 2017, pp. 1–10, 2017.

[14] A. Nshimiyimana, D. Agrawal, and W. Arif, "Comprehensive survey of V2V communication for 4G mobile and wireless technology," in 2016 International Conference on Wireless Communications, Signal Processing and Networking (WiSPNET), March 2016, pp. 1722–1726.

[15] E. Uhlemann, "Connected-vehicles applications are emerging [connected vehicles]," IEEE Vehicular Technology Magazine, vol. 11, no. 1, pp. 25–96, Mar. 2016.

[16] A. Festag, "Standards for vehicular communication—from ieee 802.11p to 5g," e & i Elektrotechnik und Informationstechnik, vol. 132, no. 7, pp. 409–416, Nov 2015. [Online]. Available: https://doi.org/10.1007/s00502-015-0343-0

[17] M. G. Sanchez, M. P. T´ aboas, and E. L. Cid, "Millimeter wave radio´ channel characterization for 5G vehicle-to-vehicle communications," Measurement, vol. 95, pp. 223–229, 2017.

[18] Y. Zheng, S. Eben Li, J. Wang, D. Cao, and K. Li, "Stability and scalability of homogeneous vehicular platoon: Study on the influence of information flow topologies," IEEE Transactions on Intelligent Transportation Systems, vol. 17, no. 1, pp. 14–26, 2016.

[19] A. Geiger, M. Lauer, F. Moosmann, B. Ranft, H. Rapp, C. Stiller, and J. Ziegler, "Team AnnieWAY's entry to the 2011 Grand Cooperative Driving Challenge," IEEE Transactions on Intelligent Transportation Systems, vol. 13, no. 3, pp. 1008–1017, Sep. 2012.

[20] J. Martensson, A. Alam, S. Behere, M. A. A. Khan, J. Kjellberg,˚ K. Liang, H. Pettersson, and D. Sundman, "The development of a cooperative heavy-duty vehicle for the gcdc 2011: Team scoop," IEEE Transactions on Intelligent Transportation Systems, vol. 13, no. 3, pp. 1033–1049, Sep. 2012.

[21] V. Milanes, S. E. Shladover, J. Spring, C. Nowakowski, H. Kawazoe, and M. Nakamura, "Cooperative adaptive cruise control in real traffic situations," IEEE Transactions on Intelligent Transportation Systems, vol. 15, no. 1, pp. 296–305, Feb. 2014.

[22] R. Kianfar, B. Augusto, A. Ebadighajari, U. Hakeem, J. Nilsson, A. Raza, R. S. Tabar, N. V. Irukulapati, C. Englund, P. Falcone et al., "Design and experimental validation of a cooperative driving system in the Grand Cooperative Driving Challenge," IEEE Transactions on Intelligent Transportation Systems, vol. 13, no. 3, pp. 994–1007, 2012.

[23] L. Guvenc, I. M. C. Uygan, K. Kahraman, R. Karaahmetoglu, I. Altay, M. Senturk, M. T. Emirler, A. E. H. Karci, B. A. Guvenc, E. Altug, M. C. Turan, . S. Tas, E. Bozkurt, U. Ozguner, K. Redmill, A. Kurt, and B. Efendioglu, "Cooperative adaptive cruise control implementation of Team Mekar at the Grand Cooperative Driving Challenge," IEEE Transactions on Intelligent Transportation Systems, vol. 13, no. 3, pp. 1062–1074, Sep. 2012.

[24] SAE International On-Road Automated Driving (ORAD) committee, Taxonomy and Definitions for Terms Related to On-Road Motor Vehicle Automated Driving Systems, Jan 2014. [Online]. Available: https://doi.org/10.4271/J3016 201401

[25] D. Gonzlez, J. Prez, V. Milans, and F. Nashashibi, "A review of motion planning techniques for automated vehicles," IEEE Transactions on Intelligent Transportation Systems, vol. 17, no. 4, pp. 1135–1145, April 2016.

[26] J. Ziegler and C. Stiller, "Spatiotemporal state lattices for fast trajectory planning in dynamic on-road driving scenarios," in 2009 IEEE/RSJ International Conference on Intelligent Robots and Systems, Oct 2009, pp. 1879–1884.

[27] P. Hao, G. Wu, K. Boriboonsomsin, and M. J. Barth, "Eco-approach and departure (ead) application for actuated signals in real-world traffic," IEEE Transactions on Intelligent Transportation Systems, vol. 20, no. 1, pp. 30–40, Jan 2019.

[28] S. E. Shladover, C. Nowakowski, and X.-Y. Lu, "Using cooperative adaptive cruise control (CACC) to form high-performance vehicle streams. Definitions, literature review and operational concept alternatives," California PATH Program, Tech. Rep., 2018.

[29] K. C. Dey, L. Yan, X. Wang, Y. Wang, H. Shen, M. Chowdhury, L. Yu, C. Qiu, and V. Soundararaj, "A review of communication, driver characteristics, and controls aspects of cooperative adaptive cruise control (CACC)," IEEE Transactions on Intelligent Transportation Systems, vol. 17, no. 2, pp. 491–509, Feb. 2016.

[30] B. van Arem, C. J. G. van Driel, and R. Visser, "The impact of cooperative adaptive cruise control on traffic-flow characteristics," IEEE Transactions on Intelligent Transportation Systems, vol. 7, no. 4, pp. 429–436, Dec. 2006.

[31] M. di Bernardo, A. Salvi, and S. Santini, "Distributed consensus strategy for platooning of vehicles in the presence of time-varying heterogeneous communication delays," IEEE Transactions on Intelligent Transportation Systems, vol. 16, no. 1, pp. 102–112, Feb. 2015.

[32] M. di Bernardo, P. Falcone, A. Salvi, and S. Santini, "Design, analysis, and experimental validation of a distributed protocol for platooning in the presence of time-varying heterogeneous delays," IEEE Transactions on Control Systems Technology, vol. 24, pp. 413–427, 2016.

[33] S. van de Hoef, K. H. Johansson, and D. V. Dimarogonas, "Fuel-efficient en route formation of truck platoons," IEEE Transactions on Intelligent Transportation Systems, vol. 19, no. 1, pp. 102–112, Jan. 2018.

[34] V. Turri, B. Besselink, and K. H. Johansson, “Cooperative look-ahead control for fuel-efficient and safe heavy-duty vehicle platooning,” IEEE Transactions on Control Systems Technology, vol. 25, no. 1, pp. 12–28, 2017.

[35] S. E. Shladover, “Path at 20history and major milestones,” IEEE Transactions on Intelligent Transportation Systems, vol. 8, no. 4, pp. 584–592, Dec 2007.

[36] J. Ploeg, B. T. M. Scheepers, E. van Nunen, N. van de Wouw, and H. Nijmeijer, “Design and experimental evaluation of cooperative adaptive cruise control,” in 2011 14th International IEEE Conference on Intelligent Transportation Systems (ITSC), Oct. 2011, pp. 260–265.

[37] J. Ploeg, S. Shladover, H. Nijmeijer, and N. van de Wouw, “Introduction to the special issue on the 2011 Grand Cooperative Driving Challenge,” IEEE Transactions on Intelligent Transportation Systems, vol. 13, no. 3, pp. 989–993, Sep. 2012.

[38] S. Tsugawa, S. Jeschke, and S. E. Shladover, “A review of truck platooning projects for energy savings,” IEEE Transactions on Intelligent Vehicles, vol. 1, no. 1, pp. 68–77, March 2016.

[39] C. Nowakowski, S. E. Shladover, X.-Y. Lu, D. Thompson, and A. Kailas, “Cooperative adaptive cruise control (CACC) for truck platooning: Operational concept alternatives,” California PATH Program, Institute of Transportation Studies University of California, Berkeley and Volvo Group North America, Tech. Rep., 2015.

[40] S. Tsugawa, “An overview on an automated truck platoon within the Energy ITS project,” IFAC Proceedings Volumes, vol. 46, no. 21, pp. 41 – 46, 2013, 7th IFAC Symposium on Advances in Automotive Control. [Online]. Available: http://www.sciencedirect.com/science/ article/pii/S1474667016383409

[41] R. Kunze, R. Ramakers, K. Henning, and S. Jeschke, “Organization and operation of electronically coupled truck platoons on german motorways,” in Intelligent Robotics and Applications, 2009, pp. 135– 146.

[42] V. Milanes, J. Godoy, J. Villagra, and J. Perez, “Automated on-ramp merging system for congested traffic situations,” IEEE Transactions on Intelligent Transportation Systems, vol. 12, no. 2, pp. 500–508, Jun. 2011.

[43] J. Rios-Torres and A. A. Malikopoulos, “A survey on the coordination of connected and automated vehicles at intersections and merging at highway on-ramps,” IEEE Transactions on Intelligent Transportation Systems, vol. 18, no. 5, pp. 1066–1077, May 2017.

[44] R. Scarinci and B. Heydecker, “Control concepts for facilitating motorway on-ramp merging using intelligent vehicles,” Transport Reviews, vol. 34, no. 6, pp. 775–797, 2014.

[45] A. Uno, T. Sakaguchi, and S. Tsugawa, “A merging control algorithm based on inter-vehicle communication,” in Proceedings 199 IEEE/IEEJ/JSAI International Conference on Intelligent Transportation Systems, Oct. 1999, pp. 783–787.

[46] X.-Y. Lu and K. J. Hedrick, “Longitudinal control algorithm for automated vehicle merging,” in Proceedings of the 39th IEEE Conference on Decision and Control, vol. 1, Dec. 2000, pp. 450–455.

[47] T. Dao, C. M. Clark, and J. P. Huissoon, “Distributed platoon assignment and lane selection for traffic flow optimization,” in IEEE Intelligent Vehicles Symposium (IV), Jun. 2008, pp. 739–744.

[48] J. Rios-Torres and A. A. Malikopoulos, “Automated and cooperative vehicle merging at highway on-ramps,” IEEE Transactions on Intelligent Transportation Systems, vol. 18, no. 4, pp. 780–789, Apr. 2017.

[49] H. Liu, X. D. Kan, S. E. Shladover, X.-Y. Lu, and R. E. Ferlis, “Impact of cooperative adaptive cruise control on multilane freeway merge capacity,” Journal of Intelligent Transportation Systems, vol. 22, no. 3, pp. 263–275, 2018. [Online]. Available: https://doi.org/10.1080/15472450.2018.1438275

[50] X.-Y. Lu, H.-S. Tan, S. E. Shladover, and J. K. Hedrick, “Automated vehicle merging maneuver implementation for AHS,” Vehicle System Dynamics, vol. 41, no. 2, pp. 85–107, 2004.

[51] D. Fernandez, M. A. Sotelo, J. Alonso, R. Garcia, T. de Pedro, C. Gonzalez, J. E. Naranjo, D. Fernandez, M. A. Sotelo, J. Alonso, R. Garcia, T. de Pedro, C. Gonzalez, and J. E. Naranjo, “Autopia architecture for automatic driving and maneuvering,” in 2006 IEEE Intelligent Transportation Systems Conference, Sep. 2006, pp. 1220– 1225.

[52] J. Ma, X. Li, S. Shladover, H. A. Rakha, X. Lu, R. Jagannathan, and D. J. Dailey, “Freeway speed harmonization,” IEEE Transactions on Intelligent Vehicles, vol. 1, no. 1, pp. 78–89, March 2016.

[53] M. Wang, W. Daamen, S. P. Hoogendoorn, and B. van Arem, “Connected variable speed limits control and car-following control with vehicle-infrastructure communication to resolve stop-and-go waves,” Journal of Intelligent Transportation Systems, vol. 20, no. 6, pp. 559–572, 2016. [Online]. Available: https://doi.org/10.1080/ 15472450.2016.1157022

[54] B. Khondaker and L. Kattan, “Variable speed limit: A microscopic analysis in a connected vehicle environment,” Transportation Research Part C: Emerging Technologies, vol. 58, pp. 146–159, 2015.

[55] X.-Y. Lu, S. E. Shladover, I. Jawad, R. Jagannathan, and T. Phillips, “A novel speed-measurement based variable speed limit/advisory algorithm for a freeway corridor with multiple bottlenecks,” in Transportation Research Board 94th Annual Meeting, Jan. 2015.

[56] Y. Li, C. Xu, L. Xing, and W. Wang, “Integrated cooperative adaptive cruise and variable speed limit controls for reducing rear-end collision risks near freeway bottlenecks based on micro-simulations,” IEEE Transactions on Intelligent Transportation Systems, vol. 18, no. 11, pp. 3157–3167, Nov. 2017.

[57] R. L. Bertini, S. Boice, and K. Bogenberger, “Dynamics of variable speed limit system surrounding bottleneck on german autobahn,” in Transportation Research Board 84th Annual Meeting, Jan. 2006.

[58] X.-Y. Lu and S. E. Shladover, “Review of variable speed limits and advisories: Theory, algorithms, and practice,” Transportation Research Record, vol. 2423, no. 1, pp. 15–23, 2014. [Online]. Available: https://doi.org/10.3141/2423-03

[59] S. Nygardhs and G. Helmers, “Vms - variable message signs: A˚ literature review,” Infrastructure maintenance, Tech. Rep. 570A, 2007.

[60] O. D. Altan, G. Wu, M. J. Barth, K. Boriboonsomsin, and J. A. Stark, “Glidepath: Eco-friendly automated approach and departure at signalized intersections,” IEEE Transactions on Intelligent Vehicles, vol. 2, no. 4, pp. 266–277, Dec 2017.

[61] K. Katsaros, R. Kernchen, M. Dianati, and D. Rieck, “Performance study of a green light optimized speed advisory (glosa) application using an integrated cooperative its simulation platform,” in 2011 7th International Wireless Communications and Mobile Computing Conference, July 2011, pp. 918–923.

[62] M. Abubakr, O. Abuchaar, S. Al-Stouhi, M. Buchard, S. Das, U. Ibrahim, A. Kailas, H. Konet, V. Kumar, J. Meier, M. Yamamoto, K. Balke, B. Kuhn, M. Lukuc, C. Poe, D. LeBlanc, M. Barth, R. Deering, and R. Goudy, “Eco-approach and eco-departure planning study final report,” U.S. Department of Transportation Federal Highway Administration, Tech. Rep., 2016.

[63] H. Yang, H. Rakha, and M. V. Ala, “Eco-cooperative adaptive cruise control at signalized intersections considering queue effects,” IEEE Transactions on Intelligent Transportation Systems, vol. 18, no. 6, pp. 1575–1585, Jun. 2017.

[64] W. Zhao, D. Ngoduy, S. Shepherd, R. Liu, and M. Papageorgiou, “A platoon based cooperative eco-driving model for mixed automated and human-driven vehicles at a signalised intersection,” Transportation Research Part C: Emerging Technologies, vol. 95, pp. 802 – 821, 2018. [Online]. Available: http://www.sciencedirect.com/science/article/pii/S0968090X18307423

[65] U.S. Department of Transportation. (2013) Applications for the environment: Real-time information synthesis (AERIS). [Online]. Available: https://www.its.dot.gov/research archives/aeris/ pdf/Eco-SignalOperationsConOps021814.pdf

[66] ——. Multi-modal intelligent traffic safety system (MMITSS). [Online]. Available: https://www.its.dot.gov/research archives/dma/ bundle/mmitss plan.htm

[67] N. Neuendorf and T. Bruns, “The vehicle platoon controller in the decentralised, autonomous intersection management of vehicles,” in Proceedings of the IEEE International Conference on Mechatronics, 2004. ICM ’04, Jun. 2004, pp. 375–380.

[68] A. I. M. Medina, N. van de Wouw, and H. Nijmeijer, “Automation of a T-intersection using virtual platoons of cooperative autonomous vehicles,” in 2015 IEEE 18th International Conference on Intelligent Transportation Systems, Sep. 2015, pp. 1696–1701.

[69] ——, “Cooperative intersection control based on virtual platooning,” IEEE Transactions on Intelligent Transportation Systems, vol. 19, no. 6, pp. 1727–1740, 2018.

[70] B. Xu, S. E. Li, Y. Bian, S. Li, X. J. Ban, J. Wang, and K. Li, “Distributed conflict-free cooperation for multiple connected vehicles at unsignalized intersections,” Transportation Research Part C: Emerging Technologies, vol. 93, pp. 322–334, 2018.

[71] M. Bashiri and C. H. Fleming, “A platoon-based intersection management system for autonomous vehicles,” in IEEE Intelligent Vehicles Symposium (IV), Jun. 2017, pp. 667–672.

[72] Q. Jin, G. Wu, K. Boriboonsomsin, and M. Barth, “Platoon-based multi-agent intersection management for connected vehicle,” in 2013 16th International IEEE Conference on Intelligent Transportation Systems (ITSC)), Oct. 2013, pp. 1462–1467.

[73] H. Diab, I. B. Makhlouf, and S. Kowalewski, “A platoon of vehicles approaching an intersection: A testing platform for safe intersections,” in 2012 15th International IEEE Conference on Intelligent Transportation Systems (ITSC), Sep. 2012, pp. 1918–1923.

[74] L. Bouraoui, S. Petti, A. Laouiti, T. Fraichard, and M. Parent, “Cybercar cooperation for safe intersections,” in 2006 IEEE Intelligent Transportation Systems Conference, Sep. 2006, pp. 456–461.

[75] A. de La Fortelle, “Analysis of reservation algorithms for cooperative planning at intersections,” in 13th International IEEE Conference on Intelligent Transportation Systems, Sep. 2010, pp. 445–449.

[76] Gustafsson, L., and Sternad, M., “Consistent Micro, Macro, and State-Based Population Modelling,” Mathematical Bioscience, vol. 225, no. 2, 2010, pp. 94-107.

[77] Macal, C. M., North, M. J., “Tutorial on Agent-Based Modeling and Simulation,” Proceedings of IEEE Winter Simulation Conference, 2005.

[78] Boesch, P. M., Ciari, F. Agent-Based Simulation of Autonomous Cars. Proceedings of American Control Conference, 2015, pp. 2588-2592.

[79] Matlab. https://www.mathworks.com/products/matlab.html

[80] Simulink. https://www.mathworks.com/products/simulink.html

[81] PTV Vissim. http://vision-traffic.ptvgroup.com/en-us/products/ptv-vissim/.

[82] Sumo - Simulation of Urban Mobility. https://sumo.dlr.de/index.html.

[83] Aimsun. https://www.aimsun.com/.

[84] Unity. https://Unity.com/.

[85] Craighead, J., Burke, J., and Murphy, R., "Using the Unity Game Engine to Develop SARGE: A Case Study," Computer, Jan. 2007.

[86] Estreen, T., and Nord, S., "Visualization of Platooning in Unity," Degree Projects in Technology, 2018.

[87] Khosravi, M., Yassiry, A., "Virtual Truck Platooning Implementation in Unity," Degree Projects in Technology, 2018.

[88] Yamaura, M., Arechiga, N., Shiraishi, S., Eisele, S., Hite, J., Neema, S., Scott, J., and Bapty, T., "ADAS Virtual Prototyping Using Modelica and Unity Co-Simulation via OpenMETA," Proceedings of Japanese Modelica Conference, 2016.

[89] Kim, B., Kashiba, Y., Dai, S., and Shiraishi, S., "Testing Autonomous Vehicle Software in the Virtual Prototyping Environment," IEEE Embedded Systems Letters, vol. 9, no. 1, Mar. 2017, pp. 5-8.

[90] Dai, S., Hite, J., Masuda, T., Kashiba, Y., Arechiga, N., Shiraishi, S., Eisele, S., Scott, J., and Bapty, T., "Control Parameter Optimization for Autonomous Vehicle Software Using Virtual Prototyping," Proceedings of IEEE 28th International Symposium on Software Reliability Engineering, 2017.

[91] R. Rajamani and S.E. Shladover, "An Experimental Comparative Study of Autonomous and Co-Operative Vehicle-Follower Control System," Trans. Res. Part C: Emerg. Technol., vol. 9, no. 1, pp. 15–31, Feb. 2001.

[92] R. O. Saber, J. A. Fax and R. M. Murray, "Consensus and Cooperation in Networked Multi-Agent Systems," in Proc. IEEE, vol. 95, no. 1, pp. 215–233, Jan. 2007.

[93] W. Ren, and E.M. Atkins, "Second-order consensus protocols in multiple vehicle systems with local interactions," presented at the AIAA Guidance, Navigation, Control Conf. Exhib., San Francisco, CA, 2005.

[94] Zhang, Y., Kosmatopoulos, E. B., Inannou, P. A., and Chien, C. C., "Autonomous Intelligent Cruise Control Using Front and Back Information for Tight Vehicle Following Maneuvers," IEEE Transactions on Vehicular Technology, vol. 48, no. 1, pp. 319–328, Jan. 1999.

[95] Xiao, L., and Gao, F., "Practical String Stability of Platoon of Adaptive Cruise Control Vehicles," IEEE Transactions on Intelligent Transportation Systems, vol. 12, no. 4, pp. 1184–1194, Dec. 2011.

[96] Wang, Z., Wu, G., and Barth, M., "Developing a Distributed Consensus-Based Cooperative Adaptive Cruise Control System for Heterogeneous Vehicles with

Predecessor Following Topology," Journal of Advanced Transportation, vol. 2017, Aug. 2017.

[97] Jia, D. and Ngoduy, D., "Platoon Based Cooperative Driver Model with Consideration of Realistic Inter-Vehicle Communication," Transportation Research Part C, vol. 68, Jul. 2016, pp. 245-264.

[98] Unity Asset Store, Simple Waypoint System. URL: https://assetstore.Unity.com/packages/tools/animation/simple-waypoint-system-2506.

[99] MOtor Vehicle Emission Simulator (MOVES). URL: https://www.epa.gov/moves.

[100] R. Rajamani and S.E. Shladover, "An Experimental Comparative Study of Autonomous and Co-Operative Vehicle-Follower Control System," Trans. Res. Part C: Emerg. Technol., vol. 9, no. 1, pp. 15–31, Feb. 2001.

[101] Y. Zheng, S. E. Li, J. Wang, L. Y. Wang, and K. Li, "Influence of Information Flow Topology on Closed-Loop Stability of Vehicle Platoon with Rigid Formation," in Proc. IEEE 17th ITSC, 2014, pp. 2094–2100.

[102] C. Lei, E. V. Eenennaam, W. Wolterink, G. Karagiannis, G. Heijenk, and J. Ploeg, "Impact of Packet Loss on CACC String Stability Performances," in Proc. ITST, 2011, pp. 381–386.

[103] G. Naus, R. Vugts, J. Ploeg, M. van de Molengraft, and M. Steinbuch, "String-Stable CACC Design and Experimental Validation: A Frequency-Domain Apprach," IEEE Trans. Veh. Technol., vol. 59, no. 9, pp. 4268–4279, Nov. 2010.

[104] M. di Bernardo, A. Salvi, and S. Santini, "Distributed Consensus Strategy for Platooning of Vehicles in the Presence of Time-Varying Heterogeneous Communication Delays," IEEE Trans. Intell. Transp. Syst., vol. 16, no. 1, pp. 102–112, Feb. 2015.

[105] X. -Y. Lu, J. K. Hedrick, and M. Drew, "ACC/CACC—Control Design, Stability and Robust Performance," in Proc. of the 2002 Amer. Control Conf., vol. 6, 2002, pp. 4327–4332.

[106] R. E. Wilson, and J. A. Ward, "Car-Following Models: Fifty Years of Linear Stability Analysis—A Mathematical Perspective," Transport. Planning and Technol., vol. 34, no. 1, pp. 3–18, Jan. 2011.

[107] M. Amoozadeh, H. Deng, C.-N. Chuah, H. M. Zhang, and D. Ghosal, "Platoon Management with Cooperative Adaptive Cruise Control Enabled by VANET," Veh. Commun., vol. 2, no. 2, pp. 110 – 123, Apr. 2015.

[108] A. A. Peters, R. H. Middleton, and O. Mason, "Leader Tracking in Homogeneous Vehicle Platoons with Broadcast Delays," Automatica, vol. 50, no. 1, pp. 64–74, Jan. 2014.

[109] J. Laumônier, C. Desjardins, and B. Chaib-draa, “Cooperative Adaptive Cruise Control: A Reinforcement Learning Approach,” in Proc. 4th Workshop Agents Traffic Transp., Hakodate, Japan, 2006, pp. 1–9.

[110] W. H. V. Willigen, M. C. Schut, and L. J. H. M. Kester, “Approximating Safe Spacing Policies for Adaptive Cruise Control Strategies,” in Proc. IEEE VNC, 2011, pp. 9–16.

[111] W. B. Qin, M. M. Gomez, and G. Orosz, “Stability Analysis of Connected Cruise Control with Stochastic Delay,” in Proc. IEEE ACC, 2014, pp. 4624–4629.

[112] D. Swaroop, and J. K. Hedrick, “String Stability of Interconnected Systems,” IEEE Trans. Autom. Control, vol. 41, no. 3, pp. 349–355, Mar. 1996.

[113] H. Xing, J. Ploeg, and H. Nijmeijer, “Padé Approximations of Delays in Cooperative ACC Based on String Stability Requirements,” IEEE Trans. Intell. Veh., vo. 1, no. 3, pp. 277–286, Sept. 2016.

[114] K. Santhanakrishnan and R. Rajamani, “On Spacing Policies for Highway Vehicle Automation,” IEEE Trans. Intel. Transp. Syst., vol. 4, no. 4, pp. 198–204, Dec. 2003.

[115] USDOT, Connected Vehicle Reference Implementation Architecture-Applications, https://www.iteris.com/cvria/html/applications/applications.html.

[116] F. Bai, D. D. Stancil, and H. Krishnan, “Toward Understanding Characteristics of Dedicated Short Range Communication (DSRC) from a Perspective of Vehicular Network Engineers,” in Proc. 16th Annu. Int. Conf. on Mobile Comput. and Netw., 2010, pp. 329–340.

[117] Q. Chen, D. Jiang, and L. Delgrossi, “IEEE 1609.4 DSRC Multi-Channel Operations and Its Implications on Vehicle Safety Communications,” in Proc. IEEE VNC, 2009.

[118] R. Miucic, Z. Popovic, and S. Mahmud, “Experimental Characterization of DSRC Signal Strength Drops,” in Proc. IEEE 12th ITSC, 2009

[119] S. Santini, A. Salvi, A. S. Valente, A. Pescapè, M. Segata, and R. Lo Cigno, “A Consensus-Based Approach for Platooning with Inter-Vehicular Communications,” in Proc. 34th IEEE INFOCOM, 2015, pp. 1158–1666.

[120] R. Horowitz, C. -W. Tan, and X. Sun, “An Efficient Lane Change Maneuver for Platoons of Vehicles in an Automated Highway System,” California PATH Research Report. UCB-ITS-PRR-2004-16. University of California Berkeley, 2004.

[121] S. E. Shladover, C. Nowakowski, X. -Y. Lu, and R. Ferlis, “Cooperative Adaptive Cruise Control (CACC) Definitions and Operating Concepts,” in Proc. Trans. Res. Board 94th Annu. Meeting, Jan. 2015.

[122] P. Seiler, B. -S. Song, and J. K. Hedrick, “Application of Nonlinear Control to a Collision Avoidance System,” in Proc. 5th World Congr. ITS, 1998.

[123] K. Yi, and J. Chung, “Nonlinear Brake Control for Vehicle CW/CA Systems,” IEEE/ASME Trans. Mechatronics, vol. 6, no. 1, pp. 17–25, Mar. 2001.

[124] M. Barth and K. Boriboonsomsin, “Real-world carbon dioxide impacts of traffic congestion,” Transp. Res. Rec., vol. 2058, no. 1, pp. 163–171, 2008.

[125] M. Zabat, N. Stabile, S. Frascaroli, and F. Browand, “The Aerodynamic Performance of Platoons: Final Report”, California PATH Research Report, Oct. 1995.

[126] INRIX. Los Angeles Tops INRIX Global Congestion Ranking, accessed on Feb. 9, 2018. [Online]. Available: http://inrix.com/press-releases/scorecard-2017/.

[127] National Safety Council. NSC Motor Vehicle Fatality Estimates, accessed on Feb. 9, 2018. [Online]. Available: http://www.nsc.org/NewsDocuments/2017/12-month-estimates.pdf.

[128] U.S. Department of Transportation. Bureau of Transportation Statistics, accessed on June 17, 2017. [Online]. Available: https://www.rita.dot.gov/bts/sites/rita.dot.gov.bts/files/publications/transportation_statistics_annual_report/2015/chapter7.html.

[129] Jiang, J. Hu, S. An, M. Wang, and B. B. Park, “Eco Approaching at an Isolated Signalized Intersection Under Partially Connected and Automated Vehicles Environment,” Transportation Research Part C: Emerging Technologies, vol. 79, pp. 290–307, Jun. 2017.

[130] B. Asadi and A. Vahidi, “Predictive Cruise Control: Utilizing Upcoming Traffic Signal Information for Improving Fuel Economy and Reducing Trip Time,” IEEE Transactions on Control Systems Technology, vol. 19, no. 3, pp. 707–714, May 2011.

[131] M. A. S. Kamal, S. Taguchi, and T. Yoshimura, “Intersection Vehicle Cooperative Eco-Driving in the Context of Partially Connected Vehicle Environment,” in Proceedings of IEEE 18th International Conference on Intelligent Transportation Systems, 2015.

[132] M. Treiber, A. Hennecke, and D. Helbing, “Congested Traffic States in Empirical Observations and Microscopic Simulations,” Physical Review E, vol. 62, no. 2, pp. 1805–1824, Aug. 2000.